Studies in Theoretical Investigations on Catalytic Properties of Gold Clusters

THESIS SUBMITTED TO THE
UNIVERSITY OF PUNE

FOR THE DEGREE OF
**DOCTOR OF PHILOSOPHY
IN CHEMISTRY**

BY
HIMADRI SEKHAR DE

**RESEARCH ADVISOR
DR. SOURAV PAL**

PHYSICAL CHEMISTRY DIVISION
NATIONAL CHEMICAL LABORATORY
PUNE-411 008

NOVEMBER, 2011

Certificate

This is to certify that the work presented in this thesis entitled, *"Studies in Theoretical Investigations on Catalytic Properties of Gold Clusters"* by Himadri Sekhar De, for the degree of Doctor of Philosophy in Chemistry, was carried out by the candidate under my supervision at the Physical Chemistry Division, National Chemical Laboratory, Pune, India. Any material that has been obtained from other sources has been duly acknowledged in the thesis.

Date:

Place:

Dr. Sourav Pal

(Research Advisor)

Physical Chemistry Division

National Chemical Laboratory

Pune, India - 411 008

Abstract

Density Functional Theory (DFT)[1] has come up as a powerful computational strategy in recent times and has influenced quantum chemistry to an appreciable extent. DFT has provided excellent methodologies in the past two decades to compute the energetics, structure and properties of the molecules, especially having large number of electrons with high accuracy using low computational costs as compared to the wavefunction based methods (WFT). In the last few years DFT in computation has emerged for calculation of large number of properties for a wide variety of systems [2]. DFT has thus played a decisive role in evolution of quantum chemistry in specialized regime, not only for larger systems but, onto smaller systems too, to various types of spectroscopic studies, for the use of materials engineering and chemistry, computational biochemistry and a wide field of scientific community as a boon [3]. Historically, although DFT came into picture for calculation of the properties of molecules and solids in 50s of last century by Slater in his X_α method, [4]it became a sustainable theory after introduction of Hohenberg-Kohn Theorems [5]. A major breakthrough came in the year 1995 when Walter Kohn and Sham, could make the orbitals included into the formalism. Parr and Yang revolutionized DFT as a theory and tool for calculating molecular energetics. Based on their idea, that the electron density is the fundamental quantity for describing atomic and molecular ground states, many pioneering chemical

concepts have been introduced in the field of chemistry. One of them was the description of properties like electronegativity, and also, a completely new frontier, the theory of reactivity evolved for further analysis.

Pal and co-workers have done extensive work in the field of chemical reactivity using Density Functional Theory. Pal et al. [6] showed that the change in chemical hardness and chemical potential are intrinsically related to the binding energies of the molecule. Pal and Roy[7, 8] further showed that chemical hardness, softness and polarizability of molecules with the corresponding electronegativity of the atoms and anions and a new concept of "local bond hardness" was proposed.

Roy et al.[9] used both the local hardness and local softness to calculate the intra and intermolecular reactivity of nucleophilic attack on carbonyl compounds. From the local softness values and the newly introduced concepts of relative electrophilicity s_k^+/s_k^- and nucleophilicity s_k^-/s_k^+ calculated for these compounds, and it was concluded that the electrophilic attack occurs on carbonyl compounds. Furthermore, Deka, et al.[10], did extensive study on the DFT based descriptors for the isomorphous substitution influence on the acidity of model systems. Krishnamurthy and Pal[11] used the concept of group softness in the study of nucleophilic additions to carbonyl compounds and in a study of relative acidity of acetic and propionic acid.

Condensed Fukui functions and local softness came out as a popularized tool for

computing reactivity and rational interaction between several molecules. Krishnamurti and Pal[12], studied the interaction of CO, NH_3 and H_2O with a cluster model of faujasite X-type zeolite using the concept of condensed fukui function. Pal and Chandrakumar[13] used the local HSAB principle in the study of the interaction of N_2, CO_2 and CO with a series of zeolite A model systems. They further proposed the mechanism of charge transfer at the reactive site. An important work in the era was a systematic and rigorous approach towards the problem of non-negativity of Fukui functions with the computational results published by Roy and Pal [14]. Chandrakumar and Pal [15] furthur extended the local HSAB principle to the case of multiple site interaction and reactivity of Lewis acid-base complexes[16].

A. Goursot et $al.$[17] presented an in-depth study on an extension of cluster model of Fe-BEA zeolite for description of catalytic cycle of N_2O reduction by CO using density functional based deMon2K code. The minimum energy paths for N_2O decomposition and reduction with CO were rigorously calculated. The metal encapsulated zeolite shows consistent results for energetics and conformational orientation compared with experimental values. Krishnamurty et $al.$ did extensive study on finite temperature behavior of Au_{19} and Au_{20} tetrahedral gold clusters[18]. This background gives an opportunity to work on novel transition metals like gold, which has been recently found to possess relativistic effect and a rich chemistry.

The present decade has witnessed the "capabilities" and "personalities" of gold in

the form of not only an essential component electronic devices but nanoclusters and nanowires. wide range of applicability from catalysis, medicine, electronics and so on [19]. Although, gold has been thought to as a yellow noble metal, it has been discovered as to have a rich chemistry. Not only in organometallics, but aided by powerful computers and advanced computational codes it has been possible to enumerate various properties of metals like gold which have been considered as 'noble' or 'inert' for centuries. It is possible now to calculate these properties by applying the principles of quantum mechanics. It is a challenge at the doorstep to simulate the chemical composition of the material which are yet to be synthesized and still have no existence.

The simulation by the application of quantum mechanics would not have been possible for large number of atoms without a way of simplifying the problem, especially without the help of Density Functional Theory computations.

Gold is an unique element in it and that possesses high relativistic effects than its neighbors in the periodic table. Relativistic effects in gold can be qualitatively attributed to the high speed of electrons when they move near heavy nucleus. This consequences in the increase in mass of the electrons which leads to stabilization in energy and radial contraction [20]. The mostly influenced orbitals are s and p, since they are closest to the nucleus. The contraction of these results in better screening of the nuclear attraction leading to the destabilization and expansion of the d and f orbitals. In case relativity is absent, it leads to a situation that the energy difference between the 5d and 6s of gold is very similar to 4d and 5s energy

gap of silver. Thus the entire orbital-energy difference between Au and Ag is due to relativity.

For calculating the properties of molecules with heavy elements, it is expensive to carry out all-electron calculations, large savings can be made with the utilization of valence electrons by replacing the core with an effective core potential (ECP), also called Pseudopotential (PP). The valence part being still treated *ab initio*. By this approach the inner electrons and their basis functions are bypassed. There has been large number of articles where the pseudopotential approach has been adopted without loosing the accuracy[21–23]. Once when derived from relativistic calculations, they include relativistic effects. Such potentials are called Relativistic Effective Core Potentials, or simply, RECPs. There has been many RECPs available for the calculation of Au clusters, some of them are:

1. Los Alamos 11 electron ECPs [24], 19 electron ECPs [25], designated as Lanl1DZ and Lanl2DZ.

2. 19 electron Steven-Basch-Krauss ECP[26], derived from Dirac-Fock Theory.

3. 19 electron Stuttgart-Dresden ECPs and RECPs[27] designated as SDD. These energy-consistent ECPs/RECPs are constructed to reproduce experimental observables of a single-atom, like ionization potentials and excitation energies, without/with relativistic Dirac-Fock Theory, etc.

In this entire work, SDD ECPs and RECPs have been used to incorporate and compare relativistic effects of gold in the calculations included in deMon 2K.

deMon[28] (<u>de</u>nsity of <u>Mon</u>treal) is a code for density functional theory (DFT) calculations. It uses the Linear Combination of Gaussian Type Orbitals (LCGTO) approach for the self consistent solution of the Kohn-Sham (KS) DFT equations. Some of the features of deMon package are:

1. Geometry Optimization and Transition State Search.

2. Molecular Dynamic Simulations (MD).

3. Calculation of properties like polarizabilities, hyperpolarizabilities, NMR, IR and Raman spectra intensities, population analysis (Mulliken, Lowdin, Bader), etc.

4. Parallelized code (MPI).

5. Interfaces for Visualization Software (Molden, Molekel).

6. Portability to Unix and Linux computer platforms.

Computational methods for analysis of structures of gold clusters have undergone a rapid progress in the recent past[30–32]. Since the discovery that small gold clusters can selectively catalyze reactions, there has been a great interest from both experimentalists and theoreticians in understanding the origin of catalytic behavior and correlation with electronic structure. Combined with new and

better computational technologies, most importantly the development of parallel hardware and software, provides exciting new opportunities to investigate quantitatively bonding, structure and reactivity of gold clusters from the entire size and shapes. Since geometrical structures and electronic structures are related to each other in an intertwined fashion, understanding of structural transition from planar Au_n to non-planar structure at particular size has been a debated issue for quite some time[29]. In the present work we have deeply focused on this aspect of structural transition from planar to non-planar structures of Au_n with rigorous computation using Density Functional Theory.

Density Functional Theory has to be combined with approximate exchange correlation (XC) functionals [33] in order to calculate various properties of molecules. Without the advent of various functionals DFT it would have remained mere a semiemperical theory. Despite these limitations, various XC functionals are widely used for modeling of various systems. Formerly XC functionals relied upon the homogeneous electron density, and were solely based upon Local Density Approximation (LDA). Later on XC functionals included energy dependence on the gradient of density, Generalized Gradient Approximations, GGA. Further developments on kinetic energy density dependent functionals, which are known as meta-Generalized Gradient Approximations, meta-GGA. This motivated immense efforts in testing of various XC functionals within the framework of DFT for Au clusters of various size and shapes and for various properties, viz. energetics, reactivity, IR frequencies, density of states (DOS) and potential energy surfaces

(PES).

Because the size, shape, thermal states and electronic structure of gold nanoparticles play immense role in determining the chemical reactivity, appreciable effort has been devoted to correlate between the structural properties and dynamics. The reign of traditional molecular dynamics and electronic structure methods was greatly extended by the family of techniques that is called here "*ab initio* molecular dynamics". Other names that are currently in use are for instance Car Parrinello, first principles, Born-Oppenheimer, quantum chemical, etc. molecular dynamics. The basic idea underlying every *ab initio* molecular dynamics method is to compute the forces acting on the nuclei from electronic structure calculations that are performed "on-the-fly" as the molecular dynamics trajectory is generated[35].

Along with an increase in the temperature there is a corresponding change in the shape of the cluster. Following this, the type and number of surface reactive sites available for a reacting molecule, (in other words, the cluster's functional catalytic activity) is modified. Hence, stability of a given geometry or an understanding of different isomers co-existing for a cluster at its working temperature is quite important. This is not very well understood and hence a limitation in their practical applications. This motivated us to carry out density functional based Born-Oppenheimer molecular dynamics (BOMD) for Au clusters of various size in a wide range of temperature.

The thesis gives a step by step approach for the study of theoretical presentation

of quantum chemistry that brings together Density Functional Theory focusing on relativistic effects in gold, structures, chemical reactivity and molecular dynamics simulations. The essence of relativistic effects in density functional theory of reactivity and molecular dynamics has been emphasized in the thesis. The thesis covers with an extensive and critical literature survey on the current status in the chemistry of gold and overall presentation of computational chemistry approaches towards detailed understanding of relativistic effects in gold, chemical reactivity and molecular dynamics. The formal steps of chemical reactivity are systematically computed from structures, IR spectra, *Fukui functions* or *frontier functions*, global hardness parameter, Born-Oppenheimer Molecular Dynamics in a wide range of temperature.

CHAPTER 1: INTRODUCTION

This introductory chapter presents a brief overview of various aspects of historical and present status of rich chemistry of gold. The peculiarities of gold chemistry when the metal is in the nanosize regime are presented. Fascinating in its properties, the chemistry of gold, emphasizing on the relativistic effects on structure and chemical trends, etc. is described in here. In consequent sections, we will focus on the factors pertaining to the bonding in gold clusters which leads to the formation of gold nanowires, clusters in shape of flat cages and closed spherical structures. Followed will be highlighted the recent trends in experimental and theoretical chemistry of gold. The planar to non-planar conversion of gold clusters and shape sensitivity, depending upon their thermal states and its implications to catalysis will be highlighted furthur. A brief overview on the motivation behind the research work has been discussed at the end of the chapter.

CHAPTER 2: THEORETICAL BACKGROUND

This chapter describes the various methods of many-body quantum chemical calculations adopted for computation of properties of gold clusters herein presented in the thesis. A brief discussion on Hartree, Hartree-Fock approximation and post-hartree fock approach emphasizing on Density Functional Theory will be highlighted. Calculation of density functional based reactivity descriptors, atom condensed *Fukui functions* will be discussed in details. The essence of relativistic effects in Density Functional Theory of reactivity descriptors, vibrational spectra

and global hardness parameters will be overviewed. The incorporation of relativistic effect using SDD-RECP in density functional theory code deMon2K which has been used throughout is discussed in brief. In subsequent sections we will highlight various aspects and plausible methods of Born-Oppenheimer molecular dynamics simulations. The analysis of generated trajectory with Mean Squared Displacements (MSD), Root Mean Squared Bond Length Fluctuations (RMS-BLF, δ_{rms}) and heat capacities will be explained in detail to describe the "phase transitions", "structural fluctionalities" and stabilities of Au clusters.

CHAPTER 3: RELATIVISTIC EFFECT ON Au CLUSTERS: STRUCTURE AND PROPERTIES

This chapter describes the influence of relativistic effects on the structure, vibrational modes, and reactivity of tetrahedral gold clusters (Au_{19} and Au_{20}). The properties are investigated using density functional methods. The intramolecular reactivity of the clusters was analyzed using density functional-based reactivity descriptors. We present in this work that that whereas the structural properties and vibrational modes are considerably affected by the relativistic effects, the reactivity trends based on Fukui function calculation on various atoms within this cluster remain unaffected by the absence or presence of relativistic effects. The work demonstrates the importance of relativistic effects in gold and without incorporation of the same, the calculated properties show large deviation from the experimental results.

CHAPTER 4: STRUCTURE, BONDING AND REACTIVITY OF SMALL Au CLUSTERS

This chapter deals with the details of Density Functional Theory based calculations, incorporating the relativistic corrections for 6-13 atom small gold clusters. Along with various details, that atoms in a ground state conformation have been classified into distinct types of reactive sites in a given geometry. Based on symmetry, susceptibility of various types of reactive sites in the ground state geometry toward an impending electrophilic and/or a nucleophilic attack has also been highlighted using DFT based reactivity descriptors. The studies have also been extended to high energy isomers in these cluster sizes. The reactivity of various sites as a function of cluster size and shape is thus analyzed. The descriptive details of general rule the size and shape of the cluster influencing the number and position of available sites for an electrophilic and/or nucleophilic attack has been described in critical manner. The occurrence of planar to non-planar transition as a function of the cluster is discussed in detail. We propose the term "amphiphilicity" in context of reactive sites based on values of relative electrophilicity and nucleophilicity.

CHAPTER 5: SENSITIVITY OF EXCHANGE-CORRELATION FUNCTIONALS ON STRUCTURE AND REACTIVITY OF Au CLUSTERS

This chapter deals with employment of Density Functional Methods to study the

sensitivity of exchange-correlation (XC) functionals of DFT towards various properties of small Au clusters. Results for geometry optimizations, IR frequencies, charge distribution across various reactive atom sites, local reactivity descriptors, density of states have been evaluated. Potential energy surface has also been presented with PBE96-PBE XC-functionals. We report the trends of the mentioned properties with GGA, meta-GGA and LDA XC functionals. Exploration of XC-functional dependence on Density Functional Theory for computing the properties of Au clusters is highlighted in this chapter.

CHAPTER 6: FINITE TEMPERATURE BEHAVIOR OF SMALL Au CLUSTERS

The present chapter describes the Density Functional based molecular dynamical simulations for Au_3-Au_{10} atom clusters with relativistic correction, with an aim of understanding their finite temperature behavior. A detailed analysis of conformations of a cluster coexisting at different temperatures is presented. Based on Born-Oppenheimer Molecular dynamics simulations, we present here the various phase transitions, melting and "structural fluctionality" of Au clusters highlighting the unique temperature behavior of the gold clusters of different sizes. The analysis of the trajectory is critically done with traditional parameters like Mean Squared Displacements (MSD), Root Mean Squared Bond Length Fluctuations (RMS-BLF, δ_{rms}) and heat capacities. We propose the existence of "planar-liquid" like region for Au clusters across the studied wide range of temperature.

CHAPTER 7: MOLECULAR DYNAMICS STUDY OF ICOSAHEDRAL Au_{32} CLUSTER

This chapter deals with the molecular dynamics study of fullerene or cage-like structure of Au_{32} cluster. Au_{32} has the same symmetry, namely, I_h group, as that of C_{60}. The fascinating "hollow cage" like structure of the cluster is discussed. This leads to the platform for evaluation of method for properties of large clusters with density functional based molecular dynamics approach. The summary of the present thesis and future goals are also presented in this chapter.

Bibliography

[1] Parr, R. G.; Yang, W. *Density-Functional Theory of Atoms and Molecules*; Oxford University Press: Oxford, 1989.

[2] Koch, W.; Holthausen, M. C. *A Chemist's Guide to Density Functional Theory*; Wiley-VCH: Weinheim, 2000.

[3] Geerlings, De Proft, P. F.; Langenaeker, W. *Chem. Rev.* **2003**, *103*, 1793.

[4] Slater, J. C. *Phys. Rev.* **1951**, *81*, 385.

[5] Hohenberg, P.; Kohn, W. *Phys. Rev. B*, **1964**, *136*, 864.

[6] Pal S.; Roy, R.; Chandra, A. K. *J. Phys. Chem.* **1994**, *98*, 2314.

[7] Roy, R.; Chandra, A. K.; Pal, S; *J. Phys. Chem.* **1994**, *98*, 10447.

[8] Roy, R. K.; Pal, S.; *J. Phys. Chem.* **1995 99**, 17822.

[9] Roy, R. K., Krishnamurti, S.; Geerlings, P.; Pal, S., *J. Phys. Chem. A* **1998** *102*, 3746.

[10] Deka, R.; Vetrivel, R.; Pal, S. *J. Phys. Chem. A* **1999**, *103*, 5978.

[11] Krishnamurti, S.; Pal, S. *J. Phys. Chem. A* **2000**, *104*, 7639.

[12] Krishnamurti, S.; Roy, R. K.; Vitrivel, R.; Iwata, S.; Pal, S. *J. Phys. Chem. A* **1997**, *101*, 7253.

[13] Pal, S.; Chandrakumar, K. R. S. *J. Am. Chem. Soc.* **2000**, *122*, 4145.

[14] Roy, R. K.; Hirao, K.; Pal, S. *J. Chem. Phys.* **2000**, *113*, 1372.

[15] Chandrakumar, K. R. S.; Pal, S. *J. Phys. Chem. A* **2002**, *106*, 5737.

[16] Chandrakumar, K. R. S.; Pal, S. *J. Phys. Chem. A* **2002**, *106*, 11775.

[17] Fischer, G.;Goursot A.; Coq, B.; Delahay, G.; Pal, S. *ChemPhysChem* **2006**, *7*, 1795.

[18] Krishnamurty, S; Shafai, G. S.; Kanhere, D. G.; Soule de Bas, B.; Ford, M. J. *J. Phys. Chem. A* **2007**, *111*, 10769.

[19] Jansen, M.; Mudring, A. V. *Gold. Progress in Chemistry, Biochemistry and Technology (Ed.: H. Schmidbaur)*, Wiley, New York, 1999.

[20] Rose, S. J.; Grant, I. P.; Pyper, N. C. *J. Phys. B* **1978**, *11*, 1171.

[21] Kaldor, U.; Hess, B. A. *Chem. Phys. Lett.* **1994**, *230*, 1.

[22] Schwerdtfeger, P.; Brown, J. R.; Laerdahl, J. K.; Stoll, H. *J. Chem. Phys.* **2000**, *113*, 7110.

[23] Lee, H. -S.; Han, Y. -K.; Kim, M. C.; Bae, C.; Lee, Y. S. *Chem. Phys. Lett.* **1998**, *293*, 97.

[24] Hay, P. J.;Wadt, W. R. *J. Chem. Phys.* **1985**, *82*, 270.

[25] Hay, P. J.;Wadt, W. R. *J. Chem. Phys.* **1985**, *82*, 299.

[26] Stevens, W. J.; Krauss, M.; Basch, H.; Jasien, P. G. *Can. J. Chem.*, **1992**, *70*, 612.

[27] Schwerdtfeger, P.; Dolg, M.; Schwarz, W. H. E.; Bowmaker, G. A.; Boyd, P. D. W. *J. Chem. Phys.*, **1989**, *91*, 1762.

[28] *deMon2k*, Koster, A.M.; Geudtner, G.; Calaminici, P.; Casida, M. E.; Dominguez, V. D.; Flores-Moreno, R.; Goursot, A.; Heine, T.; Ipatov, A.; Janetzko, F.; del Campo, J. M.; Reveles, J. U.; Vela, A.; Zuniga B.; Salahub, D. R. The deMon Developers, CINVESTAV, Mexico (2011).

[29] Olson, R. M.; Varganov, S.; Gordon, M. S.; Metiu, H.; Chretien, S.; Piecuch, P.; Kowalski, K.; Kucharski, S. A.; Musial. M. *J. Am. Chem. Soc. 2005*, *127*, 1049

[30] Balasubramanian, K.; Liao, D.-W. *J. Chem. Phys.*, **1991**, *94*, 5233.

[31] Liao, D.-W.; Balasubramanian, K. *J. Chem. Phys.*, **1992**, *97*, 2548.

[32] Arratia-Perez, R.; Hernandez-Acevedo, L. *THEOCHEM*, **1993**, *282*, 131.

[33] Geerlings, P.; De Proft, F.; Langenaeker, W. *Chem. Rev. (Washington, D.C.)* **2003**, *103*, 1793.

[34] Zhao, Y; Truhlar, D. G. *Acc. Chem. Res.*, **2008**, *41*, 157.

[35] Marx, D.; Hutter J. *Ab initio molecular dynamics: Theory and Implementation, Modern Methods and Algorithms of Quantum Chemistry*, John von Neumann Institute for Computing, Julich, 2000.

Acknowledgements

No words of gratitude are enough to express my thoughts and feelings for my research advisor Prof. Dr. Sourav Pal for being always enthusiastic and showing a great interest in my work and molding me into the person I am today. My heartfelt thanks for accepting me as your student and caring me always, specially in crucial moments of crisis and those times when things didn't look moving. Thank you for supporting me in these immensely vital days of my career and life. Thank you very much for nurturing my thoughts which eventually has led me to this thesis and guidance for a lifetime. His expertise and research insight have provided me an excellent basis for the present thesis and paved a path for my future career, without which I would have been knocked down certainly.

Special thanks to Dr. Sailaja Krishnamurthy for her time to time help in my thesis, writing the papers. I am grateful to her for introducing me to the novel gold nanoclusters and also for your extreme patience with me. I appreciate all her contributions of time to make my Ph. D. experience productive and stimulating. I am grateful to Dr. Nayana Vaval for helping me with the day to day problems in the lab, the issues related to high-performance computing, scrutinizing the thesis in the last hours and constant encouragement throughout these years, which paved the path for my work and eventually led me to this thesis. I am also thankful for the excellent example she has provided as a successful woman physicist and scientist. I am thankful to Dr. Rahul Kar, Dr. Arijit Bag and Subrata

Adhish Jaiswal, friends from other groups in NCL, Debashis, Sujit, Arpan, Binoy, Joyashis, Animesh, Prithviraj, and many others making my life comfortable outside lab schedules. Also acknowledged the staffs of Physical Chemistry Division, Mr. Dipak D. Jori, Mr. Punekar and Mr. Ganguly of Center for Materials Characterization for their timely help in official matters. I also appreciate for the time I spent with my friends and mess-staffs at Golden Jubilee Hostel and their help at needy moments.

I am also thankful to Dr. S. Sivaram, Former Director, NCL for allowing me to initiate the research work in his institute and CSIR (New Delhi) for the Junior and Senior Research Fellowship. I also acknowledge NCL for the financial support to participate in the conference of "Modeling Chemical and Biological Reactivity (MCBR-II)" held in Kreuth, Germany in 2009.

My final words of thanks and gratitude goes to my parents who have supported and encouraged me all these years and for my loving and supportive Arti, who never let me down.

Himadri Sekhar De

Pune.

Contents

List of Figures

List of Tables

Abbreviations

AE	All Electron
AO	Atomic orbital
BSSE	Basis set Superposition Error
BOMD	Born Oppenheimer Molecular Dynamics
BSSE	Basis set superposition error
CC	Coupled Cluster Approximation
CCSD	Coupled Cluster Approximation with Singles Doubles
CCSD(T)	Coupled cluster approximation with singles doubles including Perturbative triples correction
CI	Configuration interaction
CP	Car Parinello
DF	Dirac Fock
DFT	Density Functional Theory
DK	Douglas Kroll Approximation
EA	Electron Affinity
ECP	Effective Core Potential
FMO	Frontier Molecular Orbital
PES	Potential Energy Surface
GGA	Generalized Gradient Approximation
GTO	Gaussian Type orbitals
HF	Hartree-Fock
IP	Ionization Potential

LDA	Local Density Approximation
MD	Molecular Dynamics
MBPT	Many body Perturbation Theory
MO	Molecular orbital
MPn	nth order M⊘ller Plesset
PP	Pseudopotential
SO	Spin orbit coupling
SR	Scalar Relativistic
STO	Slater typer orbitals
TD-DFT	Time Dependant DFT
WFT	Wave function theory
XC	exchange corrlelation
ZORA	Zeroth order regular approximation

Physical Constants

Speed of Light	c	$=$	$2.997\ 924\ 58 \times 10^8$ ms^{-1}
Electron volt	eV	$=$	$1.602\ 176\ 46 \times 10^{-19}$ joules
Calorie	cal	$=$	$4.184\ 00$ joules
Pi	π	$=$	$3.141\ 592\ 65$

Dedicated To my Late Father

"If God created the world, his primary concern was certainly not to make its understanding easy for us."

-Albert Einstein

Chapter 1

Introduction

The present decade has witnessed the "capabilities" and "personalities" of gold in the form of not only an essential component of electronic devices but nanoclusters and nanowires. Although, gold has been thought to as a yellow noble metal, it has been discovered to have a rich chemistry. Not only in organometallics, but aided by powerful computers and advanced computational codes, it has been possible to enumerate various properties of metals like gold which have been considered as 'noble' or 'inert' for centuries. It is possible now to calculate these properties by applying the principles of quantum mechanics. It is a challenge knocking at the doorstep to simulate the chemical composition of the material which are yet to be generated and still have no existence.

The simulation by the application of quantum mechanics would not have been possible for large number of atoms without a way of simplifying the problem, especially without the help of Density Functional Theory computations. The thesis begins with a theoretical presentation of quantum chemistry that brings together Density Functional Theory focusing on relativistic effects in gold, chemical reactivity and molecular dynamics simulations. The essence of relativistic effects in density functional theory of reactivity and molecular dynamics has been emphasized in the thesis. The thesis covers with an extensive and critical literature

survey on the current status in the chemistry of gold and overall presentation of computational chemistry approaches towards detailed understanding of relativistic effects in gold, chemical reactivity and molecular dynamics. The formal steps of chemical reactivity are systematically computed from structures, *Fukui functions* or *frontier functions*, global hardness parameter, Born-Oppenheimer Molecular Dynamics in a wide range of temperature.

1.1 Chemistry of Gold

Gold has been an icon of wealth, culture and prosperity for millenia throughout the history of mankind. 'Carat' is the conventional measure of gold content and purity in alloys of gold coins, jewelery, artifacts of almost all the present and past cultures of the world, in dentistry and engineering.

The yellow color and metallic lustre of gold have fascinated mankind ever since the metal was discovered. Initially just as a discovery and later on as a result of methodic and rigorous academic research, the last two decades have witnessed the smaller counterparts of bulk gold as "clusters in chemical compounds" at the molecular level[18]. The chemistry of gold is fascinating because of the "personalities" and "peculiarities" of its characteristics and anomalies in behavior at atomic scale when compared to bulk. The gas phase chemistry of gold is surprisingly different as compared to the bulk. Thought to be "noble" for centuries, gold forms compound with sufficient number of organic groups like cyanides, phosphanes, thiolates, halides, etc. Gold cations have been found to form stable compounds with "noble" gases like xenon. Because of its wide applicability in the fields of material science, homo and heterogeneous catalysis, biochemistry and medical applications, chemistry of gold cluster has emerged as one of the most fast spreading and competitive fields of research in chemistry in the last two decades.

1.1.1　Oxidation states

The most common oxidation states of gold are +I and +III. +V state is rare and found in fluoro gold compounds. Local coordination in these are linear, quadratic planar and octahedral respectively. Due to the presence of relativistic effect in gold and expansion of 5d shells which in turn favors higher oxidation states for Au as compared to Ag, where only +I oxidation state is prevalent. An explicit discussion on effect of relativity in change of oxidation states of Au from +I to +III or +III to +V in halides is demonstrated by Schwerdtfeger et *al.*[1]. Au^0, is found in Au_n compounds.

1.1.2　Gold Complexes

1.1.2.1　Gold with water

No Au^I(aq.) or Au^{III}(aq.) has been known so far. However, the existence of $[Au(H_2O)_n]^+$; n≤10 in gas phase has been reported by Poisson et *al.*[2] More than two closely coordinated water molecules has been found, although the larger part of the hydration sphere encompasses other water molecules instead of gold as central atom.

1.1.2.2　Multiple bonds with Au

Gold is known to form multiple bonds with carbenes. $[Au=CH_2]^+$ double bonded to Au has one σ and one π bond. Au=C bond energy has been calculated to be 393 kJ mol^{-1}[3]. Experimental limit of dissociation energy has been confirmed in a later study by Aguirre et *al.*[4] and was found to be 372 kJ mol^{-1}. Multiple bonded species like $[Au\equiv C]^+$ also exist and the nature of bonding are found to be partially resembling to triple bond. Au 5dπ should delocalize to the empty 2pπ orbitals of the carbon[5]. $[Au\equiv N]^+$ also exist but have bond order slightly less

than three. The two further electrons after $[Au\equiv C]^+$ goes to the antibonding π^* orbital and thereby reducing the bond order further down from three. The gas phase $[Au\equiv N]^{2+}$ ion has a bond length of 180 pm as similar to that of $[Au\equiv C]^+$[6].

1.1.2.3 Gold with rare gases

Ab initio calculations have explicitly produced strong, covalent nature of bonding between Au and rare gases, viz., Xe. The $5p\sigma$ orbitals of Xe in $[XeAuXe]^+$ were found to donate charges to empty 6s orbitals of Au^+[7]. These were one of the first chemical bonds between Au and rare gases. The compound $[AuXe_4]^{2+}[Sb_2F_{11}]_2^-$ was synthesized containing Au^{II} cation $[AuXe_4]^{2+}$. The salt of the complex was formed from Au^{2+} dissolved in HF/SbF_5 in an atmosphere of Xenon[8]. The salt was also found to be stable under larger pressure of Xenon till upto room temperature. Spectroscopically well characterized entities include [ArAuCl], [KrAuCl], [ArAuF], [ArAuBr] etc. Ab initio calculations show that the nature of the bond between Au with the rare gas is mostly weakly covalent in nature[9–11].

1.1.3 Aurophilicity

An attraction between two or more monovalent Au^I ions in compounds is known as aurophilicity. This "aurophilic" or generally "metallophilic" attraction leads to the formation of dimers, oligomers, infinite chains or infinite two-dimensional sheets. The term aurophilicity was coined by Schmidbaur for the phenomenon[12]. The typical Au-Au bond distances in literature is found in the order of 300 pm. Temperature dependent NMR spectroscopy revealed that the interaction energy per pair of Au is in the range of 29-46 kJ mol^{-1}[13, 14]. This attraction is attributed to the hybridization between the filled $5d^{10}$ orbitals and empty 6s and 6p orbitals of Au. Also it was rigorously calculated that if the Au 6p functions are omitted from basis, more than half of the aurophilic attraction was omitted. If

the Au 5d orbitals were removed from the basis, the aurophilic attraction disappears completely[15, 16]. It was realized at a later stage that not only the 6s and 5d orbitals are of sole importance but basis set superposition error (BSSE) was also taken into account as it was considered of substantial importance along with the "counterpoise correction"[17]. Furthermore two f functions were considered mandatory for proper description of the aurophilicity.

1.1.4 Gold Halides

Experimental generation of AuF by Schwarz et *al.* has been a breakthrough in the field of metal halides [19]. Based on advanced electronic structure calculations, the AuF is supposed to undergo disproportionation to $Au^0(s)$ and $Au^{III}F_3(s)$[20] in the gas phase. This particular discovery was well established by means of various experimental evidences like emission and microwave spectra of AuF[21, 22]. These methods established the various aspects of the structural parameters of AuF, viz., equilibrium bond distance of sole Au-F, bond dissociation energies (BDE) of neutral AuF, etc., which were in well agreement with the electronic structure calculations of gas phase AuF molecule[23, 24]. Electronic structure theory calculations reveal that the nonrelativistic vs. relativistic stabilization to the bond energy of AuF is one of the largest for any diatomic molecule.

Heavier diatomic halides are also mentioned in the literature with their thermochemical properties derived from combined experimental and theoretical approach[25]. Of particular interest was the comparison between bond dissociation energies of light and heavy gold halides Au-F and Au-I at 0 K. This has led to conclusion that bonding in Au^I and Au^II with halides, viz., Au-F which has a dissociation energy of 18 kcal mol^{-1}[26, 27] represents one of the weakest metal-fluoride bond in the chemistry of halides. It also resembles the ionized alkali-halides in terms of bond dissociation energies. This also reveals that for the sake of covalent binding of the Au^+ with X· involves excitation of $5d^{10}6s^0$ to $5d^9 6s^1$ state, resulting in unfavorable

triplet Au^{II} state. Contrarily, the Au^+-X bond is better described as ion-dipole complex of Au^I cation with a X· free radical.

AuCl has been considered a classical case for studying relativistic shortening of bond length and weakening of bond in literature. While the contraction of bond is observed, there occurs the relativistic enhancement of the ionization potential (IP) of Au. As a consequence, the partial donation of bond from Au atom to the ligand takes place, which consequently decreases the dissociation limit, D_e, of the molecule[105]. The molecule as solid has a chain-like structure. The structure is well studied in literature[28]. The cubic and chain-like structures are also close in terms of energy to the linear structure. The preferential existence of the linear structure is attributed mostly to relativistic effects in gold[29]. $AuCl_3(s)$ exist as a planar dimer in the form of $[Au_2Cl_6]$. Structural elucidation with electron diffraction agrees well with the *ab initio* calculations. An augmented, correlation consistent triple-zeta basis was used for the agreement at MP2 level[30].

Stability of Au iodides also has been well studied by Söhnel et *al.* in the gas as well as solid phase. The chemistry of ions $[AuI_2]^-$ and $[AuI_4]^-$ are well known in literature[31]. AuI in its solid state has zig-zag chain-like structure. The non-existent $[Au_2I_6]$ was predicted to be stable[30].

The classic example of $[AuF_n]^-$ has been studied extensively. The vibrational frequencies of $[AuF_n]^-$, n=2, 4, 6 have been compared rigorously with the experiments[32, 33].

1.1.5 Aurides

Gold has been reported to act as a pseudohalogen and form aurides very similar to halides. One of the oldest reported aurides is cesium auride[34] in the year 1943 by Sommer et *al.*. Na alloys with gold dissolve to some extent in molten NaBr [35]. The deep blue adduct Cs·$AuNH_3$ has been studied experimentally as well

TABLE 1.1: Available ab initio on solids or molecular aurides. The table is
taken from the reference of Pyykkö[42]

Authors	System	Comments
Solids		
Wood and Reitz	CsAu	Band structure by using QDM; ionic.
Liu and Amar	CsAu	Band structure by using QDM KKR.
Norris	RbAu, CsAu	Exp. photoelectron spectra.
Hasegawa	CsAu	R semiconductor, NR metal.
Overhof et *al.*	RbAu, CsAu.	Photoelectron spectra.
Christensen	CsAu	R/NR.
Robertson	CsAu	Tigh-binding, Can F centers exist?
Wertheim et *al.*	CsAu	Charge transfer.
Watson	CsAu	R/NR.
Grosch	MAu,	M=alkali
Grosch	MAu5,	M=alkali
Mudring	$Rb_5Au_3O_2$	Contains both Au^{-I} and Au^I.
Mudring	$CsAuNH^3$	Bonding analysis.
Molecules		
Saue	[CsAu]	DF/HF.
Gagliardi	[MAu4], M=Ti-Hf,	
		Th, U
Fossgaard et *al.*	[CsM]; M=Cu-Au	D_e revised to 2.53 eV.
	CsAu	

as theoretically by Mudring et *al.*[36]. The experimental studies on aurides have
been explicitly reviewed by Pyykkö[42].

Band structure calculations of CsAu also exist in literature. Comparison between
relativistic and nonrelativistic calculations have revealed that without considera-
tion of relativity the system would behave like a metal instead of semiconductor[37].

Aurides with group 3 metals like [AuLa] and [AuLu] are also known to exist.
It has been explicitly observed that among the gaseous diatomic intermetallic
group-11 compounds those containing gold have the highest dissociation energy.
Except for the compounds, AuCu, AuAg and Au_2, corresponding copper or silver
intermetallic compounds are always less stable than the gold compounds[38]. Also

for the intermetallic compounds [AuCu] and [AuAg], the bond lengths are the mean of their pure dimers[39].

A particular "peculiarity" of gold is the formation of multiple Au^I cations, often undergo aggregation, and Au-Au binding energies are found to be comparable as that of strong hydrogen bonds although both atoms bear unipositive charges. Apart from possessing a stable closed-shell cation, gold forms another entirely new class of auride, Au^{-I} compounds, which have a comparable electron affinity as that of iodine. Much of these properties of gold has been explained to be the outcome of relativistic effects on valence orbitals of gold [40].

1.2   Gold hydrides

Another "fascinating" class of compounds are the gold hydrides. Gold hydrides are stable molecules and have been characterized well by electronic band spectroscopy in gas phase, although no solid gold hydrides are found stable. The monohydride, [AuH], is well characterized in the gas phase, however, the higher gold hydride molecules [AuH$_3$], possesses a [(H$_2$)AuH] structure and have been elucidated as well. Quantum chemical calculations reveal that [AuH$_3$] is a planar "Y" shaped molecule and, is the stable equilibrium structure. Higher complexes [AuH$_5$], having a [(H$_2$)AuH$_3$] structure has been observed by Andrews et *al.*[43].

In relativistic pseudo potential calculations on diatomic gold hydride it was noticed that Mulliken populations were almost equal ($Au^{0.02}H^{-0.02}$). Nonrelativistic calculations, by contrast, led to erroneous predictions and to differences in excitation energies[44]. Further investigations show that the dipole moment of AuH to be 1.08 D at the GGA level and 1.017 D at CCSD level[45, 46].

1.3 Medical Applications of Gold

Medical application of gold is quite primitive and can be traced back to 4, 500 years old[69]. Since the element was available in its pure form, metallic gold was considered to be a cure-all medicine till eighth century. Auric chloride was a medicine for treatment of leprosy in thirteenth century and till nineteenth century gold compounds were most effective for cure of many diseases. In late nineteenth century, the effect of AuCN on bacterial growth was the milestone for gold pharmacology and beginning of an attempt to design Au drugs. Early twentieth century, gold was popularly used for treatment of tuberculosis. This period was named as "gold decade"[70]. Common Biological applications of gold include:

- chemotherapy, where Au^I thiomalate and thioglucose are used for treatment of rheumatoid arthritis, $[Au^V(5\text{-diazouracil})_2Cl_2]Cl$ used for treatment of tumor.
- Labelling, where the heavy atom is used for labelling macromolecules and whole cells for viewing electron-microscopy and X-ray crystallography.
- Gold nanospheres/colloidal gold, for plausible treatment of cancer
- Obesity, where Au^I thioglucose is found to induce obesity in mice.
- Destruction of tissue, by means of radioactive and colloidal ^{198}Au.

Au^I compounds were found to have severe toxic effects on human body, viz., the cyanide of Au^I species. But soon the cyanide was replaced by thiol and substituted thiols and gave positive results[71]. Aurous compounds are still effective in medical treatment as any other available drug for many complicated cases[72] like chemotherapy.

Colloidal gold had been quite popular for medicinal purposes too. Since they can be identified by electron microscopy, they can be successfully used for labelling purposes[73].The surfaces of colloidal Au can bear charge by absorption of ions[74].

Also, the antibodies are found to favorably bind with the the colloidal gold. Colloidal radioactive ^{198}Au has been used for destruction of unwanted tissues, e.g., in radiosynovectomy.

The injection of aurothioglucose in mice causes obesity[75]. There it is observed a fast deposition of tissue lipid and increase in body weight upto 33% and reveals that glucose ligand in Au to permeate the macromolecules of living tissue.

Biomedical application of Au in fighting cancer has been a much discussed research area for last two decades. Gold nanoparticles have been explored and investigated in broad areas of medical research involving cancer therapy and drug delivery. Most studies on cancer therapy of gold involves induced thermal therapy by irradiation of pulsed laser on gold nanoparticles, nanorods and nanocages for destruction of cancer cells and tumor tissues[76–78].

1.4 Gold Clusters

Last two decades have witnessed the smaller counterparts of bulk gold as "clusters in chemical compounds" which has sparked a flurry of research in recent times. The chemistry of clusters become surprisingly different from their bulk counterpart. Clusters are aggregates of atoms or molecules, intermediate in size between individual atom and bulk. The distinction between molecules and clusters is that molecules are stable under certain conditions, whereas clusters are synthesized in laboratory and are metastable in nature. Molecules have definite stoichiometry whereas clusters' constitutions are variable and largely dependent upon the method of synthesis. So all molecules can be called as clusters, but very few clusters can be identified as molecule[47], like C_{60}[55], which has been explained a little later in this section. Clusters of nonmagnetic elements viz., Pd, Rh and Ru are found to be magnetic[48]. Semiconducting materials and metals loose their bulk properties[49], color of the particles at cluster size becomes different to their

bulk[50], noble metals turn out to be reactive, viz., Au[51]. These fascinating features arise because of high gap between the Highest Occupied Molecular Orbitals (HOMO) and the Lowest Unoccupied Molecular Orbitals (LUMO) when explained in terms of electronic structure. As a result of these differences, gold clusters show large number of important electronic, optical, chemical and catalytic properties which has led to an exponential growth in volume of experimental and theoretical research.

A large amount of data exists in literature on pure gas phase Au clusters and wires. A systematic study on gas phase positively charged Au_n clusters was performed by Glib et *al.* with n=4, 13, which have been supported by ion mobility experiments[52]. These structural isomers were generated from *ab initio* molecular dynamics simulation by "simulated annealing" technique and from various other structures already reported in the literature for neutral and charged species. Followed to that the structures were optimized using Density functional based methods with relativistic pseudopotentials. The lowest energy structures were further analyzed for their cross-sections and matched against the experimental results of ion-mobility experiments.

Experimentally and computationally, $[Au_n]^-$ are considered to be planar till n≤11. For n=12, both planar and nonplanar isomers have been observed in close proximity with respect to the electronic energy, whereas, for n=13, has been experimentally understood to be nonplanar[53].

Based on the collision cross section of ion mobility experiments the cations of $[Au_n]^-$ are understood to be planar till n≤7[52]. For n=8-10, 3D structures were found to exist. As far as neutral clusters are concerned, planar trigonal raft structures are favored to be the minimum energy till n=7. For the open shell Au_3 cluster, where spin-orbit coupling is found to be dominant to Jahn-Teller distortion, the cluster takes the shape of an equilateral triangle[54]. Neutral and anionic
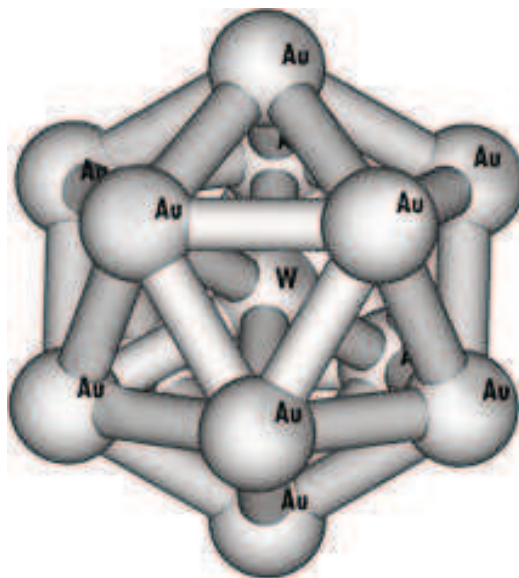
FIGURE 1.1:   The calculated structure of [WAu$_{12}$] molecule. The figure
is taken from article of Pyykkö and Runeberg[66].

tetrahedral Au$_{20}$, a fragment of fcc bulk gold, has an experimental electron affinity of 2.745 eV and a large HOMO-LUMO gap of 1.77 eV, which is reported to be the largest when compared to the coinage metal cluster and is 0.2 eV higher than the gap in C$_{60}$ cluster, i.e., buckminsterfullerene[55].

As an example of electron counts for clusters, molecules like [WAu$_{12}$] in figure 1.1, eight a$_g$ + t$_{1u}$ electrons and ten h$_g$ electrons of the central atom are accounted for the participation in bonding. The a$_g$, t$_{1u}$ and h$_g$ MOs bond to the 6s, 6p and 5d orbitals respectively, of the central atom. h$_g$ is considered the HOMO of [WAu$_{12}$]. So these systems are supposed to be stable because eighteen electron rule holds good, aurophilicity and presence of strong relativistic effects in Au.

The molecules [WAu$_{12}$] and [MoAu$_{12}$] were produced experimentally by evaporating W/Mo in a helium atmosphere and their structures were determined experimentally and theoretically as well, to be icosahedral, I_h[67].

Transition metal clusters, including gold, have multiple structures separated by small energy differences. The barriers between these structures are also found to

be considerably low. The particular phenomenon for existence of such alternative structures in metal clusters is known as "fluxionality"[68].

1.5   Molecular Dynamics

Classical molecular dynamics (MD) studies on melting of large sized gold clusters upto 459 atoms reveals the existence of icosahedral structures. Although the atomicity of these clusters in this study seems to be large, there exist numerous number of structurally well characterized heteronuclear gold metal cluster compounds, viz., Na_xAu and Cs_xAu[65]. Further work by Cleveland et *al.*[56] revealed the thermal evolution of gold clusters from the low-temperature optimal structures to icosahedral structures. The melting of gold nanoclusters has been further studied and was found that the melting process has three characteristic time periods for the intermediate sized nanoclusters. The whole process includes disordering and reordering, followed by surface melting and then overall melting[57]. The surface melting of Mackay icosahedral gold clusters was also investigated. It was found that the facets on the cluster surface soften but do not pre-melt below the bulk melting temperature[58]. The cluster is found to be nearly spherical at the verge of melting. Also, there have been studies on freezing of gold nanoparticles with Molecular Dynamics. It was established that with decreasing cooling rate, the final structure of the particle changes from amorphous to crystalline via an icosahedron-like structure[59]. It was further demonstrated the formation of an icosahedral structure through a surface-induced mechanism. Just after freezing, ordered nanosurfaces with a five-fold symmetry were formed with an interior atom remaining in the disordered state. Further lowering of the temperature induced crystallization of core atoms that proceeded from the surface towards the core region, finally leading to an icosahedral structure[60].

Molecular Dynamics studies on the structure, phase transition, thermal stability and mechanical properties of one-dimensional nanostructures exist in literature. Gold nanowires were first investigated via classical simulations by Bilabegovi$\acute{c}$[61]. Followed by the structural evolution of gold nanowires of different diameters was investigated[62]. In addition to structural properties, phase transitions in one-dimensional gold nanostructures have also been studied. Recently, surface-stress-induced phase transformation in gold nanowires has been predicted using the EAM potential[63]. It was also found that the transformation of nanowires could be controlled by the wire size, initial orientation and temperature. Further studies were performed in which shape transition of gold nanorods exposed to low-energy laser pulses were investigated. A mechanism was suggested that explains the intermediate structures and internal defects of gold nanorods observed in laser vaporization techniques[64].

1.6   Catalysis

1.6.1   Homogeneous Catalysis

Homogeneous catalysis includes all catalytic processes in which the substrate(s) and the catalyst are in the same phase. Often the gold catalysts are highly volatile so their activities are limited to the liquid phase mostly as compared to gas phase. One of the earliest of gold catalyst is AuCl and $AuCl_3$ for catalyzing chlorination of napththalene to octachloronaphthalene[79] as shown in Figure1.6.1. Although the Lewis acids like $FeCl_3$ are more efficient in carrying out the conversion.

The strong Lewis acidity of Au^I imparts reactivity towards homogeneous gold catalysts. In homogeneous catalysis, both Au^I and Au^{III} complexes have also been widely investigated mostly for alkynes towards nucleophilic reactions. The
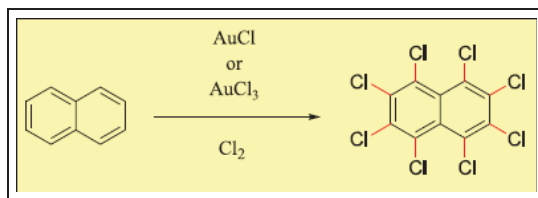
FIGURE 1.2: Substitution of all hydrogen atoms of naphthalene by chlorine

addition reactions were rigorously studied for whether the alkynes add up in an intermolecular or intramolecular fashion[80, 81].

The most important complexes of Au(I) relevant to homogeneous catalysis are complexes of Au clusters of various sizes with phosphine ligands. Johnson et *al.* reported the use of triphenylphosphine stabilized Au_{55} clusters for the oxidation of styrene using molecular oxygen[91]. Apart from gold stabilized by triphenylphosphine a large number of other Au clusters with triphenylphosphines are reported to be stable[92]. They are almost always linear 2 coordinate compounds in the form [LAuX] where L is a phosphine ligand and X is an anionic species. Au(I) can accommodate up to 4 triphenylphosphine ligands, thus satisfying the 18 electron rule. Au bonds more strongly to phosphines than to the analogous arsine or stibine compounds[93]. Gold(I) complexes with two phosphine ligands are either linear or trigonal planar geometries, depending upon the anion and the steric properties of the phosphine ligand. In $[Au(PPh_3)_2]^+$, the presence of more strongly coordinating counterions such as Cl^- gives trigonal planar $[Au(PPh_3)_2Cl]$. However, in presence of less strongly coordinating anion, viz., NO_3^- or PF_6^-, the complex is found to be always linear[92]. Gold(I) complexed with three phosphine ligands again have two possible geometries, depending upon the anion. Complexes of the type $[AuL_3]^+$ are trigonal planar, with the anion sometimes causing slight perturbation of the structure. Four coordinate complexes of $[AuL_3]X$ are also reported. These usually have slightly distorted tetrahedral structures, although trigonal pyramidal complexes have been reported. Gold(I) with four phosphine ligands, $[AuL_4]^+$, is coordinatively saturated with ligands like(L= PPh_3, PEt_3, $PMePh_3$). In these

cases, the spatial arrangement of the phosphines around the gold is dependent on the angle of the ligands by which they approach the central Au atom.

1.6.2 Heterogeneous Catalysis

Heterogeneous catalysis involves catalytic processes in which substrate(s) and catalyst are in different states. The noble metals platinum, palladium and rhodium are excellent catalysts, e.g. in hydrogenation reactions or in the automotive industry as 'catalytic converters'. Au has been used as a promoter for long time in the area of heterogeneous catalysis, e.g., in the gas phase synthesis of vinyl acetate monomer in the form of supported Pd/Au catalysts. Since the size of the particle alters the electronic and structural properties of the particles, the presence or absence of certain sites, like edges, kinks, steps and corner atoms can strongly affect a heterogeneously catalyzed reactions[86]. Different sites or the different amounts of low coordinated atoms as a result of a different particle size leads to different activities and selectivities, e.g., in hydrogenation reactions on Au catalysts[87] and other selective oxidations[88]. It has been shown that the activity of Au nanoparticles in the oxidation of CO increases with decreasing particle size and is strongly affected by nature and surface properties of the support[51, 89].

The oxidation of alcohols using gold catalysts has been a topic of great interest recently. Gold on activated carbon and TiO_2 is utilized for the oxidation of diols[90]. Catalysis by clusters of gold first came into picture after the oxidation of CO on Au/CoO, Au/NiO or Au/Fe_2O_3 carried out at low temperature of -70° and in moistened gas atmosphere by Haruta et *al.*[82]. It was revealed that the gold clusters produced by coprecipitation produced the optimum activity for CO oxidation at lower temperatures. The size of the particles plays a critical role in the mentioned reaction. For study of oxidative carbonylation process, the interaction of molecular oxygen with cationic and anionic gold clusters were also rigorously studied[52, 53]. Interaction of O_2 with the specific cluster sizes has been studied

for $[Au_n]^q$. It was found that in general, molecular O_2, adsorption takes place n $\leq$ 3, whereas adsorption followed by dissociation occurs for n $\geq$ 4. This dissociation mechanism involves a barrier of more than 1 eV due to the large distortion in the shape of the host cluster. All these planar clusters' interaction with molecular oxygen involves the charge transfer mechanism and activation of O-O bond to a superoxo-like state[83]. Similar behavior for O_2 adsorption was found for $[Au_{10}]$ clusters. In this particular case, the cluster splits molecular oxygen to superoxo-like O_2^-. Not only that, the adsorbed O was found to be sufficiently stable[84]. After the formation of the superoxo complex, the barrier to CO_2 was low and oxidative carbonylation took place fast. The d levels of the gold cluster lies higher in this activated state of superoxo-like complex state and this favors the strengthening of the chemical interactions with the adsorbates. Experimentally, Au_8, bound to F-centers of magnesia surface, is the smallest cluster that serves as catalyst for oxidative carbonylation at low temperatures of 140 K[85].

1.7 Relativistic Effects in Gold

Gold is undoubtedly, a unique element in it bearing very high relativistic effect. Among the neighboring elements in periodic table and atoms among $Z < 100$, gold shows the highest relativistic effects [42]. Due to this particular property of the element, theoretical chemistry of gold has been fascinating since last two decades.

Relativistic effects in gold arises due to the high speed of electrons when they move near a heavy nucleus. Since special theory of relativity tells that it is not possible to accelerate particles to speeds higher than c, a consequence is the mass increase,

$$m = \frac{m_0}{\sqrt{1 - (v/c)^2}} \tag{1.1}$$

For the atom Hg, the average v/c component for 1s shell is 80/137=0.58[96], which indicates that electron in 1s shell has an average velocity of 58% of the speed of light. Another conclusion from equation 4.1 is that for the electrons in 1s shell of Hg, the average mass is m $\approx 1.2m_0$.

Since the Bohr radius contains mass in denominator,

$$a_0 = 4\pi\epsilon_0 h^2/mZe^2 \tag{1.2}$$

Relativistic radius was found to be 20% smaller when compared with the non-relativistic radius. All s-shells from core to valence contract as a consequence of the high speed of electrons. The p-shells contract too. and is comparable to the s-shells. As another consequence the d- and f-shells expand and gets destabilized energetically.

A pertinent example of the importance of relativistic effects is the various difference as well as similarity among the elements of fifth and sixth row in the periodic table, viz., a classic case of silver and gold. The non-relativistic, "NR" $5d$ and $6s$ orbital energies of Au are similar to the $4d$ and $5s$ orbital energies of Ag, whereas the relativistic "R" energies do differ much in metal atoms as well as their hydrides [94–96]. The original data of ref.[94] is shown in figure 1.3.

Pyykkö and Desclaux have critically discussed[94] that due to relativistic effect in atoms, the mass of electron will increase which leads to an energetic stabilization accompanied by the contraction of orbitals. So the large contraction of s orbitals, which are closest to the nucleus, leads to a higher screening of the nuclear attraction, and hence a destabilization on d and f orbitals.

The relativistic contraction of the Au 6s shell explains the shorter covalent bonds and an explanation towards stronger bonds with Au and hence to aurophilicity too. Not only that, it also explains large ionization potential (IP) and electron
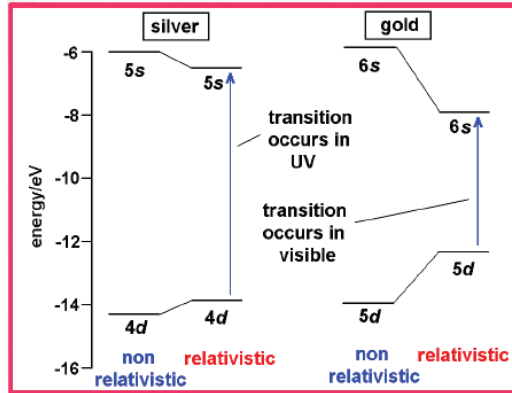
FIGURE 1.3: The relativistic (R) and nonrelativistic (NR) orbital energies of AgH and AuH. The figure is reproduced from the article of Desclaux and Pyykkö, [94] who concluded from them and the bond length data "...that the chemical difference between silver and gold may mainly be a relativistic effect." E in electron volts.

affinity (EA) of gold[97, 98]. Destabilization of 5d shells qualitatively explains the existence of trivalency and pentavalency of gold too. Yellow color of gold is also attributed to the high relativistic effects in gold. Color undoubtedly indicates electronic transition from lower energy level to Fermi level. The same for Au is around 2.3 eV. Thus gold reflects yellow and red color strongly and absorbs blue and violet. As observed in figure 1.3 the analogous 4d-5s energy gap is much higher due to absence of strong relativistic effects in Ag, the absorption is in the range of UV, which is higher than 3.5 eV. Nonrelativistic optical properties of Au differ largely from the experimental results, whereas the relativistic data correspond to realistic picture[99].

The lanthanide contraction is attributed too because of the relativistic effects in Au. The Lanthanides have vacant 4f shell while the 6s and 6p shells are completely filled. Due to the presence of strong relativistic effects 5d and 6s orbital energies (like in Au) are very different from 4d and 5s orbital energies (as in Ag). Thus entire orbital energy differences arise due to relativity. So the chemical and physical properties of Au are largely due to the strong relativistic effects.

Inert pair effect is another consequence of relativistic effects in chemistry. The tendency of the $6s^2$ electron pair to remain formally unoxidised in compounds of certain transition metal elements. In other words, the core-like behavior of $6s^2$ electron pair which results in anomalous physical properties of heavy elements and low reactivity of elemental mercury. Contraction of the 6s orbital along with the other lower valence s and p-orbitals due to the relativistic effect causes an overall contraction of the 6s density[100].

From figure 1.3 it is also clear that relativistic effects in gold lead to a more successful s-p-d hybridization. This leads to vacant hybrid orbitals which eventually leads to bond formation with other molecules as well as other Au atoms (aurophilicity[101]). Most of the stable clusters reported in the literature are known to possess large energy gap in their electronic structure between the highest occupied molecular orbital (HOMO) and the lowest occupied molecular orbital (LUMO) levels, the behavior of electrons in the HOMO largely projects the electronic and geometrical properties.

One of the first systematic studies on the structure of the clusters, $[Au]_n$ was performed for cationic clusters with $4 \leq n \leq 10$[102]. The structures were obtained from combined experimental and theoretical studies, where collision cross sections were measured using ion mobility experiments and the cross sections were compared against theoretical calculations. The density-functional-theory (DFT) studies were performed using BP86 parametrization (Becke-Perdew) for the exchange-correlation (XC) potential, a relativistic pseudopotential for Au ($5s^25p^65d^{10}6s^1$) valence electron and a localized basis set.

It is evident from the pattern that upto N=7, the experimental and the calculated values for the lowest energy structures for the ion mobility coincide with each other, but for cluster sizes, $N \geq 8$, good match was observed for three dimensional (3D) structures. Further studies on the 3D structures of higher size planar anionic clusters of $N \geq 8$, the error bars arising are considered to be due to the tendency of
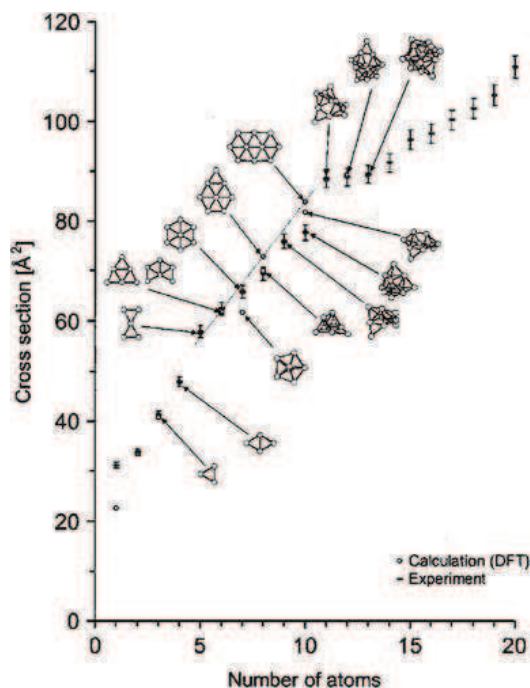
FIGURE 1.4: Measured and predicted ion mobility cross sections for gold cluster cations. The figure is taken from article of Glib et *al.* from reference [102].

DFT to overestimate the stability of planar gold clusters with gradient-correction approximations (GGA) to the exchange-correlation (XC) energy.

Structural determinations for anionic clusters for sizes upto N=14 was soon performed using photoelectron spectroscopy combined with density functional (DF) calculations[103]. The planar structures were reported to be always more stable than the three dimensional structures. The stability of the planar was accounted to be the relativistic effects in gold[105], which induces a strong 5d-6s hybridization and contraction of the Au-Au bond lengths[104].

Furthermore, along a row of periodic table, between group I to group 18, gold shows a local maximum for highest pronounced relativistic effects [96, 105] at Group 11, i.e., for the coinage metals Cu-Au indicating that these metals show higher relativistic effects than its neighbors. Such a trend is seen for all the *ns* orbital of these metals. The data of ref.[96] is shown in figure 1.5.
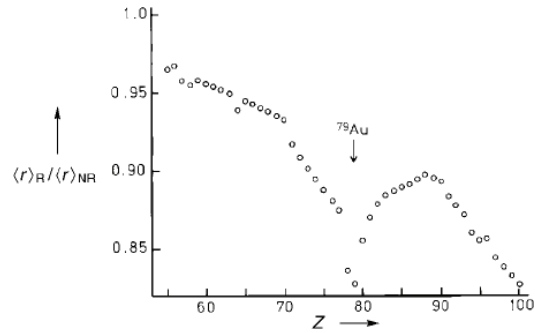
FIGURE 1.5: The ratio of relativistic and nonrelativistic $6s$ shell radii in the atomic ground states of the elements 55-100.

Such kind of anomalous behavior has been described qualitatively because of the relativistic effect in particular because of the the overlap between $(n-1)d$ and ns orbitals.

The model systems of Au_2 and AuH have been the classical test systems for study and demonstration of relativistic effects[106, 107]. For solids the relativistic effects rectify Au to the experimentally obtained interatomic distances. Yellow color of gold already mentioned as an effect of relativity, lies on the fact that the energy difference between the 5d shell and the Fermi level is $h\nu$ =2.4 eV against the experimentally observed value of 2.38 eV, whereas the nonrelativistic interband energy is quite high. Furthermore, the experimental electron affinity (EA) for gold is 2.308 eV against the relativistic calculation which is just lower by 0.014 eV. Nonrelativistic electron affinity is 1.012 eV lower than the experimental value. So it is evident that a large portion of electron affinity comes from relativity.

1.8 Relativistic effects in elements other than gold

Although, Au is the only element with Z<100, showing the highest relativistic effect, considerable relativistic effect is shown by its neighboring elements, some

elements show the additional stabilization of the 6s electrons, which plays a dominant role in their chemical properties:

Platinum ($5d^9 6s^1$): Platinum is the second element in the periodic table after gold which shows large relativistic effects. While gold can be compared to the halogens which also need one more electron to achieve a closed shell, for platinum the group reference are the chalcogens which need two electrons for a closed shell. When comparing with the chalcogens, the electron affinity of platinum (2.13 eV[108]) even exceeds the corresponding value of sulfur (2.08 eV[108]), which is the highest among all other chalcogens in the periodic table and as a non-metal readily forms divalent anions.
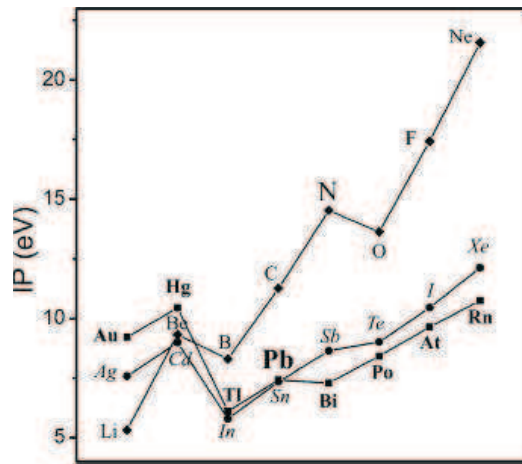
FIGURE 1.6: First ionization potentials of the elements. Diamonds, circles and squares labels correspond to the 2nd, 5th and 6th periods respectively. The figure is taken from the article of M. Jansen[111].

Mercury ($6s^2$): The relativistic effect of the element mercury is the fact that it is the only metal which is liquid at room temperatures[112]. The reason attributed to the liquid state is that since the outermost electrons are stable due to strong relativistic effects, the interatomic interactions are weaker in Hg as compared to the other metals. Interactions in neutral Hg_n clusters are weak van der Waals type for lower values of n, to covalent bonding at $n \sim 13$, which becomes metallic as $n > 100$[113].

Thallium ($6s^26p^1$): Thallium shows compounds with stable oxidation states +I and +III. Tl(III) species is prevalent as salts like TlI^3 and TlI^{4-}. Mixed metal oxides of Tl in the form of Tl_4O_3 have potent applications as superconductors[117]. The oxides of thallides M_8Tl_8O (M = Cs, Rb) have been characterized structurally. A few alkali thallides featuring novel and important structural properties were synthesized with Tl_8^{6-} cluster anion in the shape of a bicapped octahedron[118].

Lead ($6s^2$ $6p^2$): For the case of Pb, the relativistically stabilized 6s as well as 6p electrons gives more stability to the lead atom making it further nonreactive. Pb has higher ionization energy than Tl. Oxidation states of Pb are either +2 or +3. The former is better known as plumbous and the latter plumbic. Pb(II) compounds tend to be ionic with some covalent character whereas Pb(IV) compounds are polar covalent, and usually good oxidizing agents. Loss of two electrons gives Pb a $6s^2$ configuration which is stabilized due to the inert pair effect, which in turn, a consequence of relativistic effect in chemistry.

Superheavy elements: By superheavy elements it is meant for those having Z>103, often called transactinide elements. According to results of various calculations, in the nine of the transactinide elements(Z =104 to 112) the filling of the 6d shell takes place. Chemical properties of these elements influenced by all these mixed electronic shells will then be also so different to anything known before that any classification just of the basis of their knowledge will be impossible. It is interesting to note, however, that without relativistic effects, the chemistry of the heaviest superheavy elements would also be different to that of their lighter homologues due to very large shell structure effects.

1.9 Motivation and outline of the thesis

In accordance with the motivation of the present study, which is an overall presentation of theoretical chemistry using density functional theory approaches towards

detailed understanding of relativistic effects in gold, electronic and geometric structures of novel Au nanoclusters, chemical reactivity, vibrational spectra, molecular dynamics and potential energy surface (PES). The formal steps of chemical reactivity are systematically computed from structures, atom condensed *Fukui functions* or *frontier functions*, global hardness parameter and Born-Oppenheimer Molecular Dynamics in a wide range of temperature.

The outline of the thesis is as follows: Chapter 2 provides the theoretical background and the details of computational methodologies worked out in the entire thesis. Chapter 3 provides the structural and reactivity features of tetrahedral Au_{19} and Au_{20} clusters using relativistic density functional theory. Detailed results on the electronic and structural parameters of the clusters and reactivities of individual sites of the clusters are provided using atom condensed *Fukui functions* as reactivity descriptors. In chapter 4, we have presented a detailed study of the much of debated issue of (planar/two dimensional-nonplanar/three dimensional) 2D-3D transition of small Au clusters as a function of size. Moreover, we have presented a detailed analysis of the reactivity for each site of the ground state as well as thermally excited clusters using atom condensed *Fukui functions*. We have also interpreted in details the reactivity of the sites of Au_n (n=6-13) impending towards electrophilic and nucleophilic reactions. The 'amphiphilicity' of various sites in the clusters have been highlighted too. In chapter 5, we have presented the dependence of various exchange-correlation (XC) functional towards correct interpretation of structure and various properties like IR, reactivity of individual sites, density of states (DOS), potential energy (PE) surfaces and HOMO-LUMO gaps as a function of various GGA, meta-GGA and LDA XC-functionals. In chapter 6, we deal with the finite temperature behavior of small Au clusters using relativistic density functional based Born-Oppenheimer molecular dynamics (BOMD). We have calculated the traditional thermodynamics parameters like mean square displacements (MSDs) and bond length fluctuations, δ_{rms} (BLF-δ_{rms}), potential

energy surface (PES) at elevated temperatures and interpreted the results on 'solid-like' to 'liquid-like' phase transitions, behavior of Au cluster as quasi planar liquid at specific temperature, structural fluctionality and planar fluidity of small Au_n clusters $3 \leq n \leq 10$. In chapter 7, we deal with the molecular dynamics study of icosahedral Au_{32} clusters and summarize the important results of the thesis and evaluate the prospects and scope of the future work.

Bibliography

[1] Schwerdtfeger, P.; Boyd, P. D. W.; Brienne, S.; Burrell, A. K. *Inorg. Chem.* **1992**, *31*, 3411.

[2] Poisson, L.; Lepetit, F.; Mestdagh, J.-M.; Visticot, J.-P. *J. Phys. Chem. A* **2002**, *106*, 5455.

[3] Irikura, K. K.; Goddard III, W. A. *J. Am. Chem. Soc.* **1994**, *116*, 8733.

[4] Aguirre, F.; Husband, J.; Thompson, C. J.; Metz, R. B. *Chem. Phys. Lett.* **2000**, *318*, 466.

[5] M. Barysz, P. Pyykkö, *Chem. Phys. Lett.* **1998**, *285*, 398.

[6] Pyykkö, P.; Tamm, T. *Theor. Chem. Acc.* **1998**, *99*, 113.

[7] Schrder, D; Schwarz, H.; Hrušák, J.; Pyykkö, P. *Inorg. Chem.* **1998**, *37*, 624.

[8] Seidel, S.; Seppelt, K. *Science* **2000**, *290*, 117.

[9] Evans, C . J.; Lesarri, A.; Gerry, M. C. L. *J. Am. Chem. Soc.* **2000**, *122*, 6100.

[10] Evans, C. J.; Rubino-, D. S.; Gerry, M. C. L. *Phys. Chem. Chem. Phys.* **2000**, *2*, 3943.

[11] Pyykkö, P. *Science* **2000**, *290*, 64.

[12] Scherbaum, F.; Grohmann, A.; Huber, B.; Krüger, C.; Schmidbaur H. *Angew. Chem. Int. Ed. Engl.* **1988**, *27*, 1544.

[13] Pyykkö, P. *Chem. Rev.* **1997**, *97*, 597.

[14] Pyykkö, P. *Angew. Chem. Int. Ed.* **2004**, *43*, 4412.

[15] Pyykkö, P.; Zhao, Y.-F. *Angew. Chem. Int. Ed. Engl.* **1991**, *30*, 604.

[16] Pyykkö, P.; Li, J.; Runeberg, N. *Chem. Phys. Lett.* **1994**, *218*, 138.

[17] Li, J.; Pyykkö, P. *Chem. Phys. Lett.* **1992**, *197*, **586**.

[18] Clusters and Colloids, (Ed. G. Schmid), VCH, Weinheim **1994**.

[19] (a) Schalley, C. A.; Hornung, G.; Schröder, D.; Schwarz, H.; *Int. J. Mass Spectrom. Ion Processes* **1998**, *172*, 181; (b) Schalley, C. A.; Hornung, G.; Schröder, D.; Schwarz, H. *Chem. Soc. Rev.* 1998, *27*, 91; (c) Cacace, F. *Chem. Eur. J.* **2002**, *8*, 3839.

[20] Schwerdtfeger, P.; Dolg, M.; Schwarz, W. H. E., Bowmaker, G. A.; Boyd, P. D. W. *J. Chem. Phys.* **1989**, *91*, 1762.

[21] Andreev, S.; BelBruno, J. J.; *Chem. Phys. Lett.* **2000**, *329*, 490.

[22] Evans, C. J.; Gerry, M. C. L. *J. Am. Chem. Soc.* **2000**, *122*, 1560.

[23] Ilias, M.; Fardik, P.; Urban, M. J. *Phys. Chem. A* **1998**, *102*, 5263.

[24] Van Wüllen, C. *J. Chem. Phys.* **1998**, *109*, 392.

[25] Brown, J. R.; Schwerdtfeger, P.; Schröder, D.; Schwarz, H. *J. Am. Soc. Mass Spectrom.* **2002**, *13*, 485.

[26] Schröder, D.; Hrušák, J; Tornieporth-Oetting, I. C.; Klapötke, T. M.; Schwarz, H. *Angew. Chem.* **1994**, *106*, 223; *Angew. Chem. Int. Ed. Engl.* **1994**, *33*, 212.

[27] Schwerdtfeger, P.; Dolg, M.; Schwarz, W. H. E.; Bowmaker, G. A.; Boyd, P. D. W. *J. Chem. Phys.* **1989**, *91*, 1762.

[28] Doll, K.; Pyykkö, P.; Stoll, H. *J. Chem. Phys.* **1998**, *109*, 2339.

[29] Söhnel, T.; Hermann, H.; Schwerdtfeger, P. *Angew. Chem. Int. Ed.* **2001**, *40*, 4381.

[30] Schulz, A.; Hargittai, M.; *Chem. Eur. J.* **2001**, *7*, 3657.

[31] Söhnel, T; Brown, R.; Kloo, L.; Schwerdtfeger, P. *Chem. Eur. J.* **2001**, *7*, 3167.

[32] Bartlett, N . *Gold Bull.* **1998**, *31*, 22.

[33] Seth, M.; Cooke, F.; Schwerdtfeger, P.; Heully, J.-L.; Pelissier, M. *J. Chem. Phys.* **1998**, *109*, 3935.

[34] Sommer, A. *Nature* **1943**, *152*, 215.

[35] Heymann,E.; Weber, H. P. *Trans. Faraday Soc.* **1938**, *34*, 1492.

[36] Mudring, A.-V .; Jansen, M.; Daniels, J.; Krämer, S.; Mehring, M.; Prates Ramalho, J. P.; Romero, A. H.; Parrinello, M. *Angew. Chem. Int. Ed.* **2002**, *41*, 120.

[37] Watson, R. E.; Weinert, M. *Phys. Rev. B* **1994**, *49*, 7148.

[38] Schwerdtfeger, P.; Dolg, M. *Phys. Rev. A* **1991**, *43*, 1644.

[39] Liu, W.-J.; Wüllen, C. van *J. Chem. Phys.* **1999**, *110*, 3730.

[40] Gold. Progress in Chemistry, Biochemistry and Technology (Ed.: H. Schmidbaur), Wiley, Chichester, **1999**, 894.

[43] Wang, X.-F .; Andrews, L.; *J. Phys. Chem. A* **2002**, *106*, 3744.

[42] (a) Pyykkö, P. *Angew. Chem.* **2002**, *114*, 3723. (b) Pyykkö, P. *Angew. Chem. Int. Ed.* **2002**, *41*, 3573.

[43] Desclaux, J. P.; Pyykkö, P. *Chem. Phys. Lett.* **1976**, *39*, 300.

[44] Hay, P. J.; Wadt, W. R.; Kahn, L. R.; Bobrowicz, F.W. *J. Chem. Phys.* **1978**, *69*, 984.

[45] Lenthe, E. van; Snijders, J. G.; Baerends, E. J. *J. Chem. Phys.* **1996**, *105*, 6505.

[46] Schwerdtfeger, P.; Brown, J. R.; Laerdahl, J. K.; Stoll, H. *J. Chem. Phys.* **2000**, *113*, 7110.

[47] Castleman, A. W.; Jena, P *Proc Natl Acad Sci USA* **2006**, *103*, 10552.

[48] Kumar, V.; Kawazoe, Y. *Eur. Phys. J. D* **2003**, *24*, 81.

[49] Issendorff, B. V.; Cheshnovsky O. *Annu. Rev. Phys. Chem.* **2005**, *56*, 549.

[50] Link, S.; El-Sayed, M. A. *Int. Rev. Phys. Chem.* **2000**, *19*, 409.

[51] Haruta, M. *Catal. Today* **1997**, *36*, 153.

[52] Gilb, S.; Weis, P.; Furche, F.; Ahlrichs, R.; Kappes, M. M. *J. Chem. Phys.* **2002**, *116*, 4094.

[53] Furche, F.; Ahlrichs, R.; Weis, P.; Jacob, C.; Gilb, S.; Bierweiler, T.; Kappes, M. M. *J. Chem. Phys.* **2002**, *117*, 6982.

[54] Guo, R.; Balasubramanian, K.; Wang, X.-F.; Andrews, L. *J. Chem. Phys.* **2002**, *117*, 1614.

[55] Li, J.; Li, X.; Zhai, H.-J.; Wang, L.-S. *Science* **2003**, *299*, 864.

[56] (a) Cleveland, C. L.; Luedtke, W. D.; Landman, U. *Phys. Rev. Lett.* **1998**, *81*, 2036. (b) Cleveland, C. L.; Luedtke, W. D.; Landman, U. *Phys. Rev. B* **1999**, *60*, 5065.

[57] Liu, H. B.; Ascencio, J. A.; Perez-Alvarez, M.; Yacaman, M. J. *Surf.Sci.*, **2001**, *491*, 88.

[58] (a) Wang, Y.; Teitel, S.; Dellago, C. *Chem. Phys. Lett.*, **2004**, *394*, 257. (b) Wang, Y.; Teitel, S.; Dellago, C. *J. Chem. Phys.*, **2005**, *122*, 214722.

[59] Shim, J. -H.; Lee, S. -C.; Lee, B. -J.; Suh, J. -Y.; Cho, Y. W. *J. Crystal Growth*, **2003**, *250*, 558.

[60] Nam, H. -S.; Hwang, N. M.; Yu, B. D.; Yoon, J. -K. *Phys. Rev. Lett.*, **2002**, *89*, 275502.

[61] (a) Bilabegović, G. *Phys. Rev. B*, **1998**, *58*, 15412. (b) Bilabegović, G. *Comp. Mater. Sci.*, **2000**,*18*, 333.

[62] Wang, B.; Yin, S.; Wang, G.; Buldum, A.; Zhao, J. *Phys. Rev. Lett.*, **2001**, *86*, 2046.

[63] (a) Diao, J.; Gall, K.; Dunn, M. L. *Nature Mater.*, **2003**, *2*, 656. (b) Diao, J.; Gall, K.; Dunn, M. L. *Phys. Rev. B*, **2004**, *70*, 075413.

[64] Wang, Y.; Dellago, C. *J. Phys. Chem. B*, **2003**, *107*, 9214.

[65] Heiz, U .; Vayloyan, A.; Schumacher, E.; Yeretzian, C.; Stener, M.; Gisdakis, P.; Rösch, N. *J. Chem. Phys.* **1996**, *105*, 5574.

[66] Pyykkö, P .; Runeberg, N.; *Angew. Chem. Int. Ed.* **2002**, *41*, 2174.

[67] Li, X.; Kiran, B.; Li, J.; Zhai, H.-J.; Wang, L.-S. *Angew. Chem. Int. Ed.* **2002**, *41*, 4786.

[68] Mingos, D. M. P. *Polyhedron* **1986**, *3*, 1289.

[69] Dyson, G.M. *Pharm. J. 1929*, *123*, 249 and 266.

[70] D' Arcy Hart, P. *Brit. Ivied. J.* **1946** Nov. 30 and Dec. 7, 805 and 849.

[71] Forestier, J. *Lancet*, **1932**, *2*, 441.

[72] Constable, T.J.; Crockson, A.P.; Oockson, R. A .; McConkey, B. *Lancet* , **1975**, *May 24*, 1176.

[73] Gosselin, R.E. *J. Gen. Physiol.* **1956**, *39*, 625.

[74] (a) Pauli, W. *Trans. Farad. Soc.* **1935**, *31*. (b) Pauli, W. *Hev. Chim. Acta. 1949*, *32*, 795.

[75] Landé, K. *Miineh. Med. Woehensehr.* **1927**, *74*, 1132.

[76] Loo, C.; Hirsch, L.; Lee, M. H., *Opt. Lett.* **2005**, *30*, 1012.

[77] Huang, X.; El-Sayed, I. H., Qian, W., *J. Am. Chem. Soc.* **2006**, *128*, 2115.

[78] (a) Huang, X.; Jain, P. K.; El-Sayed, I. H. *Photochem. Photobiol.* **2006**, *82*, 412.
(b) Chen, J.; Wang, D.; Xi, J. *Nano Lett.* **2007**, *7*, 1318.

[79] Schwemberger, W.; Gordon, *W. Chem. Zentralbl.* **1935**, *106*, 514.

[80] Asao, N.; Takahashi, K.; Lee, S.; Kasahara, T.; Yamamoto, Y. *J. Am. Chem. Soc.* **2002** *124*, 12650.

[81] Fukuda, Y.; Utimoto, K. *J. Org. Chem.* **1991**, *56*, 3729.

[82] Haruta, M.; Kobayashi, T.; Samo, H.; Yamada, N. *Chem. Lett.* **1987**, 405.

[83] Varganov, S. A.; Olson, R. M.; Gordon, M. S.; Mills, G.; Metiu, H. *Chem. Phys. Lett.* **2003**, *368*, 778.

[84] Lopez, N .; Nskov, J. K. *J. Am. Chem. Soc.* **2002**, *124*, 11262.

[85] Sanchez, A.; Abbet, S.; Heiz, U.; Schneider, W.-D.; Häkkinen, H.; Barnett, R. N.; Landman, U. *J. Phys. Chem. A* **1999**, *103*, 9573.

[86] Davis, S.M.; Zaera, F.; Somorjai, G.A. *J. Am. Chem. Soc.* **1982**, *104*, 7453.

[87] Mohr, C.; Hofmeister, H.; Radnik, J.; Claus, P. *J. Am. Chem. Soc.* **2003**, *125*, 1905.

[88] Claus, P.; Bruckner, A.; Mohr, C.; Hofmeister, H. *J. Am. Chem. Soc.* **2000**, *122*, 11430.

[89] Yoon, B.; Hakkinen, H.; Landman, U.; Worz, A.S.; Antonietti, J.M.; Abbet, S.; Judai, K.; Heiz, U. *Science* **2005**, *307*, 403.

[90] Porta, F.; Prati, L.; Rossi, M.; Scari, G. *J. Catal.* **2002**, *211*, 464.

[91] Turner, M.; Golovko, V. B.; Vaughan, O. P. H.; Abdulkin, P.; Berenguer-Murcia, A.; Tikhov, M. S.; Johnson B. F. G.; Lambert, R. M. *Nature* **2008**, *454*, 981.

[92] Gimeno, M. C.; Laguna, A. *Chemical reviews* **1997**, *97*, 511.

[93] Tripathi, U. M.; Schier A.; Schmidbaur, H. *Journal of Chemical Sciences* **1998**, *53*, 171.

[94] Desclaux, J. P.; Pyykkö, P. *Chem. Phys. Lett.* **1976**, *39*, 300.

[95] Pyykkö, P. *Adv. Quantum Chem.* **1978**, *11*, 353.

[96] Pyykkö, P.; Desclaux, J. P. *Acc. Chem. Res.* **1979**, *12*, 276.

[97] Jackschath, C.; Rabin, I.; Schulze, W.; Ber. Bunsenges, *Phys. Chem.* **1992**, *86*, 1200.

[98] Taylor, K. J.; Jin, C.; Conceicao, J.; Cheshnovsky, O.; Johnson, B. R.; Nordlander, P.J.; Smalley, R. E. *J. Chem. Phys.*, **1991**, *93*, 7515.

[99] Christensen, N . E.; Seraphin, B. O. *Phys. Rev. B* **1971**, *4*, 3321.

[100] Schwerdtfeger, P., Heath, G. A., Dolg, M., Bennet, M. A. *J. Am. Chem. Soc.* **1992**, *114*, 7518.

[101] Pyykkö P. *Chem. Soc. Rev.* **2008**, *37*, 1967.

[102] Gilb, S.; Weis, P.; Furche, F.; Ahlrichs, R.; Kappes, M. M. *J. Chem. Phys.* **2002**, *116*, 4094.

[103] Häkkinen, H.; Yoon, B.; Landman, U.; Li, X.; Zhai H.-J.; Wang, L.-S. *J. Phys. Chem. A* **2003**, *107*, 6168.

[104] Häkkinen, H.; Moseler M.; Landman, U. *Phys. Rev. Lett.*, **2002**, *89*, 033401.

[105] Pyykkö, P. *Chem. Rev.*, **1988**, *88*, 563.

[106] Hay, P. J.; Wadt, W. R.; Kahn, L. R.; Bobrowicz, F. W. *J. Chem. Phys.*, **1978**, *69*, 984.

[107] Lee, Y. S.; Ermler, W. C.; Pitzer, K. S.; McLean, A. D. *J. Chem. Phys.*, **1979**, *70*, 288.

[108] Andersen, T.; Haugen, H. K.; Hotop, H. *J. Phys. Chem. Ref. Data*, **1999**, *28*, 1511.

[109] Karpov, A.; Wedig, U.; Dinnebier, R. E.; Jansen, M. *Angew. Chem.* **2005**, *117*, 780; *Angew. Chem., Int. Ed.* **2005**, *44*, 770.

[110] Karpov, A.; Nuss, J.; Wedig, U.; Jansen, M. *J. Am. Chem. Soc.* **2004**, *126*, 14123.

[111] Jansen, M. *Solid State Sci.* **2005**, **7**, 1464.

[112] Jacoby, M. *Chem. Engr. News* **1998**, *March 23*, 48.

[113] Moyano, G. E.; Wesendrup, R.; Sohnel, T.; Schwerdtfeger, P. *Phys. Rev. Lett.* **2002**, *89*, 103401.

[114] Olenev, A. V.; Shevelkov, A. V. *Angew. Chem., Int. Ed. Engl.* **2001**, *40*, 2353.

[115] Ulvenlund, S.; Rosdahl, J.; Fischer, A.; Schwerdtfeger, P.; Kloo, L. *Eur. J. Inorg. Chem. 1999*, 633.

[116] Borisov, S. V.; Magarill, S. A.; Pervukhina, N. V. *J. Struct. Chem.* **2003**, *44*, 441.

[117] Wahlbeck, P. G.; Myers, D. L. *J. Chem. Phys.* **1997**, *106*, 10383.

[118] Corbett, J. D. *Angew. Chem. Int. Ed.* **2000**, *39*, 670.

Chapter 2

Theoretical Background

2.1   The Many-Body Problem

The most important part of the many body problem is the interaction among the many bodies. Otherwise the many body problem could easily be tackled as "many-one-body" problem. Conventionally the motion of moon-earth-sun has been considered as one of the oldest many-body-problem, which has three bodies interaction and does not possess any exact solution[1]. It was one of the oldest scientific inquiry in the history of science. The present day many-body problem in quantum mechanics is solved regularly, of course with the introduction of approximations into the many-body interacting systems.

The ground state of a quantum mechanical system can be described by simple equation, the time independent Schrödinger equation,

$$H\psi = E\psi \tag{2.1}$$

For a molecule, the Hamiltonian can be expressed as:

$$H = -\frac{\hbar^2}{2}\sum_{j}^{nucl}\frac{\nabla_{\mathbf{R}_j}^2}{M_j} - \frac{\hbar^2}{2m_e}\sum_{i}^{elec}\nabla_{\mathbf{r}_i}^2 - \sum_{i}^{elec}\sum_{j}^{nucl}\frac{e^2 Z_j}{|\mathbf{r}_i - \mathbf{R}_j|} + \sum_{j<i}^{elec}\frac{e^2}{|\mathbf{r}_i - \mathbf{r}_j|} + \sum_{j<i}^{nucl}\frac{e^2 Z_i Z_j}{|\mathbf{R}_i - \mathbf{R}_j|}$$

(2.2)

where $\hbar$ is the Planck's constant, R_j being the nuclear coordinate for the jth nucleus, R_i being the coordinate of ith nucleus, r_i being the electronic coordinate for the i'th electron and M_j and m_e are the corresponding masses. Z_j are the nuclear charges. ψ is the many-body wavefunction and is a function of all the positions and coordinates of the electrons of the molecular system. To solve this many-body problem, there are important and necessary approximations associated with it.

2.2 Born-Oppenheimer approximation

Börn-Oppenheimer approximation, where the motion of the nuclei is separated from the electronic degrees of freedom and the electrons are considered as moving in an external field generated by the collection of nuclei. This has been a valid approximation since the mass of the nuclei is much larger than the mass of the electrons and hence the nuclei motions are much slower than that of the electrons. The Börn-Oppenheimer approximation still leaves a difficult many-body problem with us. A fascinating way to approach is the Hartree-Fock Approximation (HF). The entire many-body wavefunction is defined by a Slater determinant of single electron wavefunctions and fulfill the Pauli exclusion principle. As a consequence of which a non-local exchange potential appears.

2.3   Hartree Theory

Hartree theory deals with the many-body wavefunction as simply the product of the many one electron wavefunctions.

$$\psi(1, 2, ..., N) = \psi_1(1)\psi_2(2) \cdots \psi_N(N) = \Pi_{i=1}^{N}\psi_i(i) \qquad (2.3)$$

This expression for the wavefunction is the **Hartree product**. Since the probability density of any N-electron system is given by the product of the wavefunction and its complex conjugate, ψ^*, the N-electron probability density is reduced to a product of N one-electron probability densities,

$$\psi^*(1, 2, ..., N)\psi(1, 2, ..., N) = \Pi_{i=1}^{N}\psi_i^*(i)\psi_i(i) \qquad (2.4)$$

According to probability theory, if a probability can be written as the product of individual probabilities, the events associated with those probabilities must occur independently of one another. Thus, the orbital approximation is based on an independent electron model, implying that the motion of each electron is independent of all the other electrons.

The Hartree product given above describes the spatial distribution of the N electrons within the system. However, for the complete description of any electron, the spin state of each electron must also be included. This is most easily accomplished by multiplying each spatial function (ψ_i) by a spin function (α or β), producing a unique spin orbital, denoted by χ_i. Thus the wavefunction is a product of one-electron spin orbitals.

With the wavefunction expressed as a product of one-electron functions, it is also important to consider the overall symmetry of this expression. Electrons are indistinguishable particles, and as such, no property can be affected simply by the

interchange of any two electrons[2]. Consider the electron probability density as shown in equation 2.4, in order for this result to remain constant following the interchange of two electrons, there are only two possible solutions,

$$\psi(1, 2, ...i, j, ...N) = \psi(1, 2, ...j, i, ...N) \tag{2.5}$$

However, it is known from experiment that electrons, and in fact all fermions, must have antisymmetric wavefunctions with respect to the interchange of any two electrons. Thus, if the interchange of two electrons is affected by a permutation operator, the resultant wavefunction must have the opposite sign, $\hat{P}_{ij}$,

$$\begin{aligned}
\hat{P}_{ij}\psi(1, 2, \cdots, i, j, \cdots, N) &= \psi(1, 2, \cdots, j, i, \cdots, N) \\
&= -\psi(1, 2, \cdots, i, j, \cdots, N)
\end{aligned} \tag{2.6}$$

2.4   The Hartree-Fock Approximation

The many body wavefunction ψ is approximated as antisymmetrized product of N orthonormal spin orbitals $\chi_i(\mathbf{x})$, with each being a product of spatial orbital $\phi_k(\mathbf{r})$ and the spin function $\sigma(s) = \alpha(s)$ or $\beta(s)$, the rows refer to the electron indices and the column to the spin orbitals. the result is an N-electron system Slater determinant, which is represented as:

$$\psi_{HF} = \frac{1}{\sqrt{N!}} \begin{vmatrix} \chi_1(1) & \chi_2(1) & \cdots & \chi_N(1) \\ \chi_1(2) & \chi_2(2) & \cdots & \chi_N(2) \\ \vdots & \vdots & \ddots & \vdots \\ \chi_1(N) & \chi_2(N) & \cdots & \chi_N(N) \end{vmatrix} \tag{2.7}$$

where $(N!)^{-\frac{1}{2}}$ is normalization constant, found by imposing the condition $\int \psi^* \psi d\tau = 1$

If two rows are interchanged, determinant changes sign. If two rows are identical, determinant vanishes. Determinant automatically satisfies Pauli's Exclusion Principle due to its inherent antisymmetric nature. HF determinant among all other determinants is the one which is minimum in energy.

As a direct consequence of this construction, a non-local exchange potential appears naturally. Although good for two-particles problem, the Hartree-Fock approximation has deficiencies making it useless for applications in molecules and clusters. The many body wavefunction is expressed in terms of single Slater determinant is inadequate for the expression of energy of a multielectronic electronic structure problem.

The spin orbitals that provides the 'best' n-electron determinantal wavefunction are estimated by means of variational principle (discussed in later section), which involves the minimization of the Rayleigh Ratio:

$$\epsilon = \frac{\psi^*(i)\hat{H}\psi(i)dx}{\psi^*(i)\psi(i)dx} \tag{2.8}$$

where the spin orbitals are considered to be orthonormal. The minimum value of the ϵ for the electronic energy is considered to be the best for nuclear configuration.

The HF equation for spin-orbital $\phi_a(1)$, where arbitrarily assigned electron 1 to spin orbital ϕ_a, has the form:

$$f(1)\phi_a(1) = \epsilon_a \phi_a(1) \tag{2.9}$$

ϵ_a being the orbital energy of the spin orbital $f(1)$ is the known as the *fock operator*.

$$f_1 = h_1 + \sum_u \{J_u(1) - K_u(1)\} \tag{2.10}$$

where $h(i)$ is the core hamiltonian for electron 1, the sum is over all spin orbitals $u = a, b, \cdots, z$ and $J_u(1)$ is the *Coulomb Operator*, $K_u(1)$ being the *Exchange Operator* which are defined as:

$$J_u(1)\phi_a(1) = \left[\int \phi_u^*(2) \left(\frac{e^2}{4\pi\epsilon_0 r_{12}} \right) \phi_u(2) dx_2 \right] \phi_a(1) \tag{2.11}$$

$$K_u(1)\phi_u(1) = \left[\int \phi_u^*(2) \left(\frac{e^2}{4\pi\epsilon_0 r_{12}} \right) \phi_a(2) dx_2 \right] \phi_u(1) \tag{2.12}$$

Coulomb and exchange operators are defined in terms of spin orbitals rather than spatial wavefunctions.

The Hartree-Fock method takes into account only the lowest-lying configuration which is one of very many with comparable energies, and better approximation would result from taking a linear combination. This approach is the simplest *ab initio* method available and provides the basis for many higher order methods. Such an approach, where effects beyond the Hartree-Fock approximation (correlation effects) are included by improving the many-particle wave function, is known as configuration interaction (CI). It leads, in principle, to the exact wave functions from which most properties of interest can be calculated. CI is however even more computationally costly than HF.

2.5 Choice of basis sets

Despite the fact that the Hartree-Fock approximation allows for an expression which can be handled and the many-electron wavefunction can be expressed well

as a product of one-electron functions, the form of these functions need to be understood. To describe a spin-orbital exactly, in principle, a complete set of basis functions are supposed to be used, which implies, the use of an infinite number of functions. Since an infinite basis set is computationally not feasible, the use of a finite basis set is always desired. However, there arises the error due to the incompleteness of the basis set often called *Basis-set truncation error.* The difference between the Hartree-Fock energy limit, which is the possible lowest energy obtained variationally, and in an Hartree-Fock SCF calculation is the basis-set truncation error. On these grounds, the spin orbitals, χ_is, which are often referred to as *molecular orbitals* (MOs), are constructed as a linear combination from a set of known one-electron functions, ϕ_μ, called *basis functions*,

$$\chi_i = \sum_{\mu=1}^{K} C_{\mu i} \phi_\mu \tag{2.13}$$

where C is the coefficient in the expansion for the μth basis function in the ith MO. A particular set of K basis functions forms a basis set.

Various types and sizes of basis functions are available, as well as the way in which they can be combined. As the choice of basis set reflect heavily on the quality of the MOs, and ultimately the accuracy of the calculation, serious consideration of these factors are to be taken care of.

In most of the cases, the MOs are expanded from a set of atomic orbitals (AO) on the constituent atoms. This approach is commonly known as the *linear combination of atomic orbitals (LCAO)*, but can quickly become impractical for larger systems. Consequently, simpler functions are often used instead of the AOs.

The two most common types of basis functions employed are *Slater-type orbitals* (STO)[4] and *Gaussian-type orbitals* (GTO)[5]. Both classes of functions exhibit exponential decay. The key difference between the Slater- and Gaussian-type orbitals stems from the fact that the former decay with $\exp(-\zeta r)$ and possess a

cusp at the nucleus while the latter decay with $\exp(-\zeta r^2)$, decaying too rapidly as r increases, and exhibiting a finite value at the nucleus. The orbital exponents (ζ) can be adjusted to control the size of the orbitals.

STOs provide a better description of the molecular orbitals, and thus are considered better than GTOs. Unfortunately, the better description comes at an increased computational cost and so GTOs tend to be used more frequently.

To overcome this problem, a linear combination of GTOs are usually employed. The coefficients determining the weighting of each Gaussian used are calculated by the fitting to a single STO. It is typically the three times the number of GTOs rather than STOs for any given accuracy. The greater the number of primitive gaussians used, the more flexible the expression of the orbital and thus greater accuracy of the calculation. STO-3G is a minimal basis set as it contains only one basis function per AO. The 3G part indicates that each basis function is a contraction of three primitive gaussians. Minimal basis sets are not used for accurate calculations.

Further accuracy is achieved by representing each orbital with more number of basis function. Double zeta (ζ) or DZ basis set contains two basis functions per atomic orbital. Same quality is provided by Dunning/Huzinaga basis sets. A triple zeta or TZ basis set uses three basis functions per atomic orbital, etc. It is also understood that for most systems, the core electrons do not play a significant role in bonding, thus it is possible to save computation cost by treating the core electrons to a lesser accuracy than the valence electrons. The basis set that does this is called a split-valence or SV basis set. The smallest example of a split-valence basis set is *3-21G*. The 3 indicates that three primitive gaussians are used in the contraction of the core orbitals, 21 indicates that the outer orbitals are split into two functions; inner and outer functions where the inner function uses two gaussians and the outer function uses only one gaussian. 6-311G is a basis that is triply split, it treats the core only minimally but gives a TZ treatment of the

valence electrons. The advantage of using inner and outer functions for the valence orbitals is that they may change size, growing or shrinking to meet the particular bonding requirements of the molecule.

When atoms are in bonded state in molecules, the atomic orbitals get distorted from their actual shapes. While both split-valence and double-ζ basis set allow orbitals to change size, they do not permit changing of shape. Change of orbital shape is usually allowed by including polarization functions to the basis set. These basis functions represent orbitals higher in angular momentum than those occupied in the atom, for example adding d-orbitals to a carbon atom whose highest occupied orbitals are 2p. d-functions are used to describe polarization of p-orbitals, f-functions are used to describe polarization of d-orbitals and so on. Involving d and f orbitals increases the accuracy of the electron density around the atom. Polarization is indicated by either "*" notation or by specifying the orbitals added. In this manner 6-31G(d) and 6-31G* are equivalent. A DZP basis set means a double-ζ basis with polarization functions.

The other way of adding to the basis set to improve accuracy is by the addition of diffuse functions. These are necessary to describe weakly-bonded systems such as Hydrogen-bonding and also to describe anions or electronically excited states where the small amount of electron density far from the nucleus plays a signicant role. These functions are indicated in a basis set by the prex aug- (abbreviation for augmented) or by a + symbol as in 6-31+G(d,p).

For transition metals the choice of the basis set is quite limited. The used basis sets for transition metal atoms are the Los Alamos National Laboratory (Lanl) family of basis sets and the Stuttgart/Dresden basis set (abbreviated either as ECP-SDD or RECP-SDD). RECP19-SDD for Au atom from theochem-stuttgart is used for addressing relativistic effects in gold throughout the work in this thesis which is included in the deMon2K program. Both of these bases are of double-ζ quality.

2.6 Basis Set superposition error

While the calculations involving the interaction energy between two (or more) monomers, the choice of basis set plays a pivotal role. The interaction energy is calculated as the difference between the energy of the complex and the energy of the individual monomers. A complete basis set would be used for these calculations; however, in reality, which is not possible as discussed in the earlier section. Due to the incompleteness of the basis set, the interaction energy tends to be overestimated and leads to the the *basis set superposition error (BSSE)*. This error arises because of the lowering of the complex energy, since, the monomers in the complex have a superior description of their molecular orbitals due to the presence of the other monomer's basis functions. Although the magnitude of the BSSE is usually quite small, it can have a large effect on the calculated binding energies depending on the strength of the interactions in the complex.

2.7 Variational Theorem

The fundamental objective of quantum chemistry is to determine the form of the wavefunction in order to understand the system of consideration. The Slater determinant provides the simplest means to determine the antisymmetric wavefunction from the spin orbitals. In addition to that, the spin orbitals themselves are constructed as a linear combination of basis functions as in equation 2.13. The understanding of the coefficients, $C_{\mu i}$, in the expansion of the basis functions are enough to evaluate the spin orbitals. Computational chemistry mainly revolves around the ground state of a given system, when provided, the exact ground-state wavefunction, ψ_0, the corresponding ground-state energy, E_0, is obtained from the expectation value of the Hamiltonian operator. According to the variational theorem, given a trial function, $\tilde{\psi}$ that satisfies the boundary conditions of the system, the lowest-energy eigenvalue of the trial function,

$E_{\tilde{\psi}}$, will always be greater than or equal to the exact ground-state energy, which is expressed as,

$$\epsilon = \frac{\int \tilde{\psi}^* \hat{H} \tilde{\psi}^*}{\int \tilde{\psi}^* \hat{H} \tilde{\psi}^*} \geq E_0 \qquad (2.14)$$

Using this theorem, the exact ground-state wavefunction is approximated from the trial function that gives the lowest energy.

2.8 Roothan Equations

The Hartree-Fock approximation or the HF method provides the basis to obtain the set of spin orbitals which makes it feasible to provide the true ground-state system. Equations 2.9-2.12 are the very non-linear equations which were fundamentally used in further post Hartree-Fock methods.

A first leap to solve these non-linear equations is where the Roothaan-Hall method comes into existence. In this very method, the spin orbitals (SO), or molecular orbitals (MO) are expressed as linear combinations of atomic orbitals (AO). Also, in principle, the set of basis functions employed, constructs a complete set in order to properly describe the molecular orbitals. However, as discussed earlier in the previous section that this would require an infinite number of basis functions and thus this approach is not feasible. Furthermore, choice of basis function is the bottleneck and a proper selection of the basis set provides a better representation of the molecular orbitals, although, a finite basis has to be used for the sake of feasibility of computation[2]. In general, the larger the number of basis functions included, the more accurate the description of the molecular orbitals. An ardent application of the variational method to the Hartree-Fock equations and substitution of equation 2.13 gives the Roothaan-Hall equations, [6, 7].

$$\sum_{\nu=1}^{M} (f_{\mu\nu} - \epsilon_i S_{\mu\nu}) c_{\nu i} = 0, \qquad \mu = 1, 2, \cdots, M \qquad (2.15)$$

It results in minimum energy system when the coefficients satisfy the above equation. The Fock matrix, $f_{\mu\nu}$, consists of elements defined by, μ and ν

$$F_{\mu\nu} = H_{\mu\nu} + \sum_{\lambda=1}^{M} \sum_{\sigma=1}^{M} P_{\lambda\sigma} [(\mu\nu \mid \lambda\sigma) - \frac{1}{2}(\mu\lambda \mid \nu\sigma)] \qquad (2.16)$$

where $\mu\nu$ is a matrix element of the core Hamiltonian operator, is a matrix element of the density matrix such that,

$$P_{\lambda\sigma} = 2 \sum_{i=1}^{occ.MOs} c_{\mu i} c_{\nu i} \qquad (2.17)$$

Equation 2.15 is comprising the set of simultaneous equation, and will have a solution for each value of i, and these are known as *Roothan equations.* The entire set of equations can be represented as the single matrix equation:

$$Fc = Sc\epsilon \qquad (2.18)$$

where c is an $M \times M$ matrix of elements $c_{\mu\nu}$ and ϵ is also an $M \times M$ diagonal matrix of orbital energies ϵ_a.

2.9 Electron correlation

Although the spin orbitals obtained from variational theorem are considered the 'best', but they are not the 'exact' functions. HF methods relies on the average interaction of the electrons and has ample drawbacks. The instantaneous electronic repulsions are not taken care of and the effect of n-1 electrons on a single

electron under consideration is treated in an average way. The consideration of average interaction is a crude approximation and as a matter of fact, motion of the electrons is correlated. Since electrons repel one another, it is impossible to find two electrons with parallel spin in the same location at the same time. HF method ignores electron correlation completely. In order to get a sense of post Hartree-Fock treatment, the instantaneous interactions between electrons must be considered and have to be considered into the calculation. The difference between the exact energy (E_{exact}) of the system and that obtained at the Hartree-Fock limit (discussed in previous section)(E_{HF}) is the **correlation energy** (E_{corr})[3],

$$E_{corr} = E_{exact} - E_{HF} \tag{2.19}$$

Despite the fact that the correlation energy has less contribution to the total energy as compared to the HF energy, it is understood that it has a value similar to that of chemical bonds, and must be incorporated while studying the chemical systems and their reactions. Many methods in literature have been suggested to recover the correlation energy, which involves perturbation and variational treatments. These methods are the post-HF methods, some of which are discussed in subsequent sections.

2.10   Configuration Interaction

A well known method to take care of the electron correlation is the configuration interaction (CI). CI is a variational method in which the wavefunction can be expressed as a linear combination of Slater determinants corresponding to the ground state and various excited states. It is the addition of the excited states that accounts for electron correlation in configuration interaction. To deal with an n-electron system, first a Hartree-Fock wavefunction ϕ_0 is created. A basis

set is selected having M members resulting in $2M$ spin orbitals. So there exist $2M - n$ virtual orbitals. Since many Slater determinants can be constructed out of the $2M$ spin-orbitals and ϕ_0 is one of the many, the rest can be identified as the determinants in which how many electrons are considered promoted by exciting to virtual orbitals from the ground state ϕ_0. The Slater determinant denoting the Hartree-Fock can be expressed as:

$$\phi_0 = \mid \phi_1 \phi_2 \phi_3 \cdots \phi_a \phi_b \cdots \phi_n \mid \qquad (2.20)$$

where ϕ_a and ϕ_b are the occupied spin orbitals for the Hartree-Fock ground state.

Since the strategy is to write the ground-state and the excited state in the form of a linear combination of all possible n-electron Slater determinants arising from a complete set of spin-orbitals, so the exact electronic wavefunction, ψ, for any state of the system, in the form, may be written as:

$$\psi = C_0 \Phi_0 + \sum_{a,p} C_a^p \Phi_a^p + \sum_{\substack{a<b \\ p<q}} C_{ab}^{pq} \Phi_{ab}^{pq} + \sum_{\substack{a<b<c \\ p<q<r}} C_{abc}^{pqr} \Phi_{abc}^{pqr} + \cdots \qquad (2.21)$$

where the coefficients in this expansion, C_is, are treated variationally to find the lowest energy state. The first term in equation 2.21 is the ground-state HF determinant while the following terms correspond to single, double, triple, excitations and so on. The summations indicate that all possible excitations of a single type are included. For instance, all single excitations, (Φ_a^p), are included in which one electron from an occupied spin orbital (Φ_a) is promoted to an unoccupied virtual orbital (Φ_p). Similarly for the double excitations, (Φ_{ab}^{pq}), one electron is excited from Φ_a to Φ_p while another electron is excited from Φ_b to Φ_q, and so on for the subsequently higher excitations.

2.11   Density Functional Theory

While the Hartree-Fock method and Configuration Interaction gives an approximate solution to the many-body problem by a reasonable to heavy computational effort, the Density Functional Theory reveals a beautiful dream. Density Functional Theory (DFT) takes an entirely different approach to the many-body problem. Instead of trying for a rigorous effort to calculate the N-electron wavefunction (WFT), it only deals with the electron density $\rho(\mathbf{r})$ and energy as a functional of ρ.

The density functional theory (DFT) is based upon the theorems by Hohenberg and Kohn, stated as:

1. The ground-state electron density, $\rho(\mathbf{r})$, uniquely determines the external potential, $V_{ext}(\mathbf{r})$. Furthermore, $\rho(\mathbf{r})$ also determines the number of electrons of the system, such that, $\int \rho(\mathbf{r})d^3\mathbf{r} = N$ which follows that the electron density can predict the ground-state energy, E_0, and many other properties of the ground states[8]. In other words, density functional theory, arises from the fact that energy, and hence other properties, are functionals of the ground-state electron density, $E[\rho(\mathbf{r})]$.

2. The second Hohenberg-Kohn theorem depicts that, given any trial density, such that $\tilde{\rho}(\mathbf{r}) \geq 0$ and $\int \rho(\mathbf{r})d\mathbf{r} = N$, the ground state energy follows the variational principle,

$$E_0[\rho(\mathbf{r})] \leq E_v[\tilde{\rho}(\mathbf{r})] \tag{2.22}$$

Also, this is to keep into account that the principle holds good when the exact energy functional is used. The total energy functional further can be further

decomposed into various energy functional contributions,

$$E[\rho(\mathbf{r})] = T[\rho(\mathbf{r})] + V_{ee}[\rho(\mathbf{r})] + V_{ext}[\rho(\mathbf{r})]$$

$$= \int \rho(\mathbf{r})dv(\mathbf{r}) + F_{HK}[\rho(\mathbf{r})] \qquad (2.23)$$

$$where \qquad F_{HK}[\rho(\mathbf{r})] = T[\rho(\mathbf{r})] + V_{ee}[\rho(\mathbf{r})]$$

where, $T[\rho(\mathbf{r})]$ is the kinetic energy functional, $V_{ee}[\rho(\mathbf{r})]$ is the electron-electron repulsion energy, $V_{ext}[\rho(\mathbf{r})]$ is the external potential which in the absence of any external field comprises of the electron-nucleus attraction attraction energy. In this equation, F_{HK} is a universal functional of the density and it is given by the expectation value of the kinetic energy and of electrostatic electron repulsion terms on the ground state.The Hohenberg-Kohn theorems[9] proved that various properties of atomic and molecular systems were obtainable from the electron density rather than via the wavefunction and was a big achievement of its time indeed. Unfortunately, the HK theorem does not tell about the form of the functional dependence of energy on the electron density.

2.12   v- and N-representability

The ground state electron density is the key to the electronic energy and hence the electronic properties of the system, the electron density has to be *v-representable*. An electron density is considered to be v-representable if it is associated with an antisymmetric ground state wavefunction of a Hamiltonian of the form , corresponding to an external potential $V_{ext}[\rho(\mathbf{r})]$. It is this unique mapping between the v-representable density, $V_{ext}[\rho(\mathbf{r})]$ and the ground state wavefunction that

facilitates in obtaining all the electronic properties of the state. All the properties related to the density are defined only for v-representable electron densities. However, the electron density may or may not be v-representable. Equation 2.22 is v-representable in electron density. Interestingly, not all electron densities are v-representable, and in fact, many densities have been found to be non-v-representable by Levy. Alternatively, the electron density in the functionals and the variational principle do satisfy a much weaker condition called the N-representability by formulating the DFT from a different perspective. N-representability is a pre-requisite for the v-representability condition and any reasonable density that can be obtained from some antisymmetric wave function is N-representable.

2.12.1   Kohn-Sham equations

Density Functional Theory came out to be successful since the year 1965 when Walter Kohn and Sham[10] took care of the modifications of early density-based methods which resulted in poor representations of the kinetic energy functional. To improve the model, they introduced a new functional by mapping the many-body problem into a non-interacting electrons problem with the same ground-state electronic density. The new functional can be obtained by subtracting to F_{HK} some terms of the energy calculated for the non-interacting electrons problem by applying variational principle to the ground state electronic energy with the charge density:

$$\rho(\mathbf{r}) = \sum_{i=1}^{N} \mid \psi_i(\mathbf{r}) \mid^2 \tag{2.24}$$

If $\psi_i(\mathbf{r})$ is the single-particle wavefunction, then kinetic energy of any non-interacting electron comes out to be:

$$T_0 = \langle \psi_i \mid -\frac{1}{2}\nabla^2 \mid \psi_i \rangle \tag{2.25}$$

where the density $\rho(\mathbf{r})$ is represented as in equation 2.24. Furthermore, from $F_{HK}[\rho(\mathbf{r})]$ we can subtract an energy term which defines the non-interacting classical Coulomb interaction of a spatial charge distribution $\rho(\mathbf{r})$ as:

$$E_{classical} = \frac{1}{2} \int \int \frac{\rho(\mathbf{r}_1) - \rho(\mathbf{r}_2)}{\mid \rho(\mathbf{r}_1)\rho(\mathbf{r}_2) \mid} \tag{2.26}$$

and so we write the universal Hohenberg-Kohn functional as:

$$F_{HK} = T_0 + E_{classical} + E_{XC} \tag{2.27}$$

where E_{XC} is the so-called "exchange-correlation" functionals, which contains all terms relevant to the many-body interaction effects, which are not included in the other energy terms. Also, the interaction energy associated with the external potential is described as:

$$E_{ext} = \int V_{ext}(\mathbf{r})\rho(\mathbf{r})d^3\mathbf{r} = \langle \psi_i \mid V_{ext} \mid \psi_i \rangle \tag{2.28}$$

So equation 2.27 can further be simplified as:

$$F_{HK} = T_0 + E_{classical} + E_{XC} + E_{ext}, \tag{2.29}$$

Hence, the KS equation for one-electron orbitals $\psi_i(\mathbf{r}_1)$ have the form[2]:

$$\left\{ -\frac{\hbar^2}{2m_e}\nabla^2 - \sum_{l=1}^{N} \frac{Z_l e^2}{4\pi\epsilon_0 r_{12}}d\mathbf{r}_2 + V_{XC}(\mathbf{r}_1) \right\}\psi_i(\mathbf{r}_1) = \epsilon_i\psi_i(\mathbf{r}_1) \tag{2.30}$$

So the Kohn-Sham equations for the one-electron orbitals $\psi_i(\mathbf{r}_1)$ contains all the terms which besides external potential describes the potential arising due to many-body interactions when treated classically,

$$E_{classical}\psi_i(\mathbf{r}_1) = \left\{ \sum_{l=1}^{N} \frac{Z_l e^2}{4\pi\epsilon_0 r_{12}} d\mathbf{r}_2 \right\} \psi_i(\mathbf{r}_1) \qquad (2.31)$$

and the exchange-correlation potential:

$$V_{XC}[\rho(\mathbf{r})] = \frac{\delta E_{XC}\rho(\mathbf{r})}{\delta\rho(\mathbf{r})} \qquad (2.32)$$

From the solution of the KS equations one obtains the auxiliary single-particle wavefunctions, ψ_i, that give the ground-state electronic density through equation 2.24.

Equation 2.30 describes an electron moving in a potential generated by the nuclei and by the other electrons through their charge density. Since the ground-state charge density depends on the solution itself, in order to solve this equation, the strategy is to utilize a self-consistent iterative procedure: an initial guess for the charge density, $\rho_{org}(\mathbf{r})$, is used to compute the KS potential, V_{KS}, which is needed to diagonalize the KS Hamiltonian and get a new estimate of the density, $\rho_{step_1}(\mathbf{r})$, through the set of single-particle wavefunctions $\psi_i(\mathbf{r}_1)$. From a linear combination of the densities $\rho_{org}(\mathbf{r})$ and $\rho_{step_1}(\mathbf{r})$, another trial density $\rho_{step_2}(\mathbf{r})$ for the next iteration is built. The potential V_{KS} is recomputed from $\rho_{step_2}(\mathbf{r})$,the KS Hamiltonian is further diagonalized to obtain $\rho_{step_2}(\mathbf{r})$, and the iteration step is repeated until the difference between the solutions of two successive iterations is less that the defined tolerance value for convergence.

2.12.2   Exchange Correlation Potential

From the previous discussion it is very clear that an explicit form of $E_{xc}\rho(\mathbf{r})$ is mandatory to specify the KS equations. The search for an accurate $E_{XC}\rho(\mathbf{r})$ has been the greatest challenge in density-functional theory. In the KS scheme the kinetic energy $T_s\rho(\mathbf{r})$ is rigorously treated. One can use the homogeneous electron gas formula solely for the unknown part of the energy functional. This leads to introduction of of the *local-density approximation*, (**LDA**).

$$E_{XC}^{LDA}\rho(\mathbf{r}) = \int \rho(\mathbf{r})\epsilon_{XC}\rho(\mathbf{r})d\mathbf{r} \tag{2.33}$$

where $\epsilon_{XC}[\rho(\mathbf{r})]$ indicates the exchange and correlation energy per particle of a uniform electron gas of density $\rho(\mathbf{r})$. The corresponding exchange-correlation potential of 2.30 in terms of $\rho(\mathbf{r})$ then becomes

$$V_{XC}^{LDA}(\mathbf{r}) = \frac{\delta E_{XC}^{LDA}}{\delta\rho(\mathbf{r})} = \epsilon_{XC}[\rho(\mathbf{r})] + \rho(\mathbf{r})\frac{\partial\epsilon_{XC}\rho(\mathbf{r})}{\partial\rho(\mathbf{r})} \tag{2.34}$$

and the KS orbital equations read

$$\left[-\frac{1}{2}\nabla^2 + V(\mathbf{r}) + \int \frac{\rho(\mathbf{r}')}{|\mathbf{r}-\mathbf{r}'|}d\mathbf{r}' + v_{XC}^{LDA}(\mathbf{r})\right]\psi_i = \epsilon_i\psi_i \tag{2.35}$$

The self-consistent solution of equation 2.35 defines the Kohn-Sham local-density approximation (KS-LDA), or simply *LDA method*.

Application to an atom or molecule or solid of the local-Density approximation of equation 2.33 amounts to assuming that the exchange-correlation energy for a nonuniform system can be obtained by applying uniform electron-gas results to infinitesimal portions of the non-uniform electron electron distribution, each having $\rho(\mathbf{r})d\mathbf{r}$ electrons, and then summing over all space the individual contributions.

The LDA is applicable to systems with slowly-varying densities but cannot be formally justified for highly inhomogeneous systems such as atoms and molecules. The essential justification for its use in atoms and molecules comes from successful numerical applications. A rather improvement and commonly used extension of the LDA is the *generalized gradient approximation* (**GGA**), where the exchange-correlation energy depends locally not only on the charge density C, but also on its gradient, $\bigtriangledown\rho(\mathbf{r})$. Within the scope of this approximation, the exchange-correlation energy can be written as:

$$E_{XC}[\rho(\mathbf{r})] = \int \epsilon_{XC}^{GGA}(\rho(\mathbf{r}), \bigtriangledown\rho(\mathbf{r}))\rho(\mathbf{r})d^3\mathbf{r} \qquad (2.36)$$

In our work we used local density approximated functional by Vosko, Wilk and Nusair (VWN) and gradient-corrected functional proposed by Perdew, Burke, and Ernzerhof (PBE); Perdew and Wang (PW91); Becke exchange (1988) plus Lee-Yang-Parr correlation (B88-LYP) and *meta*-GGA functionals of Tao, Perdew, Staroverov, and Scuseria (TPSS); Perdew, Kurth, Zupan, and Blaha (PKZB), which are fairly simple to implement and still widely adopted in many transition metal cluster applications.

2.13   Effective Core Potential, ECP

Elements having high atomic number have a large number of electrons to deal with involving calculations[10]. During a chemical reaction, the core electrons have little role contributing the reflection towards the same. They are the valence electrons which are considered to provide the maximum contribution towards interpreting the energy and various other physicochemical properties. A convenient way is to expand the overall core orbitals with sufficiently large number of basis functions,

so that the electron-electron repulsions are taken well care of and for the proper description of the valence orbitals.

An additional complication for the well description of elements having higher atomic numbers is relativistic effects, which has been discussed earlier in the previous chapter. The modelling of the core orbitals separately from the valence is called *Effective Core Potential*, (**ECP**) or *Pseudopotential*, (**PP**). The neglect of the explicit treatment of the core orbitals are known to provide good results at a fraction of the price of the heavy computational resources to be used for performing all-electron calculations.

2.14 Addressing Relativistic Effects

Relativistic effects are best described within the four-component Dirac theory generalized to many-electron systems[11]. This method is not recommended often as the method is computationally expensive.

The most popular method way for the relativistic effects by modeling the inner electrons of atoms with effective core potentials (ECPs) that are fitted to the results of relativistic all-electron calculations. This is the most preferred way for inclusion of relativistic effects in self-consistent field (SCF) procedures. However, in most program systems this facility is restricted to scalar relativistic effects that include the effect of relativistic mass/velocity and the Darwin-shift, but omit spin-orbit coupling (SOC). The latter effect has been efficiently be included by a second variational treatment[12] allowing to calculate spin-orbit coupling. In this approach the spin orbit term is set up in a subspace spanned by the scalar relativistic solution with about twice the number of the occupied orbitals but much less than the full basis. The proper treatment of spin-orbit coupling may require an improved basis set, in particular for semi-core states of heavy elements. Spin

polarized calculations can provide both spin and orbital moments in magnetic materials.

2.15 DFT based Reactivity Descriptors

DFT-based reactivity descriptors represent the response of a system to a specific perturbation. This perturbation might be a change in the total number of electrons N or in the nuclear configuration $v(\mathbf{r})$. For a comprehensive and extended literature about both the theoretical aspects as well as applications, we refer to the Parr and Yang's 'Density Functional Theory of Atoms and Molecules' [8].An overview of the definitions of DFT-based indicators is given in Table 2.1. In the remainder of this section a brief discussion of their properties is given.

TABLE 2.1: DFT-based reactivity descriptors: Global and Local

Global Descriptors	**Local Descriptors**
$\mu = \left(\frac{\partial E}{\partial N}\right)_{v(\mathbf{r})}$	$\rho(\mathbf{r}) = \left(\frac{\partial E}{\partial v(\mathbf{r})}\right)_{N}$
$\eta = \frac{1}{2}\left(\frac{\partial^2 E}{\partial N^2}\right)_{v(\mathbf{r})} = \frac{1}{2}\left(\frac{\partial \mu}{\partial N}\right)_{v(\mathbf{r})}$	$\eta(\mathbf{r}) = \frac{1}{2}\left(\frac{\partial \mu}{\partial \rho(\mathbf{r})}\right)_{v(\mathbf{r})}$
$S = \frac{1}{2}\eta = \left(\frac{\partial N}{\partial \mu}\right)_{v(\mathbf{r})}$	$s(\mathbf{r}) = \left(\frac{\partial \rho(\mathbf{r})}{\partial \mu}\right)_{v(\mathbf{r})}$
$\omega = \frac{\mu^2}{2\eta}$	$f(\mathbf{r}) = \left(\frac{\partial^2 E}{\partial N \partial v(\mathbf{r})}\right) = \left(\frac{\partial \rho(\mathbf{r})}{\partial N}\right)_{v(\mathbf{r})} = \left(\frac{\partial \mu}{\partial v(\mathbf{r})}\right)_{v(\mathbf{r})}$
$\nu = \frac{2\eta}{\mu^2}$	
$\lambda_N = exp\left(-\frac{1}{10}(sgn)(\eta+\mu)\left(\frac{(\eta+\mu)^2}{2\eta}\right)\right)$	
$\lambda_E = exp\left(-\frac{1}{10}\left(\frac{(\mu-\eta)^2}{2\eta}\right)\right)$	

2.15.1 Global Reactivity Descriptors

Global descriptors are used to discuss the reactive behavior of one single molecule or a set of related molecules, providing reactivity sequences for the latter. The first order derivative towards N equals the chemical potential μ. It is the cornerstone

of "conceptual DFT" as it provides a chemical interpretation for the Lagrange-multiplier in the equation:

$$\frac{\partial F_{HK}[\rho(\mathbf{r})]}{\partial[\rho(\mathbf{r})]} + v(\mathbf{r}) = \mu \tag{2.37}$$

The aforementioned relationship points out that the chemical potential is the effective electrostatic potential experienced by the electron density. Hence, this quantity characterizes the escaping tendency of the electron cloud from the equilibrium state[13]. The chemical potential was also recognized to be equal to an important chemical concept, which is the electronegativity, χ where, $(\mu = -\chi)$.

The second derivative of the quantity of F_{HK} with respect to N, represents the *global hardness*, $\eta(\mathbf{r})$[14]. This quantity characterizes the resistance towards charge transfer, and is correlated to the stability of the reagent[15, 16]. The global hardness was found within an orbital approach using Koopmans' theorem which is to be related to the energy gap between the Highest Occupied Molecular Orbital (HOMO) and lowest unoccupied molecular orbital (LUMO). The reciprocal of the global hardness is the *global softness*, S, which is also a measure of polarizability[17]. It is usual that the small, non polarizable, and highly charged species behave as hard reagents, while larger, more polarizable, and less charged species act as soft. In the majority of the studies published in literature so far, the global descriptors are computed applying the simple finite difference method and taking the arithmetic average of the left- and right-hand-side derivatives. The vertical ionization potential (IP) and electron affinity (EA) consequently form the basic quantities. The disadvantage of this conceptually simple method is that it only requires three energy calculations (corresponding to the N, $N-1$ and $N+1$ systems). In addition with possible stability problems of the $N+1$ and $N-1$ structures, use of orbital energies, applying Koopmans' theorem to approximate the finite difference method, might be more appropriate. This particular theorem states that the IP and the EA of an N-electron system can be identified with the

orbital energy of the highest occupied molecular orbital (HOMO) and lowest un-occupied molecular orbital (LUMO), respectively. This approximation is basically applicable when orbital relaxation effects can be neglected upon addition or re-moval of an electron. That is the reason for which the finite difference method is applied to the event to the geometries undergoing vertical ionization.

Other descriptors also exist to describe the ability of a molecule to accept or donate electrons, i.e. the electrophilic or nucleophilic behavior, respectively. These properties can be identified as combinations of μ and η. In this light, the 'philicity' ω is defined as the change in energy that occurs when a reagent is placed in contact with the perfect nucleophile (that is, a reservoir of electrons with zero chemical potential and zero hardness)[18].

2.15.2 Local reactivity descriptors

Local descriptors provide direct information about the site-selectivity within a molecule and indicate at which site the reaction preferentially will occur. Using standard perturbation techniques, the second order, mixed derivative equals the Fukui function $f(\mathbf{r})$[19]. This quantity is normalized to unity and can be seen as an **intra-molecular descriptor**. The Fukui function is a general outcome of the frontier molecular orbital approach (FMO) developed by Fukui in 1952, in which the importance of the frontier orbitals (HOMO and LUMO) is most prominent. This relation is shown in the following equations, taking into account the N-discontinuity problem using the finite difference method, followed by freezing all orbitals, with exception of the frontier orbitals:

$$f^+(\mathbf{r}) \approx \rho_{N+1}(\mathbf{r}) - \rho_N(\mathbf{r}) \approx \rho_{LUMO},$$

$$f^-(\mathbf{r}) \approx \rho_N(\mathbf{r}) - \rho_{N-1}(\mathbf{r}) \approx \rho_{HOMO}, \qquad (2.38)$$

$$f^0(\mathbf{r}) \approx \frac{\rho_{N+1}(\mathbf{r}) - \rho_{N-1}(\mathbf{r})}{2} \approx \frac{\rho_{LUMO} + \rho_{HOMO}}{2}.$$

The relation between the Fukui functions and the frontier orbitals was established by Yang et *al.*[20].

The *local softness*, s($\mathbf{r}$), is another frequently used local indicator, describing intermolecular site reactivity as it contains all information of the $f(r)$ descriptor. The correlation between both quantities is $(s(\mathbf{r}) = Sf(\mathbf{r}))$, where, S is the *global softness*.

Using the finite difference method, the following equations are obtained:

$$f_k^+ = q_k^{(N+1)} - q_k^{(N)} \text{ and equivalently, } s_k^+ = S(q_k^{(N+1)} - q_k^{(N)}),$$

$$f_k^- = q_k^{(N)} - q_k^{(N-1)} \text{ and equivalently, } s_k^- = S(q_k^{(N)} - q_k^{(N1)}), \qquad (2.39)$$

$$f_0^k = \frac{(q_k^{(N+1)} - q_k^{(N1)})}{2} \text{ and equivalently, } s_0^k = \frac{S(q_k^{(N+1)} - q_k^{(N1)})}{2}.$$

In these equations $q_k^{(N)}$ is the electron population on the kth atom of the molecule with N electrons. This population can be calculated using various population analysis methods such as Mulliken[21], Lowdin [22], Natural Population Analysis (NPA)[23], Hirshfeld[24] and many others based on the electrostatic potential. The influence of the population analysis method on the resulting condensed values is most of the times remarkable, and a substantial amount of critical studies have been addressed to this topic in literature[25]. Computing condensed descriptors sometimes lead to negative values, and although this is rather peculiar, still there is no theoretical reason why this should not be acceptable. Roy et *al.* attributed

these negative values to relaxation effects and improper population analysis techniques [26]. In order to overcome the issue of negative condensed Fukui functions, new descriptors, i.e. the *relative nucleophilicity*, $(= \frac{s^-}{s^+}$ or $\frac{f^+}{f^-})$ and *relative electrophilicity* $(= \frac{s^+}{s^-}$ or $\frac{f^-}{f^+})$ were introduced[27]. In this thesis, these quantities have been computed and used to predict the intra-molecular reactivity trend among the novel gold cluster. Within the context of hard and soft species, the *local hardness descriptor*, $\eta(\mathbf{r})$, is also of similar interest.

2.15.3 HSAB principle

The hardness and softness descriptors had attained much of attention among chemists, due to their importance within the well-known hard and soft acids and bases (HSAB) principle. Pearson originally proposed this principle in 1963[28], and it was recognized as an important and fundamental chemical principle with special utility especially in inorganic chemistry. The principle indicates that hard acids prefer binding with hard bases (often forming bonds with substantial ionic character) and soft acids prefer to coordinate with soft bases (often forming bonds with substantial covalent character). The principle can be applied at a global description, $(S_A = S_B$, interaction between system A and system B) and local $(s_{Ai} = s_{Bj}$, interaction between atom i of system A and atom j of system B) level. The softness-matching hypothesis in the case of multiple sites of interaction is still a challenging subject, and further research is continued on the very topic.

Electron-transfer effects favor the formation of the soft-soft product, whereas electrostatic effects favor the formation of the hard-hard product. In this light, the categorization into two types of reactions, according to the hard or soft character of the reactants, leads to a better understanding of the HSAB principle and its validity. This twofold classification is obviously similar to that of Klopman, who made a distinction between charge controlled and frontier orbital controlled reactions[29]. The latter group corresponds to the formation of covalent bonds,

associated with partial electron transfer from the highest occupied orbital of the base to the lowest unoccupied orbital of the acid. The first group can be associated with ionic bonding, dominated by the electrostatic attraction between the acid and the base.

2.16   Optimization Techniques

Optimization of the atomic configuration to the local potential energy minimum is the basic to-do in computer simulations performed in this thesis. The minimum energy structure is needed for vibrational spectra calculations as well as for geometrical and structural comparisons and calculation of various electronic properties. The potential energy surface (PES) is a complicated, three dimensional function of the coordinates. Various efficient methods exist to determine a minimum on the potential energy surface.

2.16.1   First-order methods

Minimization techniques have been mainly classified in two different categories: first-order methods that use the first derivative and second order methods that use both first and second derivatives of the forces. The *conjugate-gradients* technique, a first-order method, in which, the stationary points of a function $F(x)$ are defined by[30]:

$$g_i = \left(\frac{\partial F(x)}{\partial x} \right)_{x_i} = 0 \tag{2.40}$$

In the absence of any information about the function $F(x)$, the first step to the optimum direction from the point x_i is done in the direction of steepest descent g_i, $x_{i+1} = x_i - \alpha g_i$, but subsequent searches are preformed along a line which is a mixture of the current negative gradient and the previous search direction, $d_i = -g_i + \beta_i d_{i-1}$, where β is a scalar constant.

2.16.2   Second-order methods

The second-order methods in addition to the first-order methods, use the second derivatives to locate a minimum. The matrix of second derivatives, the *Hessian matrix*, is:

$$\frac{\partial^2 F(x)}{\partial x^2}\bigg|_{x_i} = H_i \tag{2.41}$$

The greater advantage of the second order methods is that these provide valuable information about the curvature of the function, which can be exploited to find stationary points more efficiently and are faster than the first-order methods. If all eigenvalues of H are negative, the stationary point corresponds to a maximum and on the other hand, if they are positive, the minimum. In the case of negative and positive eigenvalues a saddle point was found. The expansion of the function $F(x)$ around x_i into a Taylor series is:

$$Fx = Fx_i g_i^{\dagger} x - x_i \frac{1}{2} x - x_i^{\dagger} H_i (x - x_i) \tag{2.42}$$

For the gradient of the second-order approximation to be zero produces the step: $(x - x_i) = -H^{-1}g$. This scheme is called the *Newton-Raphson method*. For a purely quadratic function it seeks for the minimum in first step from any point on the surface. However, in practice the surface is only quadratic to a first approximation. This implies that various number of steps will be required, at each of which the Hessian matrix must be calculated and inverted. The direct calculation of the second derivative can be a ten times more demanding than calculating the gradient. An alternative updating scheme is however popular, which is the *quasi-Newton* methods in which the inverse Hessian matrix is gradually built up in successive iterations instead of considering the exact H . The initial H matrix can be just a unit matrix, the first step resembles a steepest descent step. As the optimization proceeds, the gradients at the previous points are used to make the

Hessian a better approximation for the actual system. After two steps, the updated Hessian is a better approximation to the exact Hessian, in the direction defined by these two points. The second-order approximation method implemented in the density functional theory code 'deMon' has been used throughout this thesis. However, there are many updating schemes, one of which was also used in the calculations for this thesis, is the Broyden-Fletcher-Goldfarb-Shano (BFGS) scheme[31], its update formula is given by:

$$H_{i+1} = H_i + \frac{(x_{i+1} - x_i) \otimes (x_{i-1} - x_i)}{(x_{i-1} - x_i) \cdot (g_{i+1} - g_i)} - \frac{[H_i \cdot (g_{i+1} - g_i)] \otimes [H_i \cdot (g_{k+1} - g_i)]}{(g_{i+1} - g_i) \cdot H_i \cdot (g_{i+1} - g_i)}$$
$$+ [(g_{i+1} - g_i) \cdot H_i (g_{i+1} - g_i)] u \otimes u$$

$$(2.43)$$

where, $u = \frac{(x_{i+1} - x_i)}{(x_{i+1} - x_i) \cdot (g_{i+1} - g_i)} - \frac{[H_i \cdot (g_{i+1} - g_i)]}{(g_{i+1} - g_i) \cdot H_i \cdot (g_{i+1} - g_i)}$.

The symbol $\otimes$ when interposed between two vectors means that a matrix is to be formed. It is well known fact that the quasi-Newton method does not converge as fast as the Newton-Raphson method, but since each step of the former one takes significantly less time than the true Hessian matrix calculation, the overall computational effort is smaller.

The optimization is performed by using all distances, bending and torsional angles between atoms within bonding distance as variables, i.e. using redundant internal coordinates (the number of coordinates is larger than $3N - 6$)[32]. Internal coordinates appear to be a good choice for efficient quasi-Newton optimization[33].

2.16.3   Global minimum search

The methods described in the previous sections can only locate the "nearest" minimum, which is normally a 'local minimum', while initiating from a given set

of variables. It is notable that the energy minimum search is especially difficult if the systems with the large number of atoms to be studied. As an alternative to "static" optimization techniques, *molecular dynamics* or *simulated annealing* might be used in search for **global minimum**. Molecular dynamics methods helps the molecules to be able to overcome barriers separating minima if the barrier height is less than the total energy minus the potential energy. Given a high enough energy, which is related to the simulations temperature, the dynamics will sample the whole surface.

A search for the global minimum structure can be performed by using simulated annealing. Starting from sufficiently high temperature (for the system being investigated) at long run time, all the conformations can be sampled. The structures generated can thus be now subjected to geometry optimizations for search of global minima using the methods discussed in previous section of this chapter.

2.17   Molecular Dynamics

Molecular Dynamics describes the time dependent behavior of a group of particles in space under the influence of forces acting between the particles, as well as the external forces [34]. MD methods are routinely used to investigate the structures and dynamics of molecules, clusters and complexes. At the molecular scale, molecular dynamics simulations generate information at the microscopic level, including atomic positions and velocities. Statistical mechanics provides the rigorous mathematical expressions that relate macroscopic properties, such as energy, thermochemical properties viz., heat capacity, and so on towards the distribution and motion of the atoms of the N-body system.

2.17.1   Classical Molecular dynamics

The basic formalism of MD simulations is common for all methods (the electronic structure calculations or the force fields) and often when based on classical Newtons laws, then the formalism is called classical MD. For an assembly of N-atoms with positions r_i and masses m_i , the trajectory is obtained by solving the differential equations:

$$\frac{d^2 r_i}{dt^2} m_i = F_i \equiv -\frac{dE}{dr_i} \tag{2.44}$$

where F_i is the force exerted on the particle i. Quantum and classical approaches differ in the way of treating the potential energy function $E(r_i)$. It is computed either by solving the Schrödinger equation or by substituting a parametrized force field. The equations of motion are integrated further by using a finite difference method. The integration is further broken down into many small stages separated by a fixed small time interval, δt. The total force on each particle in the configuration at a time t is calculated as the vector sum of its interactions with other particles, which are then combined with the positions and velocities at a time t to calculate the positions and velocities at time $t + \delta t$. All the integration schemes assume that the positions and dynamic properties, can be approximated as Taylor series expansions. A number of numerical algorithms have been developed for integrating the equations of motion, and of these algorithms the 'velocity Verlet' algorithm[35], based on the original Verlet algorithm[36]. Initiating from $r_i(0)$ and $v_i(0)$, the trajectories of the N-particles are generated iteratively as:

$$r_i(t + \delta t) = r_i(t) + \delta t v_i(t) + \frac{\delta t^2}{2m_i} F_i(t),$$
$$v_i(t + \delta t) = v_i(t) + \frac{\delta t}{2m_i}[F_i(t)F_i(t + \delta t)]. \tag{2.45}$$

It is understood that the most computationally demanding part is the calculations of the forces at each iteration. The major criteria for the integration algorithm

choice are that:

1. The algorithm should conserve energy and momentum,

2. it must be computationally efficient, and

3. it should permit a long time step for integration.

The integration procedure shows that to calculate a trajectory, one only needs the initial positions of the atoms, initial distribution of velocities and the potential energy function. The equations of motion are deterministic, e.g., the positions and the velocities at time zero determine the positions and velocities at all other times, t . The initial positions can be obtained from experimental structures and velocities are usually determined from a random distribution with the magnitudes conforming to the required temperature and corrected so that there is no overall momentum, i.e., for a system of N atoms: $P = \sum_{i=1}^{N} m_i v_i = 0$. The velocities, v_i, are often chosen randomly from a Maxwell-Boltzmann or Gaussian distribution at a given temperature, which gives the probability that an atom i has a velocity v_x in the x direction at temperature T:

$$p(v_{x_i}) = \left(\frac{m_i}{2k_BT}\right)^{\frac{1}{2}} exp[-\frac{m_i v_{x_i}^2}{2k_BT}] \qquad (2.46)$$

with a temperature, T, given as:

$$T = \frac{1}{(3N)} \sum_{i=1}^{N} \frac{|p_i|}{2m_i} \qquad (2.47)$$

2.17.2 Born-Oppenheimer Molecular Dynamics (BOMD)

In this thesis we have used the Born-Oppenheimer molecular dynamics (BOMD) implemented in deMon2K code which has been discussed briefly in the later

section[37]. From equation 2.44 it is evident that MD is not tied to any particular electronic structure method. The forces can be computed at Hartree-Fock level, however, the computational time requirements is the bottleneck for post-HF methods, which is again main advantage of DFT. It is also clear that the strength as well as the weakness of a particular ab initio MD implementation is a strength and/or weakness of the chosen electronic structure method. The Newton equation of motion, equation 2.44 for BOMD in general:

$$\frac{d^2 R_i}{dt^2} m_i = - \nabla_i \, min_{\psi_0} \mid \langle \psi_0 \mid H_e \mid \psi_0 \rangle \mid \tag{2.48}$$

and for DFT:

$$\frac{d^2 R_i}{dt^2} m_i = - \nabla_i \, min_{\{\psi_i\}} E^{KS}[\{\psi_i\}] \tag{2.49}$$

Thus the static electronic structure problem in each molecular time step is solved for the set of fixed nuclear positions $\{\mathbf{R_i}\}$. The nuclei move according to classical mechanics in an effective potential due to the electrons. This potential is a function of only the nuclear positions at time t as a result of averaging H_e over the electronic degrees of freedom. In BOMD, the minimum of $\langle H_e \rangle$ has to be reached at every step, in DFT the minimum of the Kohn-Sham functional E_{KS} is obtained by varying the energy functional in the equation 2.30 with respect to the density $\rho(\mathbf{r})$. The time step choice in BOMD depends on the structure and, in particular, on the type of atoms involved. The value of the time step is a compromise between the efficiency and accuracy of algorithm and trajectory. The total energy conservation and small range of the energy fluctuations are the main indicators of the correct time step choice. The most typical time steps for the simulations are in the range of 0.5 fs to 1 fs. Ab initio MD for constant temperature simulations this is fixed by using Nose-Hoover or Berensden thermostat. In this thesis, Berensden thermostat has been used for studying the finite temperature behavior of gold clusters.

2.17.3   Car-Parinello Molecular Dynamics (CPMD)

Another very popular molecular dynamics (MD) scheme was proposed by Car and Parrinello in 1985[38]. The advantage over other MD schemes such as Born-Oppenheimer molecular dynamics is that the forces on the nuclei of the electronic structure are calculated "on-the-fly", which means that for each geometry step a single wave function is performed. This is in opposition to Born-Oppenheimer molecular dynamics (BOMD), where the Kohn-Sham equations have to be solved iteratively after each change of the atomic coordinates. The key idea of the Car-Parrinello method is the definition of a fictitious dynamical system whose potential energy surface E is an appropriate functional of both ionic and electronic degrees of freedom. The fictitious system is devised in such a way that the trajectories generated by its dynamics reproduce very closely those of the physical system with potential energy surface, ν.

The classical Lagrangian of the physical system is given by the sum of the ionic kinetic energy and the ionic potential energy with reversed sign.

$$\mathcal{L}^{el} = \frac{1}{2} \sum_I M_I \dot{\mathbf{R}}_I^2 - \nu[\{\mathbf{R}_I\}^2] \tag{2.50}$$

where M_I is the mass of atom I.

The generalized classical Lagrangian of the system is defined as:

$$\mathcal{L} = \sum_{i=1}^{N} \int \mu_i \mid \dot{\psi}_i(\mathbf{r}) \mid^2 d(\mathbf{r}) + \frac{1}{2} \sum_I M_I \dot{\mathbf{R}}_{\mathbf{I}}^2 - E[\{\psi_i\}, \mathbf{R}_{\mathbf{I}}] + \sum_{ij} \Lambda_{ij} \left(\psi_i^*(\mathbf{r})\psi_j^*(\mathbf{r})d(\mathbf{r}) - \delta_{ij} \right)$$
$$\tag{2.51}$$

$\mathcal{L}$ is a functional of two sets of classical degrees of freedom, i and R_I. The ψ_i are arbitrary parameters of units $(\text{mass}) \times (\text{length})^2$ which play the role of generalized

masses for the electronic degrees of freedom. For simplicity a unique μ is used for the Ψ_i, which is independent from the electronic state. The first and second terms in equation 2.51 are the kinetic energy of the electronic and ionic degrees of freedom. E is the potential energy of the coupled electron-ion fictitious system. The Lagrangian multipliers Λ_{ij} are used to impose orthonormality conditions on the ψ_i.

The Euler equation associated with the Lagrangian of the *physical system* is:

$$M_I \ddot{R}_I = -\frac{\partial \nu[\{\mathbf{R_I}\}]}{\partial \mathbf{R_I}} \tag{2.52}$$

The equations of motion derived from the Lagrangian of the system under consideration are:

$$\mu \ddot{\Psi}_i = -\frac{\delta E}{\delta \psi_i^*} + \sum_j \Lambda_{ij} \psi_j,$$
$$M_I \ddot{\mathbf{R_I}} = -\frac{\partial E}{\partial \mathbf{R_I}} \tag{2.53}$$

In general the trajectories generated by equation 2.52 and those obtained from equation 2.54 do not coincide unless $E[\psi_i; \{\mathbf{R_I}\}]$ is at the instantaneous minimum. However, the parameter μ and the initial conditions for $\psi_{i,0}$, $\dot{\psi}_{i,0}$ is chosen in such a way that the time-scale for the electronic degrees of freedom is much shorter than that of the nuclei. In this case nuclear trajectories, initially lying on the Born-Oppenheimer surface, will deviate from it only after times that are significantly longer than the MD time step. In other words, if these parameters are chosen so that the two sets of classical degrees of freedom, ions and electrons, are only weakly coupled, the transfer of energy between them is small enough to allow the electrons to follow adiabatically the ionic motion, remaining close to the Born-Oppenheimer surface.

2.17.4 Vibrational Spectroscopy Calculation

Similar to that of molecular dynamics simulations, first principles vibrational spectroscopy calculations are not tied to any particular electronic structure method.

DFT is effective and sufficiently accurate method for vibrational spectra calculations and in particular applicable to clusters and molecules. In practice, the calculated harmonic vibrational frequencies, depending on the computational method, are underestimated or overestimated as compared to fundamentals observed experimentally. However, the error is relatively systematic, and as a result frequency scaling factors are often applied[39]. The major source of this disagreement is the neglect of the anharmonicity, finite basis set size, and the errors due to the XC-functionals. Several studies reported the quality of the harmonic frequencies predicted by various DFT functionals as compared to other methods[40]. One more practical issue in the vibrational normal modes calculations is the optimized molecular geometry. If the fundamental frequencies for rotations are not "close enough" to zero, or they are vibrational frequencies are "negative" it most probably means that the system is not at the equilibrium.

2.17.5 Potential energy surface calculation

In the Born-Oppenheimer approximation, the Potential Energy Surface (PES) of a molecule can be defined as the surface described by the potential energy function of the molecule with respect to the molecular geometry. The surface dimension depends on the number of atoms of the molecule (3N-5 for polyatomic molecules, with N being the number of atoms, and the potential energy the extra dimension). Due to the large number of dimensions of these polyatomic surfaces, they are commonly known as hyper-surfaces. The hyper-surfaces are described by the Schrödinger equation, whose solution gives the molecular energy as a function of the nuclear coordinates. However, the Schrödinger equation has an infinite

number of solutions, which correspond to the different electronic states of the molecule, and each state has its own hyper-surface. The topology of the hyper-surface drives all the processes of the molecule in that particular electronic state. The PES topology of the excited states is different from that of the ground state, and hence, the regions (geometries) that the molecule can access are different too. Consequently, there are also processes which can only take place in excited states.

2.17.6 Traditional Parameters for analysis of BOMD trajectories

The insight of the cluster system and the motion of atoms within it is understood and analyzed through two traditional thermodynamic parameters viz. RMS and MSD[41] in the work presented in this thesis. For the sake of completeness we briefly discuss these properties below:

2.17.6.1 Root-Mean Squared BLF

The parameter **root-mean squared bond-length fluctuation** (RMS-BLF or δ_{rms}) are computed for trajectory at each temperature for individual clusters. The parameter δ_{rms} is a measure of the fluctuations in the bond lengths averaged over all the atoms and over the total time span. It is defined as:

$$\delta_{rms} = \frac{2}{N(N-1)} \sum_{i<j} \frac{\sqrt{\langle R_{ij}^2 \rangle_t - \langle R_{ij} \rangle_t^2}}{\langle R_{ij} \rangle_t} \tag{2.54}$$

where, N is the number of particles in the system, r_{ij} is the distance between the ith and j^{th} particle in the system and $<...>_t$ denotes a time average over the entire trajectory.

2.17.6.2 Mean Squared Displacements

The MSD is another widely used parameter for analyzing a solid-like-to-liquid-like transition. In the present work, we calculate the mean-squared displacements for individual atoms, which is defined as:

$$\langle R_i^2 \rangle = \frac{1}{M} \sum_{m=1}^{M} [R_i(t_{0m} + t) - R_i(t_{0m})]^2 \tag{2.55}$$

where $\mathbf{R}_I$ is the position of the Ith atom and we average over M different time origins t_{0m} spanning the entire trajectory. The MSD indicates the displacement of an atom in the cluster as a function of time. In the solid-like region, all atoms perform oscillatory motion about fixed points resulting in negligible MSDs of individual atoms from their equilibrium positions. In a liquid-like state, on the other hand, atoms diffuse throughout the cluster and the MSDs eventually reach a saturated value of the order of the square of the cluster radius.

2.18 deMon2K code

The software package for density functional theory (DFT), by the name 'deMon', has been used for implementing the work presented in this thesis. The name de-Mon, stands for, *density of Montreal*. The earliest version of deMon was the deMon-KS set of programs. The modification of the deMon-KS further led to the new version of the deMon called the deMon2k[42]. The deMon2k software has a variety of features and can be used for a range of calculations, namely, geometry optimization, transition state search, single-point energy calculations, *Born-Oppenheimer Molecular Dynamic Simulations* (BOMD), *Time-dependent DFT* (TDDFT), Mulliken, Löwdin and Bader population analysis, and so on. Calculation of properties like polarizabilities, hyperpolarizabilities, NMR, IR and

Raman spectra and intensities, and thermodynamic data of atoms, molecules and solids. It has interfaces for visualization packages like Molden, Molekel and

FIGURE 2.1: The 128 cores Intel(R) Xeon(R) CPU 5160@3.00GHz cluster computer - BOSE, used mainly for the work in this thesis.

Vu and is portable to various computer platforms and operating systems. Several developments and implementations in deMon ranging from analytical to numerical schemes for properties and a variety of applications are available. The deMon set of programs is a modern density functional theory (DFT) package based on the Kohn-Sham (KS) method and uses the linear combination of atomic orbitals (LCAO) framework with Gaussian type orbital (GTO) basis sets centered on atoms and effective core potentials (ECP). Although both deMon-KS and deMon2K are based

on the KS method although the structure of the two programs are quite different from each other.

Bibliography

[1] Gutzwiller, M. C. *Rev. Mod. Phys.* **1998**, *70*, 589.

[2] Atkins, P. W. *Molecular Quantum Mechanics*, **1986**, Oxford University Press.

[3] Szabo, A.; Ostlund, N. S. *Modern Quantum Chemistry: Introduction to Advanced Electronic Structure Theory*, **1989**, McGraw-Hill, Inc.: New York.

[4] Slater, J. C. *Phys. Rev.* **1930**, *36*, 57.

[5] Boys, S. F. *Proc. R. Soc. (London)* **1950**, *A200*, 542.

[6] Roothaan, C. C. J. *Rev. Mod. Phys.* **1951**, *23*, 69.

[7] Hall, G. G. *Proc. Roy. Soc. (London)* **1951**, *A205*, 541.

[8] R. G. Parr and W. Yang, *Density functional theory of atoms and molecules*, **1989**, Clarendon Press, New York.

[9] Hohenberg, P., Kohn, W. *Phys. Rev.* **1964**, *B136*, 864.

[10] Jensen, F. *Introduction to Computational Chemistry, Second Edition John Wiley and Sons, Ltd.*, **2007**, West Sussex.

[11] P. Schwedtfeger (Ed.), *Relativistic Electronic Structure Theory, Part 1: Fundamentals, Elsevier Science B.V.*, **2002**, Amsterdam.

[12] MacDonald, A. H.; Pickett, W. E.; Koelling, D. D. *J. Phys. C: Solid State Phys.* **1980**, *13*, 2675.

[13] Kohn, W.; Becke, A. D.; Parr, R. G. *J. Phys. Chem.* **1996**, *100*, 12974.

[14] Parr, R. G.; Pearson, R. G. *J. Am. Chem. Soc.* **1983**, *105*, 7512.

[15] Ayers, P. W.; Parr R. G., *J. Am. Chem. Soc.* **2000**, *122*, 2010.

[16] Pearson R. G. *J. Chem. Educ.* **1987**, *64*, 561.

[17] Politzer, P. *J. Chem. Phys.* **1987**, *86*, 1072.

[18] Maynard, A. T.; Huang, M.; Rice, W. G.; Covell, D. G. *Proc. Natl. Acad. Sci. U.S.A.* **1998**, *95*, 11578.

[19] Parr, R. G.; Yang W., *J. Am. Chem. Soc.* **1984**, *106*, 4049.

[20] Yang, W.; Parr, R. G.; Pucci, R. *J. Phys. Chem. 1984*, *81*, 2862.

[21] Mulliken, R. S. *J. Chem. Phys.* **1955**, *23*, 1833.

[22] Lowdin, P. -O. *J. Chem. Phys.* **1950**, *18*, 365.

[23] Reed, A. E.; Curtiss, L. A.; Weinhold, F. *Chem. Rev. 1988*, *88*, 899.

[24] Hirshfeld, F. L. *Theor. Chim. Acta* **1977**, *44*, 129.

[25] (a)De Proft, F.; Martin, J. M. L.; Geerlings, P. *Chem. Phys. Lett.* **1996**, *256*, 400. (b) De Proft, F.; Martin, J. M. L.; Geerlings, P. *Chem. Phys. Lett.*, **1996**, *250*, 393.

[26] (a) Roy, R. K.; Pal, S.; Hirao, K. *J. Chem. Phys.* **1999**, *110*, 8236. (b) Roy, R. K.; Hirao, K.; Pal, S. *J. Chem. Phys.* **2000**, *113*, 1372. (c) Roy, R. K.; Hirao, K.; Krishnamurty, S.; Pal, S. *J. Chem. Phys.* **2001**, *115*, 2901.

[27] (a) Roy, R. K.; Krishnamurti, S.; Geerlings, P.; Pal, S. *J. Phys. Chem. A* **1998**, *102*, 3746. (b) Roy, R. K.; De Proft, F.; Geerlings, P. *J. Phys. Chem. A* **1998**, *102*, 7035.

[28] Pearson, R. G.; *Science* **1966**, *151*, 172.

[29] Klopman, G. *J. Am. Chem. Soc.* **1968**, *90*, 223.

[30] M. C. Payne, M. P. Teter, D. C. Allan, T. A. Arias, J. D. Joannopoulos. *Rev. Mod. Phys.* **1992**, *64*, 1045.

[31] Fletcher, R. *In Practical Methods of Optimization*, **1980**, *vol. 1*, Wiley, New York.

[32] Peng, C.; Ayala, P. Y.; Schlegel, H. B.; Frisch, M. J. *J. Comp. Chem.* **1996**, *17*, 49.

[33] Eckert, F.; Pulay, P.; Werner, H.-J. *J. Comp. Chem.*, **1997**, *18*, 1473.

[34] Allen, M.; Tildesley, D. *Computer Simulations of Liquids* **1989**, Oxford Press, Oxford.

[35] Swope, W. C.; Anderson, H. C.; Berens, P. H.; Wilson, K. R. *J. Chem. Phys.* **1982**, *76*, 637.

[36] Verlet, L. *Phys. Rev. 159*, **1967**, 98.

[37] Marx, D.; Hutter, J. *Ab initio molecular dynamics: theory and implementation, in Modern Methods and Algorithms of Quantum Chemistry, ed. J. Grotendorst*, **2000**, *1*, 301.

[38] Car, R.; Parrinello, M. *Phys. Rev. Lett.* **1985**, *55*, 2471.

[39] (a) Scott, A. P.; Radom, L. *J. Phys. Chem.* **1996**, *100*, 16502. (b) Wong, M. W. *Chem. Phys. Lett.* **1996**, *256*, 391.

[40] Zhou, X.; Wheeless, C. J. M.; Liu, R. *Vib. Spectrosc.* **1996**, *12*, 53.

[41] (a)Kanhere, D. G.; Vichare, A.; Blundell, S. A. *Reviews in Modern Quantum Chemistry*, edited by K. D. Sen, World Scientic, Singapore, 2001. (b) Berry, R. S., Haberland, H. *Clusters of Atoms and Molecules I*, edited by H. Haberland Springer-Verlag, Berlin, 1994.

[42] deMon2k, Koster, A. M.; Calaminici, P.; Casida, M. E.; FMoreno, R.; Geudtner, G.; Goursot, A.; Heine, T.; Ipatov, A.; Janetzko, F.; del Campo, J. M.; Patchkovskii, S.; Reveles, J. U.; Vela, A.; Salahub, D. R. deMon Developers, 2006.

Chapter 3

Relativistic Effect On Au Clusters: Structure And Properties

Abstract

The influence of relativistic effects on the structure, vibrational modes, and reactivity of recently discovered tetrahedral gold clusters (Au_{19} and Au_{20}) are investigated using density functional methods. The intramolecular reactivity of the clusters was analyzed using density functional-based reactivity descriptors. The work shows that whereas the structural properties and vibrational modes are considerably affected by the relativistic effects, the reactivity trends based on Fukui function calculation on various atoms within this cluster remain unaffected by the absence or presence of relativistic effects. The reactivity descriptors reveal that the vertex atoms are the most reactive ones in Au_{20} toward a nucleophilic attack. On the other hand, atoms connecting the missing vertex edge with the pyramid base along with the vertex atom are the most reactive for a nucleophilic attack in Au_{19}. The atoms lying at the center of each face are favorable for an electrophilic

attack in both cases. Interestingly, the atoms with a missing cap in Au_{19} are highly favorable for electrophilic attack, and Au_{20} has more sites for a favorable nucleophilic attack.

3.1   Introduction

Gold clusters have been of recent interest because of their rich chemistry and potential applications in the field of molecular electronic devices, catalysis, and as probes for biological diagnostics, and so forth.[1] The most interesting application of the gold nanoclusters is in the area of catalysis.[2, 3] Bulk gold is well-known to be chemically inert; the metal does not react with oxygen in air. However, it is now well established that gold clusters from eight atoms or more up to a cluster of 5 nanometers in diameter differ from bulk as they have several surface and corner atoms that have low coordination and hence adopt geometries that are extremely active for catalyzing certain oxidation reactions.[4, 5] Since the pioneering reports on the possible application of Au clusters as catalysts, there have been a large amount of experimental and theoretical studies devoted to understand the structural, electronic, catalytic properties, and reactivity of Au_n (n < 60) clusters.[6–10] Several interesting findings on Au clusters have been summarized in a recent review on theoretical chemical calculations on gold.[11] These studies have brought out two additional interesting aspects of Au clusters, that is enhanced stability of clusters of particular sizes and, similarly, enhanced catalytic activity of clusters of particular sizes.

A more recent exciting report based on theoretical calculations combined with photoelectron spectroscopy (PES) has established the existence of hollow golden cages for anionic gold clusters with 16-18 atoms with an average cage diameter of 5.5 Å [12]. However, Au_{20} is the most interesting gold cluster reported so far. PES studies have revealed that this anionic Au_{20} cluster has a pyramidal structure (point group, T_d) with each of the three faces and the base representing the (111) surface of the FCC gold. It is reported to have an energy gap of 1.77 eV between the highest occupied molecular orbital (HOMO) and the lowest unoccupied molecular orbital (LUMO). This energy gap is greater than that of C_{60}, thereby indicating that Au_{20} is highly stable and chemically inert.[13] On the other hand, its high

surface area and large fraction of corner sites provide ideal surface sites for binding of small molecules like CO, NO_x, and so forth for catalysis. The structure of Au_{19} is quite similar to that of Au_{20} with one missing corner atom. A more recent experimental vibrational frequency spectroscopic study in combination with the theoretical calculations have shown that neutral Au_{19} and Au_{20} clusters adopt the same symmetry as their anionic counterparts[14]. The high HOMO-LUMO gaps of these two clusters, particularly that of Au_{20} in its neutral, cationic, and anionic forms, has motivated several research groups to work on these clusters, particularly on their structure and stability. The stability of these clusters has been a topic of recent investigation. However, the reactivity of these clusters has not been explored until now. Moreover, most of the theoretical studies to date[15–17] on such clusters have been using the nonrelativistic methods. It is well established by now that gold has very high relativistic effects, much larger than its neighboring elements in the periodic table and larger than any other element with $Z < 100$. Relativistic effects are known to influence the structural aspects of Au clusters[18] as already demonstrated for the case of the small clusters Au_n, (n up to 8) predicted to be nonplanar in the nonrelativistic calculations[19].

Hence, in this work, the structural and reactivity aspects of these medium-sized Au_{19} and Au_{20} clusters have been analyzed with nonrelativistic and relativistic effects using density functional theory (DFT). The condensed Fukui function (FF) has been used to determine the site reactivity in a system or intramolecular reactivity.[20] The results bring an interesting pattern as to how a single missing cap atom in Au_{20} changes the predominantly nucleophilic attacking sites to predominantly electrophilic attacking favorite sites in Au_{19}. The chapter is organized as follows. In section 3.2, we present the brief overview of method used. In section 3.3, relevant computational details have been presented. Section 3.4 presents results and a discussion on these results.

3.2 Theoretical Method

The ground-state energy of an atom or a molecule, in DFT, can be expressed in terms of electron density $\rho(\mathbf{r})$ and the function $f(\mathbf{r})$ is defined by,

$$f(\mathbf{r}) \equiv \left[\frac{d\mu}{dv(\mathbf{r})}\right] = \left[\frac{\delta\rho}{\delta N}\right]_{v(\mathbf{r})} \tag{3.1}$$

$f(r)$ is called the Fukui function (FF) or frontier function for a molecule. The N discontinuity problem of atoms and molecules[21] in eq 3.1 leads to the introduction[22] of both right- and left-hand-side derivatives at a given number of electrons, N_0 $(= N)$.

By the finite difference method, using electron densities of N_0, $N_0 + 1$ and $N_0 - 1$ electron systems, FFs for nucleophilic and electrophilic attack can be defined respectively as,

$$f^+(\mathbf{r}) \approx \rho_{N_0+1}(\mathbf{r}) - \rho_{N_0}(\mathbf{r}) \tag{3.2}$$

$$f^-(\mathbf{r}) \approx \rho_{N_0}(\mathbf{r}) - \rho_{N_0-1}(\mathbf{r}) \tag{3.3}$$

and for radical attack

$$f^0(\mathbf{r}) \approx \frac{1}{2}(\rho_{N_0+1}(\mathbf{r}) - \rho_{N_0-1}(\mathbf{r})) \tag{3.4}$$

To describe the site reactivity or site selectivity, Yang et al.[23] proposed the condensed FF for an atom k undergoing nucleophilic, electrophilic, or radical attack as:

$$f_k^+ \approx q_k^{N_0+1} - q_k^{N_0} \tag{3.5}$$

$$f_k^- \approx q_k^{N_0} - q_k^{N_0-1} \tag{3.6}$$

$$f_k^0 \approx \frac{1}{2}(q_k^{N_0+1} - q_k^{N_0-1}) \tag{3.7}$$

where q_k values are electronic population of the kth atom of a particular species.

To determine the relative nucleophilicity indices, Roy et *al.* proposed the relative nucleophilicity as[24, 29]

$$f_{nu} = \frac{f_k^+}{f_k^-} \tag{3.8}$$

$$f_{el} = \frac{f_k^-}{f_k^+} \tag{3.9}$$

where f_{el} is the relative electrophilicity.

This quantity is quite useful to identify the reactive site at which the reaction takes place. For intramolecular reactivity, f_{nu}/f_{el} has the importance in comparing reactivity across the same molecule.

3.3   Computational Details

All of the calculations have been performed using demon.2.2.6 package[26]. The geometries of neutral Au_{19} and Au_{20} were optimized using B88 exchange and Lee, Yang, and Parr correlation functionals[27] followed by the calculation of harmonic vibrational frequencies. All of the frequencies were found to be positive, confirming the structure to be a global minima. The basis used for Au is of ECP quality with Stuttgart-Dresden ECP valence basis for nonrelativistic calculations incorporating 19 electrons for treatment and rest electrons being treated as core. For the sake of nonrelativistic calculations, the basis used for calculation is ECP quality with Stuttgart-Dresden ECP for 19 valence electrons treatment. No additional polarization functions have been added. It may be noted that these ECPS are well

FIGURE 3.1:   (a) Projection views of the clusters Au_{19} in their ground-state configuration of C_{3v} point group (note, there is no significance to the lines conn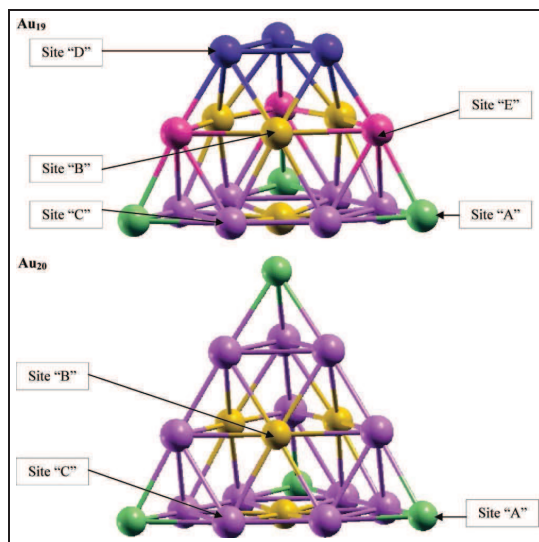ecting the nuclear positions; these are only an aid for visualization). (b) Projection views of the clusters Au_{20} in their ground-state configuration of T_d point group (note, there is no significance to the lines connecting the nuclear positions; these are only an aid for visualization).

documented for accurate prediction of structure[14] as well as spectroscopic properties[14, 28] of Au clusters. The basis set used for the relativistic calculations is RECP quality with 1997 Stuttgart-Dresden RECP for 19 valence electrons treatment. The A2 auxiliary functions were set to fit the charge density. The convergence of the geometries were based on gradient and displacement criteria with a threshold value of 10^{-5} au and the criteria for convergence of SCF cycles were set to 10^{-9}. The FFs were calculated on the basis of Lowdin SCF population analysis.[29]

3.4   Results and Discussion

3.4.1   Structure and Vibrational Frequencies

We begin the discussion with a note on the ground-state geometries of Au_{19} and Au_{20} obtained from the relativistic (R) and nonrelativistic (NR) calculations. These geometries are shown in parts a and b of Figure 3.3. Au_{20} has a T_d symmetry with a face centered cubic structure, as shown in part b of Figure 3.3, whereas Au_{19} has a C_{3V} symmetry. Au_{19} cluster differs from the Au_{20} by a single missing vertex atom of the tetrahedron. This is in good agreement with the earlier reported experimental and theoretical predictions.[14] As seen, both of the clusters are very symmetric, with ordered triangular surfaces stacked over each other. The atoms in both of the clusters are divided into various classes depending upon their symmetry types or environment. Each class of atoms will have a different reactivity. We begin with a classification of atoms in the Au_{19} cluster. This cluster having a C_{3V} point group has five different environments, as shown in part a of Figure 3.3. They are:

1. Vertex atoms of the pyramid base (site A), coordinated to three atoms.

2. Atoms lying at the center of each face (site B), coordinated to nine atoms.

3. Edge atoms of the pyramid-base (site C), coordinated to six atoms.

4. Atoms with missing vertex on the top (site D), coordinated to five atoms.

5. Atoms connecting the base of the pyramid and the missing vertex (site E). coordinated to six atoms.

TABLE 3.1: (a) Average Interatomic Distances and Bond Angles between Different Sites in Au_{19} and Au_{20}

distance (Å)/bond angles (°)	$Au_{19}(NR)$	$Au_{20}(NR)$	Au_{19} (R)	$Au_{20}(R)$
A-B	5.269 (5.249)	5.256	4.822	4.819
A-C	3.038	3.058	2.798	2.802
A-E	3.048		2.813	
B-C	3.210	3.127	2.912	2.927
B-D	3.105		2.915	
B-E	3.134		2.927	
C-C	3.020	3.019	2.737	2.745
C-E	3.213		3.075	
D-D	3.158		2.918	
D-E	3.042		2.783	
B-B	3.379	3.365	3.528 (3.437)	3.338
E-B-E	173.6		165.0	
C-B-C	176.7	174.8	169.3	170.4
A-C-C	177.7	177.5	176.0	175.6
C-A-C	64.4	64.1	67.0	67.0
C-C-C	59.9	60.0	60.0	60.0
D-E-A	176.3		174.2	
D-D-D	60.0		60.0	
C-E-A	63.7		66.5	

[a] The values in parentheses correspond to case when one of the central atom is in the pyramid base of Au_{19}.

TABLE 3.2: (a) Charges on Various Sites in Au_{19} and Au_{20} as Obtained from
Lowdin Population Analysis

Sites	Au_{19} (NR)	Au_{20} (NR)	Au_{19} (R)	Au_{20} (R)
A	0.215	0.213	0.228	0.199
B	-0.131	-0.147	-0.223	-0.226
C	-0.044	-0.022	-0.025	0.009
D	0.068		0.102	
E	-0.032		-0.004	

TABLE 3.3: (a) Reactivity of the Various Sites of Au_{19} and Au_{20}

Reactivity centers	Au_{19} (NR) $\frac{f^+}{f^-}$	Au_{19} (NR) $\frac{f^-}{f^+}$	Au_{20} (NR) $\frac{f^+}{f^-}$	Au_{20} (NR) $\frac{f^-}{f^+}$
A	1.110	0.901	2.252	0.502
B	0.975	1.029	0.283	3.609
C	0.989	1.011	1.083	1.093
D	0.920	1.086		
E	1.010	0.990		

(b) Reactivity Indices Obtained from Relativistic Calculations

Reactivity centers	Au_{19} (R) $\frac{f^+}{f^-}$	Au_{19} (R) $\frac{f^-}{f^+}$	Au_{20} (R) $\frac{f^+}{f^-}$	Au_{20} (R) $\frac{f^-}{f^+}$
A	1.043	0.959	1.341	0.746
B	0.980	1.022	0.411	2.494
C	0.974	1.027	0.996	1.024
D	0.954	1.048		
E	1.068	0.936		

[a] The values in parentheses correspond to case when one of the central atom
is in the pyramid base of Au_{19}.

On the other hand, Au_{20}, with T_d symmetry, has only first three classes (A, B, and C). The presence of an additional vertex atom in Au_{20} increases the symmetry of the cluster leading to two less reactive centers within it as compared to Au_{19}. We begin with an analysis of the geometrical parameters of each cluster. Table 5 shows some important interatomic distances and angles for all of the cases. Table 5 gives the charges obtained from the Lowdin population analysis on various sites of Au_{19} and Au_{20} for the relativistic and nonrelativistic cases. It is seen from Table 5 that the relativistic effect causes shortening of all the Au-Au bond distances (viz. A-B, A-C, A-E, B-C, B-D, B-E, C-C, C-E, D-D, and D-E) by about 0.2 Å. This shortening of bond lengths is due to the contraction and stabilization of $6s$ orbitals in contrast to $5d$ orbitals. It is also interesting to note that most of the Au-Au-Au angles are similar in nonrelativistic and relativistic cases with the exception of E-B-E and C-B-C of Au_{19}. Most of the geometric parameters are also similar between Au_{19} and Au_{20} are similar except for the B-B interatomic distances. As discussed earlier, the loss of the symmetry in Au_{19} leads to the presence of two additional sites, viz., D and E. The D-D interatomic distances in Au_{19} are longer by about 0.2 Å as compared to C-C distances in the same cluster. On incorporation of relativistic effects, E-B-E and C-B-C angles decrease significantly in Au_{19}. This decrease in the E-B-C and C-B-C angles results in a small curvature within the planes without vertex atoms in Au_{19}, thereby increasing B-B interatomic distances. B-B distances between these planes is 3.5 Å (3.4 Å when one of the atoms is in the pyramid base) as compared to 3.3 Å in Au_{20}.
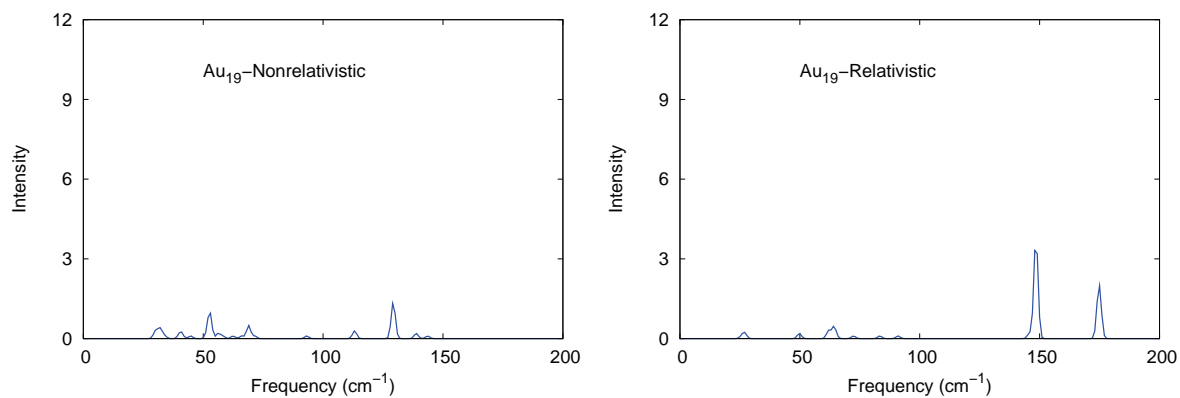
FIGURE 3.2: (a) Au_{19} nonrelativistic, (b) Au_{19} relativistic. The signals are simulated using gaussian functions with a half-width value of 1 cm^{-1}. The values were scaled by 1.29.
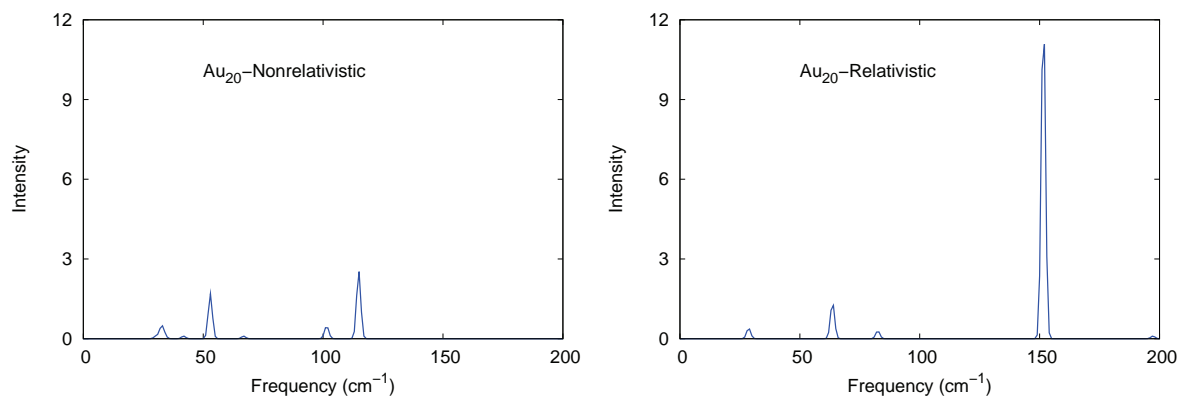

FIGURE 3.3: (c) Au_{20} nonrelativistic, and (d) Au_{20} relativistic. The signals are simulated using gaussian functions with a half-width value of 1 cm^{-1}. The values were scaled by 1.29.

The distribution of charge across the atoms in both the clusters reveals that the relativistic effects result in greater charge transfer from all of the atoms toward the central atoms. This result in a more negatively charged central atom in both clusters, for example, the average charge on central atoms (site B) of Au_{19} in nonrelativistic calculations is -0.131, which increases to -0.223 when relativistic effects are incorporated. The same in Au_{20} is increased from -0.147 to -0.226 upon incorporation of relativistic effects. This change may be attributed to the following reason: The angles connected with the central atoms (C-B-C and E-B-E) decrease by at the least 4° upon incorporation of relativistic effects. It is by now well-known that a decrease in the Au-Au-Au angle is associated with an increase in the negative charge on the central Au atom at the cost of the edge Au atoms.[30, 31] In the present case, it is seen that there is a small charge transfer from sites C, D, and E to the central atom B, leading to a higher negative charge in the B site as a net effect in relativistic cases as seen in Tables 5 and 5. This results in shorter interatomic distances between the positively charged vertex atoms and negatively charged central atoms (A-B) when the relativistic effects are incorporated (4.82 Å as compared to 5.26 Å in nonrelativistic case). Absence of a vertex atom results in positively charged D sites (0.102) as compared to the C sites, which have a small negative charge (-0.025) on them. This results in larger D-D interatomic distances as compared to the C-C distances as mentioned in the earlier paragraph. This has implications on the reactivity trends as will be discussed in the next sections. In general, it is interesting to note that the central atoms are most negatively charged in both the clusters, whereas the vertex atoms are the positively charged ones. The missing vertex atoms in Au_{19} are the next positively charged centers.

We next analyze the vibrational frequencies of Au_{19} and Au_{20} as obtained from both relativistic and nonrelativistic calculations. IR spectra for Au clusters have been studied using experimental[14, 32] and theoretical methods.[33, 34]

All of the frequencies are positive for Au_{19} and Au_{20} in both relativistic and nonrelativistic methods. In a recent report, Gruene and co-workers have reported the far-infrared (IR) photon dissociation spectrum[14] for neutral Au_{19} and Au_{20} clusters. The experimental IR spectrum of Au_{20} shows a single dominant adsorption around 148 cm^{-1} due to its symmetric structure. The lower symmetry in Au_{19} splits the single adsorption mode into a doubly degenerate vibration ($149 cm^{-1}$) and a nondegenerate vibration in Au_{19} (168 cm^{-1}). In Figure 5, we present the IR spectrum as obtained from the nonrelativistic calculations and the relativistic calculations. It is clearly seen that the nonrelativistic calculations do not follow the experimental IR spectra, whereas the relativistic calculations follow the experimental trends. It is noted that the IR spectrum of Au_{19} obtained by relativistic calculations shows a doubly degenerate vibration (e) around 148.6 cm^{-1} and a blue-shifted nondegenerate vibration (a_1) around 174.5 cm^{-1}. Relativistic calculation on Au_{20} shows a triply degenerate vibration (t_2) at 151.4 cm^{-1}. We note that the t_2 vibration in Au_{20} and a_1 vibration in Au_{19} are blue-shifted by 3 and 6 cm^{-1} respectively compared to the experiments and we attribute this difference to the absence of the polarization functions in our calculations. The spectra of both the clusters also show a peak around 63 cm^{-1} corresponding to the rocking mode in the relativistic calculations. On the other hand, nonrelativistic calculations show two dominant peaks in Au_{19} at 52.6 cm^{-1} and 129.1 cm^{-1} as well as Au_{20} at 53.0 cm^{-1} and 114.7 cm^{-1} values, respectively. It is noteworthy that the experimentally reported features are absent in the nonrelativistic calculations, highlighting the importance of the relativistic effects in energy levels of the gold clusters.

3.5   Reactivity

Reactivity of these clusters is a matter of great interest because the tetrahedral Au_{20} cluster has been discovered. Whereas charges give a brief insight

on the electron redistribution on the cluster, a qualitative understanding on the response of the atom toward an electrophilic or nucleophilic attack using density functional descriptors has been proven to be successful in several earlier studies.[24] Hence, we investigate the trend of relative electrophilicity and nucleophilicity for relativistic and nonrelativistic calculations using FFs for the two studied clusters. The q_k^0 values were calculated for the optimized geometries of neutral Au_{19} and Au_{20} clusters using Lowdin population analysis. q_{N-1}^k and q_{N+1}^k values were obtained by substituting and adding a single electron to the neutral cluster respectively and relaxing the molecular orbitals, while maintaining the same geometry of the neutral cluster. This is a standard procedure used by several groups for calculating the reactivity indices.[35, 36] As already discussed, Au_{20} has three types of reactive sites, namely, A, B, and C, whereas Au_{19} has two more additional reactive sites, namely, D and E, owing to the missing vertex atom. In this section, part a of Table 5 gives the relative nucleophilicity and relative electrophilicity of the five sites in Au_{19} and three reactive sites of Au_{20} and part b of Table 5 gives the same for relativistic calculations for the two Au clusters.

We begin with a discussion on the reactivity trends seen for the case of Au_{19}. Interestingly, despite the differences in geometry and vibrational modes seen between relativistic and nonrelativistic calculations, the reactivity descriptors obtained from these two calculations predict similar reactivity order among atoms. It is seen that site A corresponding to the vertex atoms in Au_{19} and sites E are more favorable sites for a nucleophilic attack as compared to the other three sites. Atoms with the missing vertex (site D) are least favorable sites for nucleophilic attack. For the case of an electrophilic attack, sites B (central atoms), C, and D are more favorable. Coming to the case of Au_{20}, the vertex atoms (site A) are most favorable for a nucleophilic attack as in case of Au_{19}. The central atoms, that is sites B, are the most favorable ones for electrophilic attack.

We also note that the relative nucleophilicity of the vertex atom is much higher in case of Au_{20} as compared to Au_{19}, in which, along with the vertex atoms, sites E show a higher affinity toward nucleophilic reagents. The central atoms, that is the atoms at reactive sites B, are most reactive for electrophilic attack in both the clusters. Apart from that, the sites with missing vertex C are the additional counterparts for electrophilic attack.

Interestingly, in both the cases we find that incorporation of relativistic effect does not show a marked change in the trend of the reactivity of various reactive centers in both of the Au clusters. We finally note that Au_{19} has more sites favorable for an electrophilic attack, and Au_{20} has more sites for an favorable nucleophilic attack. Thus, it is interesting to note how a single missing cap atom changes a predominately nucleophilic attack favorable Au_{20} to a predominantly electrophilic attack favorable Au_{19}.

3.6   Conclusions

The above discussion brings out clearly how the relativistic effects are important for a good description of geometry and vibrational frequencies. However, the density functional-based reactivity descriptors bring out the same trend in reactivity, irrespective of the presence or absence of these effects, emphasizing the robustness of these descriptors. These descriptors predict relative nucleophilicity of the vertex atom to be higher in case of Au_{20} as compared to Au_{19}. It is seen that relativistic effects have no influence on catalytic activity of the Au clusters. The most reactive atoms in Au_{19} correspond to the atoms that are not capped by any vertex atom. The reactivity descriptors also predict that the vertex atoms are the most reactive ones in Au_{20} toward a nucleophilic attack, whereas atoms connecting the missing vertex edge with the pyramid base along with the vertex atom are the most reactive ones for nucleophilic attack in Au_{19}. The atoms lying at the center of each face are favorable for an electrophilic attack in both the cases. The atoms with a missing cap in Au_{19}

are highly favorable for electrophilic attack. The present work clearly brings out how the presence of all of the vertex atoms in Au_{20} results in more sites for a favorable nucleophilic attack.

Bibliography

[1] Gold. *Progress in Chemistry, Biochemistry and Technology; Schmidbaur*, H., ed.; Wiley: Chichester, 1999; p 894.

[2] Teles, J. H.; Brode, S.; Chabanas, M. *Angew. Chem.* **1998**, *37*, 1415.

[3] Hashmi, A. S. K. *Gold Bull.* **2003**, *36*, 3.

[4] Haruta, M. *Gold Bull.* **2004**, *37*, 27.

[5] Haruta, M.; Daté, M. *Appl. Catal. A* **2001**, *222*, 427.

[6] Pyykkö, P. *Angew. Chem., Int. Ed.* **2004**, *43*, 4412.

[7] Pyykkö, P. *Angew. Chem., Int. Ed.* **2002**, *41*, 3573.

[8] Haruta, M. *Catal. Today* **1997**, *36*, 153.

[9] Chrétien, S.; Metiu, H. *J. Chem. Phys.* **2007**, *127*, 084704.

[10] Lemire, C.; Meyer, R.; Shaikhutdinov, Sh.K.; Freund, H-. J. *Surf. Sci.* **2004**, *552*, 27.

[11] Pykkö, P. *Chem. Rev.* **2008**, *37*, 1967.

[12] Bulusu, S.; Li, X.; Wang, L. S.; Zeng, X. C. *Proc. Natl. Acad. Sci. U.S.A.* **2006**, *103*, 8326.

[13] Li, J.; Li, X.; Zhai, H. J.; Wang, L. S. *Science* **2003**, *299*, 864.

[14] Gruene, P.; Rayner, D. M.; Redlich, B.; van der Meer, A. F. G.; Lyon, J. T.; Meiger, G.; Fielicke, A. *Science* **2008**, *321*, 674.

[15] Wang, J.; Wang, G.; Zhao, J. *Phys. Rev. B* **2002**, *66*, 035418.

[16] Garzón, I. L.; Michaelian, K.; Beltrán, M. R.; Posada-Amarillas, A.; Ordejón, P.; Artacho, E.; Sánchez-Portal, D.; Soler, J. M. *Phys. Rev. Lett.* **1998**, *81*, 1600.

[17] Michaelian, K.; Rendón, N.; Garzón, I. L. *Phys. Rev. B* **1999**, *60*, 2000.

[18] (a) Haberlen, O. D.; Chung, S. C.; Stener, M.; Rosch, N. *J. Chem. Phys.* **1997**, *106*, 5189. (b) Bowmaker, G. A.; Schmidbaur, H.; Kruger, S.; Rosch, N. *Inorg. Chem.* **1997**, *36*, 1754.

[19] Hakkinen, H.; Moseler, M.; Landman, U. *Phys. Rev. Lett.* **2002**, *89*, 033401.

[20] Parr, R. G.; Yang, W. *J. Am. Chem. Soc.* **1984**, *106*, 4049. (b) Yang, W.; Parr, R. G. *Proc. Natl. Acad. Sci. U.S.A* **1985**, *82*, 6723.

[21] Perdew, J. P.; Parr, R. G.; Levy, M.; Balduz, J. L., Jr. *Phys. Rev. Lett.* **1982**, *49*, 1691. (b) Zhang, Y.; Yang, W. *Theor. Chem. Acc.* **2000**, *103*, 346.

[22] Parr, R. G.; Yang, W. *J. Am. Chem. Soc.* **1984**, *106*, 4049.

[23] Yang, W.; Mortier, W. *J. Am. Chem. Soc.* **1986**, *108*, 5708.

[24] Roy, R. K.; Krishnamurti, S.; Geerlings, P.; Pal, S. *J. Phys. Chem. A* **1998**, *102*, 3746.

[25] Roy, R. K.; Proft, F.; Geerlings, P. *J. Phys. Chem. A* **1998**, *102*, 7035.

[26] Fischer, G.; Goursot, A.; Coq, B.; Delahay, G.; Pal, S. *ChemPhysChem* **2006**, *7*, 1795.

[27] Perdew, J. P.; Burke, K.; Erzenhof, M. *Phys. Rev. Lett.* **1996**, *77*, 3865.

[28] Schwerdtfeger, P.; Dolg, M.; Schwarz, W. H. E.; Bowmaker, G. A.; Boyd, P. D. W. *J. Chem. Phys.* **1989**, *91*, 1762.

[29] Mulliken, R. S. *J. Chem. Phys.* **1955**, *23*, 1833.

[30] Joshi, A. M.; Tucker, M. H.; Delgass, W. N.; Thomson, K. T. *J. Chem. Phys.* **2006**, *125*, 194707.

[31] Shafai, G. S.; Shetty, S.; Krishnamurty, S.; Shah, V.; Kanhere, D. G. *J. Chem. Phys.* **2007**, *126*, 014704.

[32] Pichugina, D. A.; Kuzmenko, N. E.; Shestakov, A. F. *Proc. SPIE-Int. Soc. Opt. Eng.* **2006**, *6580*, 658003.

[33] Kryachko, E. S.; Remacle, F. *Int. J. Quantum Chem.* **2007**, *107*, 2922.

[34] Molina, B.; Soto, J. R.; Calles, A. *Revisra Mexicana de Fisica* **2008**, *54*, 314.

[35] Chattaraj, P. K. *J. Phys. Chem. A* **2001**, *105*(2), 511.

[36] Kar, R.; Chandrakumar, K. R. S.; Pal, S. *J. Phys. Chem. A* **2007**, *111*, 375.

Chapter 4

Structure, Bonding And Reactivity of Small Au Clusters

Abstract

Relativistic Density Functional Theory (DFT) based calculations have been performed on gold clusters with six to thirteen atoms (Au_n; n=6-13). The ground state geometries of these clusters as obtained from our calculations, are presented and discussed. This chapter proposes that atoms in a ground state conformation can be classified into distinct types of reactive sites in a given geometry. Based on symmetry, susceptibility of various types of reactive sites in the ground state geometry towards an impending electrophilic and/or a nucleophilic attack has also been studied using DFT based reactivity descriptors. The studies have also been extended to high energy isomers in these cluster sizes. The reactivity of various sites as a function of cluster size and shape was thus analyzed. The study shows that as a general rule the size and shape of the cluster influences the number and position of available sites for an electrophilic and/or nucleophilic attack. This makes the reactivity patterns of these clusters highly complex. The chapter also highlights as to how for a cluster with seven atoms (Au_7) various conformations are likely to co-exist indicating that the reactivity patterns of various high energy conformations are also important while dealing with small sized Au clusters.

4.1 Introduction

Gold clusters with six atoms and above exhibit different chemical properties as compared to their bulk counterpart. Some of the unique properties observed in these gold clusters are high catalytic activity,[1–4] better response properties,[5–7] different melting behavior,[8] to name a few. The first two distinct properties have led to an exponential research on their applications in the areas of material science,[9] medicine,[10] and specially catalysis.[11–15] While, it was well known that the catalytic properties of the nanoclusters vary with the size of the cluster, what came as a surprise in the subnanocluster size range (clusters with 2-100 atoms) is the fact that addition or removal each atom is seen to alter these properties dramatically. The results varied depending upon the support, host molecule, geometry and the shape of the Au clusters. A detailed analysis of these aspects has been discussed in one of the recent reviews.[16] Hence, several theoretical [17–30] and experimental studies in conjunction with theoretical calculations [30–33] were carried out to understand the structural and electronic properties of Au clusters as a function of size and charge. These reports have brought out interesting and some times conflicting details on the lowest energy structure and reactivity trends for small Au clusters. One of the most debated issues has been the exact cluster size where 2D-3D transition occurs in Au clusters. This transition is seen to be at a much larger cluster size range as compared to that of Pt, Pd, Ag and Cu clusters.[34–36] Ion mobility experiments and photo electron spectroscopy studies in combination with density functional theory (DFT) calculations have shown that Au anions and cations retain their planarity up to 12 and 8 atoms[37, 38] respectively. However, there are no experimental records for neutral clusters. CCSD(T) calculations place this value to be 8 for neutral clusters [22] and DFT calculations report this value to be between 11-15 atoms.[23–29] Complete reviews are available which mention several theoretical studies carried out to investigate the lowest energy geometry of Au clusters.[39–42] Apart from the study on the lowest energy

conformation, many researchers have been interested in the catalytic activity of Au clusters in the size range of 6-13 atoms. One of the important applications of Au clusters has been for CO oxidation. This requires the simultaneous reduction of O_2 molecule and CO oxidation. In this context, interaction of ground state geometry of Au clusters with O_2 [43–48] and CO [49, 50] has been widely studied. However, detailed information on the reactivity of various Au clusters and the reacting sites within them has not yet been clearly obtained. Moreover, it has now recently been reported that in some cases, the higher energy conformations have better adsorption properties as compared to the ground state cluster.[50, 51] Many additional reports have shown that the activity of neutral clusters depends upon the type of sites exposed and their ability to absorb or donate electrons. Thus, the catalytic activity of gold clusters is more complex and is closely related to the basic electrophilicity and nucleophilicity of various sites in a given cluster. The number of electrophilic or nucleophilic sites is in turn dependent on the size and shape of the cluster.

Hence, in this chapter, we have analyzed in depth the response of various sites towards an impending electrophilic attack (which describes as to how easily it will donate the electrons) or an nucleophilic attack (which describes as to how easily it will accept the electrons). For this purpose, the ground state structure as well as few characteristic high energy isomers of Au_n ($n = 6 - 13$) were considered. The relative nucleophilicity and electrophilicity of the above conformations were calculated and an analysis of this is presented in Section 4.4. Our results show that for gas phase clusters, the ground state geometries with alternating nucleophilic and electrophilic sites are best suited for catalysis. In contrast, non-planar geometries are better candidates for adsorbing on supports and subsequent catalysis. An analysis of infra-red spectrum of Au_7 isomers clearly demonstrates that in this cluster size range, ground state conformations as well as some high energy conformations are likely to co-exist indicating that above aspects could play an important role in the overall reactivity of these clusters.

4.2 Theoretical Methods

The ground-state energy of an atom or a molecule, in density functional theory, can be expressed in terms of electron density, $\rho(\mathbf{r})$, as [52]

$$E[\rho(\mathbf{r})] = F_{HK}[\rho] + \int v(\mathbf{r})\rho(\mathbf{r})d\mathbf{r} \tag{4.1}$$

where $v(\mathbf{r})$ is the external potential and F_{HK}, the universal Hohenberg-Kohn functional is the sum of electronic kinetic energy $(T[\rho(\mathbf{r})])$ and electron-electron interaction energy $(V_{ee}[\rho(\mathbf{r})])$.

$$F_{HK}[\rho] = T[\rho] + V_{ee}[\rho] \tag{4.2}$$

The first partial derivative of $E[\rho(\mathbf{r})]$ with respect to the number of electrons N under constant external potential $v(\mathbf{r})$ is defined as the chemical potential [53], μ, for a system.

$$dE = \mu dN + \int \rho(\mathbf{r})dv(\mathbf{r})d\mathbf{r} \tag{4.3}$$

where

$$\mu = \left(\frac{\partial E[\rho(\mathbf{r})]}{\partial N}\right)_v = \left(\frac{\delta E}{\delta \rho(\mathbf{r})}\right)_v \tag{4.4}$$

For the calculation of curvature of E with respect to N at a given value of N at 0 K, using the finite difference method,

$$\mu = \left(\frac{\partial E[\rho(\mathbf{r})]}{\partial N}\right)_{v(\mathbf{r})} \approx \frac{E(N+h) - E(N-h)}{2h} \tag{4.5}$$

Since only integral values of N can be observed from data of ionization potentials (I) and electron affinity (A), the infinitesimally small quantity h, can be set equal to unity and through rearrangement, followed by using electron densities of N_0, $N_0 + 1$ and $N_0 - 1$ electron systems, the equation is modified as:

$$\mu = \frac{E(N+1) - E(N-1)}{2h} = -\frac{I+A}{2} \tag{4.6}$$

The second derivative of energy with respect to N at $0\ K$ as obtained from equation 4.4 gives the definition of hardness, η :

$$\eta = \frac{1}{2}\left(\frac{\partial \mu}{\partial N}\right)_{v(\mathbf{r})} = \frac{1}{2}\left(\frac{\partial^2 E}{\partial N^2}\right)_{v(\mathbf{r})} \tag{4.7}$$

and applying three point finite difference approximation, we obtain the formula:

$$\eta = \frac{I - A}{2} \tag{4.8}$$

From the understanding of MO theory, within the framework of density functional theory, applying Koopmans' approximation to Kohn-Sham orbitals instead of canonical Hartree-Fock molecular orbitals [54], equations 4.6 and 4.8 can be further simplified using the MO eigenvalues (ϵ) of the highest occupied (ϵ_{HOMO}) and lowest occupied (ϵ_{LUMO}) molecular orbitals. In that case, the equations 4.6 and 4.8 simplifies as :

$$\mu = \frac{\epsilon_{HOMO} + \epsilon_{LUMO}}{2} \tag{4.9}$$

$$\eta = \frac{\epsilon_{LUMO} - \epsilon_{HOMO}}{2} \tag{4.10}$$

Continuing from equation 4.3, the function $f(\mathbf{r})$ is defined as the derivative of chemical potential μ against external potential at constant electronic framework or the slope of density against number of electrons, N, at constant perturbation:

$$f(\mathbf{r}) \equiv \left(\frac{\delta\mu}{\delta v(\mathbf{r})} \right)_N = \left(\frac{\partial\rho(\mathbf{r})}{\partial N} \right)_{v(\mathbf{r})} \tag{4.11}$$

$f(\mathbf{r})$ is called the *Fukui function* or *frontier function* for a molecule.[55] Thus, the Fukui function can be interpreted either as the change of electron density at each point $\mathbf{r}$ when the total number of electrons is changed or as the sensitivity of chemical potential of a system to an external perturbation at a particular point $\mathbf{r}$. The N discontinuity problem of atoms and molecules [56] in equation 4.11 leads to the introduction of both right- and left-hand-side derivatives at a given number of electrons, $N_0 (\equiv N)$

$$f^+(\mathbf{r}) = \left(\frac{\partial\rho(\mathbf{r})}{\partial N} \right)^+_{v(\mathbf{r})} \tag{4.12}$$

for nucleophilic attack and

$$f^-(\mathbf{r}) = \left(\frac{\partial\rho(\mathbf{r})}{\partial N} \right)^-_{v(\mathbf{r})} \tag{4.13}$$

for electrophilic attack.

By the finite difference method, using electron densities of N_0, $N_0 + 1$ and $N_0 - 1$ electron systems, Fukui functions for nucleophilic and electrophilic attack can be defined respectively as,

$$f^+(\mathbf{r}) \approx \rho_{N_0+1}(\mathbf{r}) - \rho_{N_0}(\mathbf{r}) \tag{4.14}$$

$$f^-(\mathbf{r}) \approx \rho_{N_0}(\mathbf{r}) - \rho_{N_0-1}(\mathbf{r}) \tag{4.15}$$

and for radical attack:

$$f^0(\mathbf{r}) \approx \frac{1}{2}(\rho_{N_0+1}(\mathbf{r}) - \rho_{N_0-1}(\mathbf{r})) \tag{4.16}$$

To describe the site reactivity or site selectivity, Yang et *al.*[57] proposed the atom condensed *Fukui function*, based on the idea of electronic population around an atom in a molecule, similar to the procedure followed in the population analysis technique. The condensed Fukui function for an atom k undergoing nucleophilic, electrophilic, or radical attack can be defined respectively as:

$$f_k^+ \approx q_k^{N_0+1} - q_k^{N_0} \tag{4.17}$$

$$f_k^- \approx q_k^{N_0} - q_k^{N_0-1} \tag{4.18}$$

$$f_k^0 \approx \frac{1}{2}(q_k^{N_0+1} - q_k^{N_0-1}) \tag{4.19}$$

where q^k values are electronic population of the kth atom of a particular species.

To determine the relative nucleophilicity indices, Roy et *al.* proposed the relative nucleophilicity as [58, 59]

$$f_{nu} \approx \frac{f_k^+}{f_k^-} \tag{4.20}$$

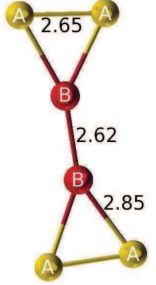$$f_{el} \approx \frac{f_k^-}{f_k^+} \tag{4.21}$$
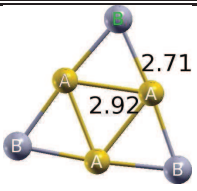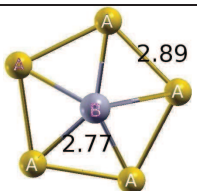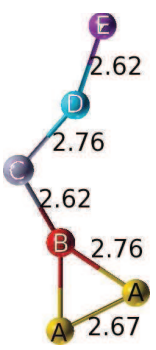
where, f_{el} is the relative electrophilicity. This quantity is quite useful to identify the reactive site at which the reaction takes place. For intramolecular reactivity, $\frac{f_{nu}}{f_{el}}$ has the importance in comparing reactivity across the same molecule. Further the relative difference between the values of f_{nu} and f_{el} is also of importance. A site for which $f_{nu} >> f_{el}$ is a site favorable for a nucleophilic attack, while a site for which $f_{el} >> f_{nu}$ is clearly a site favorable towards an electrophilic attack. A site for which f_{el} is nearly equal to f_{nu} is likely to both give or take electrons easily making it an amphiphilic site, likely to participate in both oxidation and reduction chemical reactions.

4.3   Computational Details

All calculations have been performed using *deMon.2.2.6* code.[60] The geometries of all the clusters have been optimized using B88 exchange and Lee, Yang, and Parr correlation functional[61] followed by the calculation of harmonic vibrational frequencies. All of the frequencies were found to be positive, confirming the structure to be a minima. The basis set used for the relativistic calculations is RECP quality with 1997 Stuttgart-Dresden RECP for 19 valence electrons treatment.[62] The A2 auxiliary functions were set to fit the charge density. [63] No additional polarization functions have been added. It may be noted that these ECPs are well documented for accurate prediction of structure as well as spectroscopic properties of Au clusters.[64, 65] The convergence of the geometries were based on gradient and displacement criteria with a threshold value of 10^{-5} au and the criteria for convergence of SCF cycles was set to 10^{-9}. The FFs were calculated on the basis of Lowdin population analysis. [66]Only one spin multiplicity has been investigated depending upon the cluster size. Only the lowest spin state has been considered for all the Au clusters. The spin multiplicities for even electron (even number of Au atoms) clusters are singlets and doublets for odd electron (odd number of Au

atoms) clusters. It has also been reported in an earlier literature that Au clusters prefer to be in their lowest spin state.[67]

TABLE 4.1: Structural, Electronic and Reactivity Parameters of Au_6 Conformations. The values in red, blue and black correspond to electrophilic, nucleophilic and amphiphilic attack sites respectively. The values given next to the conformations in Column II of the Table correspond to the inter-atomic distances (in $\mathring{A}$) between various unique sites.

	Structure	$\triangle$ E (eV)	No. of Unique Sites	Site	Charge	f_{el}	f_{nu}
I		0.00	2	A	-0.16	1.26	0.79
				B	0.16	0.78	1.29
II		0.90	2		0.05	1.00	1.00
				B	-0.24	0.85	1.18
III		1.53	5	A	0.12	1.94	0.52
				B	-0.11	1.83	0.55
				C	0.03	0.48	2.09
				D	-0.17	0.52	1.91
				E	0.01	0.46	2.17
IV		1.62	2	A	0.06	1.09	0.91
				B	-0.12	0.75	1.33

4.4 Results

4.4.1 Au$_6$

The structural, electronic and reactivity parameters of the lowest energy structure and a few characteristic high energy conformations of Au$_6$ are given in Table 4.3. We begin with an analysis of structural and electronic properties of the ground state Au$_6$ geometry shown in Table 4.3 ($conformation(I)$). The values given next to the conformations in Column II of the Table correspond to the inter-atomic distances (in $\mathring{A}$) between various unique sites. Consistent with the earlier reports,[28, 29] the lowest energy conformation is a planer triangle with D_{3h} point group. Depending upon the symmetry, various atoms in a this conformation have been grouped together as distinct reactive site types. This particular arrangement of six atoms results in 2 types of reactive sites having distinct chemical environments viz., (i) atoms forming an inner triangle "A" and (ii) atoms capping each edge of this triangle, "B". The inner triangle (AAA) is a perfect equilateral triangle. On the other hand, the outer triangles (BAA) are deformed equilateral triangles with the B-A-A angles reduced to 57.5° and the angle A-B-A increased to 64°. These structural features are an outcome of the charge redistribution among the six atoms. The inner triangular atoms ("A" atoms) absorb some charge from the atoms capping them ("B" atoms). As result the inter atomic distances in the inner triangle increase to nearly 2.92 $\mathring{A}$ (higher than the bulk Au-Au inter atomic distance of 2.88 $\mathring{A}$) indicating these atoms to be bonded through metallic bonds. The outer cap atoms are bonded to the equilateral triangle through bonds lengths of 2.77 $\mathring{A}$. This is in between the covalent bond length (Au dimer has an inter atomic bond distance of 2.59 $\mathring{A}$)[68] and metallic bond length seen in bulk Au.
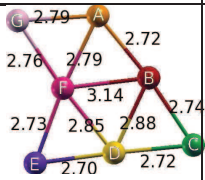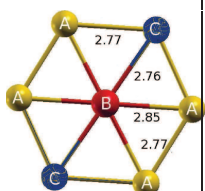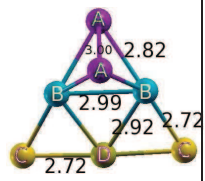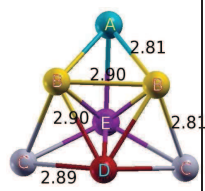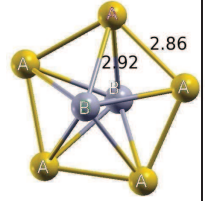
The next high lying isomer (0.90 eV) is a non-planer conformation, a capped pentagon with C_{5v} point group (Conformation-(II)) and two unique reactive sites.

The central atom (atom with highest co-ordination) in this configuration is negatively charged and the atoms surrounded are positively charged. In this case, the central atom is connected to the surrounding atoms with shorter inter atomic distances as compared to inter atomic distances between the edge atoms. All other conformations lie about 1.5-1.6 eV higher than the lowest energy conformation. Two such characteristic conformations are shown in Table 4.3. One conformation (conformation (III)) has nearly five types of reactive sites and has a open dangling trimer attached to another closed trimer. The other conformation analyzed (conformation (IV)) has two types of reactive sites. The trend of atoms with higher co-ordination (which are mostly the central atoms) being negatively charged is consistently observed is these two structures too.

The final interest in all these clusters is to understand their response towards an impending electrophilic or a nucleophilic attack which is analyzed using relative reactivity descriptors discussed in Section 4.2. It is noteworthy, that these reactivity descriptors need not follow the charges necessarily as they are indicative of the tendency of an atom to accept or loose additional charge. On the other hand, charge is a measure of the amount of electrons the atom has lost or gained within the conformation. In conformation (I), the atoms forming the caps (called as cluster tips in earlier works)[74] are favorable for the adsorption of an electrophilic guest molecule such as O_2 or an oxide support. The atoms forming the inner equilateral triangle in contrast are favorable for an attack by a nucleophilic molecule such as CO, H_2O. The reactivity trends observed in our study within the ground state isomer of Au_6 are interestingly corroborated by results from a recent work, which reported that O_2 molecule binds with Au_6 only when it collides with the tips of the cluster and not along the edges while CO prefers the inner-triangular atoms.[74, 75] In conformation (III), the atoms "C", "D" and "E" forming the open triangle are more favorable for O_2 adsorption. Rest of two chemical sites ("A" and "B") are favorable for a nucleophilic attack. Conformations (II) and

(IV) differ from conformations (I) and (III) as in the former two, it is the inner or central atoms (sites "B") that are more viable for an electrophilic attack.

TABLE 4.2: Structural, Electronic and Reactivity Parameters of Au_7 Conformations. The values in red, blue and black correspond to electrophilic, nucleophilic and amphiphilic attack sites respectively. The values given next to the conformations in Column II of the Table correspond to the inter-atomic distances (in $\mathring{A}$) between various unique sites.

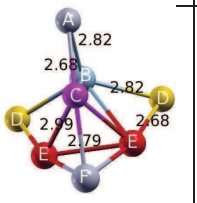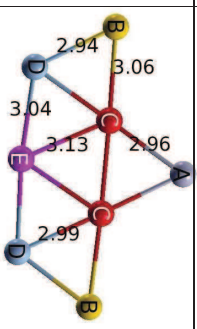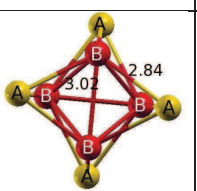|	Structure	$\triangle E$ (eV)	No. of Unique sites	Site	Charge	f_{el}	f_{nu}
I		0.00	7	A	0.04	1.07	0.93
				B	-0.10	1.94	0.98
				C	0.15	1.06	0.94
				D	-0.14	0.98	1.02
				E	0.18	1.01	0.99
				F	-0.25	0.90	1.11
				G	0.12	0.97	1.03
II		0.37	3	A	0.05	1.00	1.00
				B	-0.31	0.94	1.07
				C	0.05	1.02	0.98
III		0.46	4	A	0.10	1.04	0.96
				B	-0.22	0.91	1.10
				C	0.19	1.04	0.96
				D	-0.13	1.06	0.95
IV		0.68		A		1.00	0.99
				B		0.98	1.02
				C	0.68	1.01	0.99
				D		1.00	1.00
				E		1.01	0.99
V		0.74	2	A	0.06	1.00	1.00
				B	-0.14	1.00	1.00

4.4.2 Au_7

In Table 4.4.1, we present the structural and electronic properties of the ground state and a few characteristic high lying geometries of Au_7. The lowest energy conformation is built upon Au_6-conformation(I) and is consistent with several earlier reports.[32] The additional atom "G" breaks down the symmetrical structure of Au_6 leading to 7 unique reactive sites. As a consequence, the inner triangle (B-F-D) is no longer equilateral. The atom "F" in inner triangle absorbs some charge from the new atom "G", becoming the most negatively charged center and consequently increasing the bond distances between it and other two central atoms ("B" and "F"). Thus, "A"-"F" and "B"-"F" increase from 2.71 $\mathring{A}$ in Au_6 to 2.79 $\mathring{A}$ and from 2.92 $\mathring{A}$ to 3.14 $\mathring{A}$ respectively. However, rest of the inter atomic distances remain between 2.71-2.74 $\mathring{A}$. As in case of Au_6-conformation(I), central atoms ("F", "B", and "D") having maximum atomic coordination have a negative charge on them. Rest of the four discussed structures of Au_7 are non-planar. Conformation (II) is the first high energy conformation and lies 0.37 eV above the lowest energy conformation in our calculation and is consistent with a recent report [32]. Thus, the gap between the planar and non-planar conformation has reduced considerably in Au_7 as compared to Au_6. This geometry, based on symmetry has three unique reactive sites. The central atom is negatively charged. This trend is also consistent in conformations (III), (IV) and (V) where atoms with higher co-ordination number (central atoms) are negatively charged. Further, these negatively charged centers are bonded to each other through the largest inter atomic bond distances in the range of 2.90 $\mathring{A}$ - 3.00 $\mathring{A}$.

In a recent work, experimental infra-red (IR) vibrational modes of neutral Au_7 have been reported . Hence, we found it interesting to analyze the IR spectrum of the above mentioned isomers and compare them with the earlier reported theoretical as well as experimental studies[32]. In Figure 4.4.2, we show the IR spectra of the five conformations given in Table 4.4.1. The experimental IR spectra has been

reported to have small peaks around 56 cm^{-1}, 65 cm^{-1}, 75 cm^{-1}, 100 cm^{-1}, 120 cm^{-1}, 165 cm^{-1}, 201 cm^{-1} and one prominent peak around 186 cm^{-1}. A quick observation shows that none of the isomers show the same features. However, three isomers viz., conformation (I), (II) and (III) show prominent peaks around 185 cm^{-1}. Conformation (II) shows a peak around 56 cm^{-1}. Conformation (I) shows peaks around 120 cm^{-1}, 165 cm^{-1}, 201 cm^{-1}. Conformation (III) shows a peak around 100 cm^{-1}. Conformation (IV) does not have show any appearance in experimental spectrum and Conformation (V) shows a peak around 56 cm^{-1}. This is in contrast to earlier observations in Au$_{19}$ and Au$_{20}$ where, IR spectrum of the ground state geometry is seen to closely match with the experimentally predicted one.[32, 65] Thus, it is more likely that in these cluster ranges, various conformations are likely to co-exist leading to a mixed experimental spectrum.

The relative reactivity indices show that atoms "A", "B" and "C" in conformation (I) are good nucleophilic sites and the central edge atoms "F" and "G" are good electrophilic sites. Sites "D" and "E" are amphiphilic site as noted from the relative f$_{nu}$ and f$_{el}$ sites. An analysis of the reactivity descriptors of high energy conformations reveals that all the sites in conformations (IV) and (V) are favorable for both electrophilic and nucleophilic attack. In conformations (II) and (III), the central atoms "B" is viable for an electrophilic attack.

TABLE 4.3: Structural, Electronic and Reactivity Parameters of Au_8 Conformations. The values in red, blue and black correspond to electrophilic, nucleophilic and amphiphilic attack sites respectively. The values given next to the conformations in Column II of the Table correspond to the inter-atomic distances (in Å) between various unique sites.

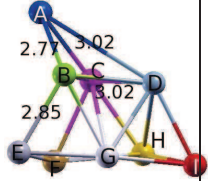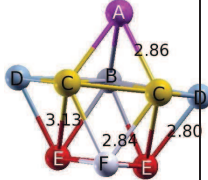|	Structure	$\triangle$ E (eV)	No. of Unique sites	Site	Charge	f_{el}	f_{nu}
I		0.00	2	A	0.17	1.06	0.94
				B	-0.17	0.92	1.08
II		0.44	5	A	-0.29	1.31	0.77
				B	0.06	1.03	0.97
				C	0.10	0.89	1.13
				D	-0.09	0.89	1.12
				E	0.15	1.00	1.00
III		0.54	6	A	0.19	0.99	1.01
				B	-0.35	0.52	1.91
				C	-0.14	0.90	1.10
				D	0.18	1.01	0.99
				E	-0.14	0.96	1.04
				F	0.19	1.69	0.59
IV		0.57	4	A	0.15	1.04	0.96
				B	0.10	1.08	0.92
				C	-0.20	0.86	1.16
				D	0.04	1.02	0.99
				E	-0.04	0.97	1.03
V		0.78	2	A	0.17	1.10	0.91
				B	-0.17	0.98	1.02
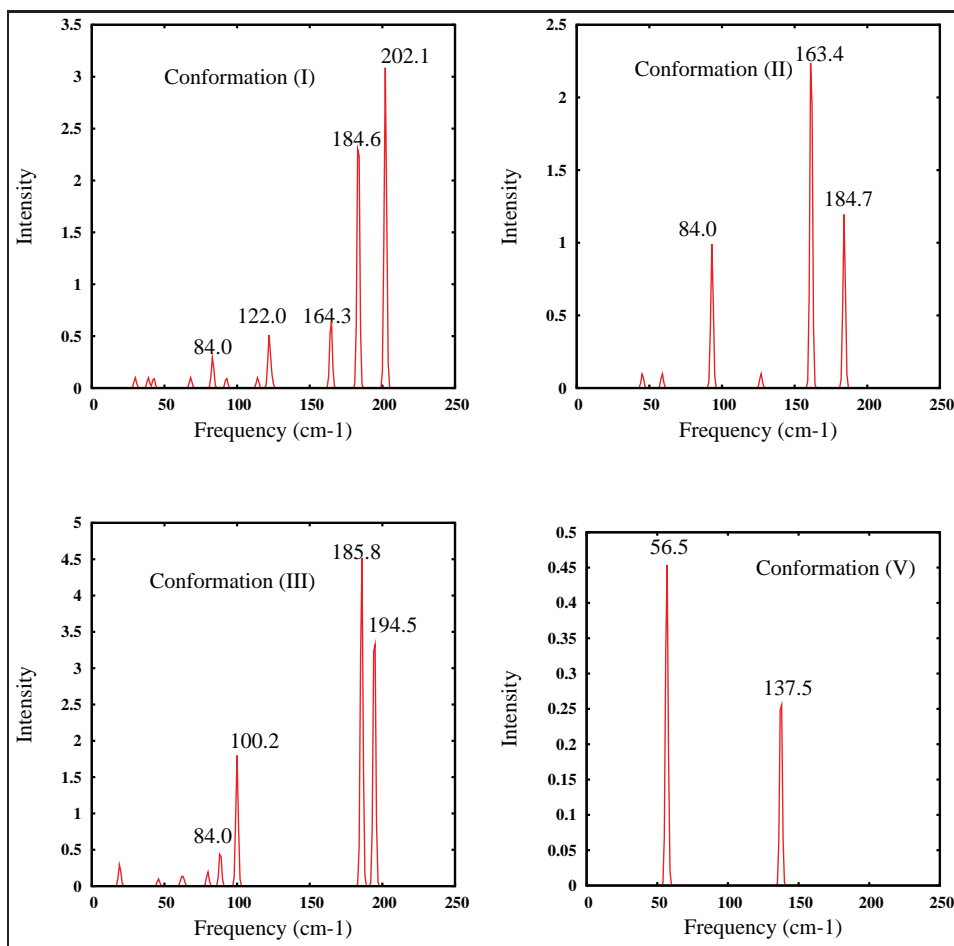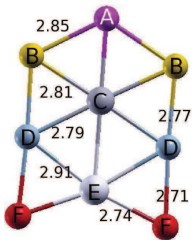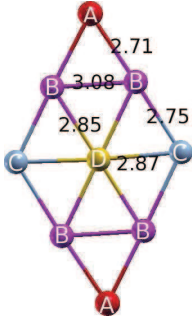
FIGURE 4.1: Calculated Infra-Red Vibration Spectra for Various Conformations of Au_7.

4.4.3 Au_8

Table 4.3 gives structural, electronic and reactivity parameters of Au_8 conformations. The lowest energy conformation (I) is a planar one with four caps ("A") to each edge of a square made up of atoms "B" as seen in Table 4.3. This is the only cluster size among Au_n (n=6-13) clusters whose lowest energy conformation is not built upon Au_6 ground state geometry. This configuration has been reported to be the lowest energy configuration also in earlier literature reports.[28, 29] The inner atoms "B" are negatively charged and bonded to each other through reasonably long bond distances of $2.88\mathring{A}$. The first high energy conformation (conformation (II)) is a planar conformation and is built upon Au_7-conformation (I). It has a C_{2v} symmetry. Due to increased symmetry, this conformation has just five distinct reactive sites. The central atoms (A-D-D) form an equilateral triangle and are bonded to each other with the largest inter atomic distances within the cluster. Atom "A" with maximum co-ordination remains negatively charged. Among the two non-linear structures considered, one of them has 6 unique reactive sites. The other non-linear conformation has D_{5h} symmetry and 2 types of reactive sites.

Analysis of the reactivity parameters indicates that the four cap atoms in the conformation (I) are favorable for a nucleophilic attack, while the atoms in the square are preferable for an electrophilic attack. Thus, the structure has alternating electrophilic and nucleophilic sites. First high energy conformation (II) has electrophilic sites located at the edges of the upper triangle while the central atom is a nucleophilic attack preferring site. The other planar conformation (IV) has favored sites of electrophilic attack inner triangle (C-C-E) surrounded by favored sites for nucleophilic attack. This arrangement is likely to be favorable for C=O oxidation which requires a simultaneous O_2 reduction and C=O oxidation. The other two non-planar conformations also show similar arrangement of the reactivity sites.

TABLE 4.4: Structural, Electronic and Reactivity Parameters of Au_9 Conformations. The values in red, blue and black are electrophilic, nucleophilic and amphiphilic attack sites respectively. The values given next to the conformations in Column II of the Table correspond to the inter-atomic distances (in Å) between various unique sites.

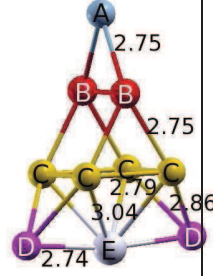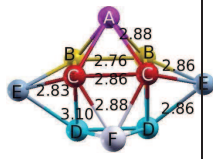|	Structure	$\triangle E$ (eV)	No. of Unique sites	Site	Charge	f_{el}	f_{nu}
I		0.00	6	A	0.05	0.92	1.09
				B	0.10	0.98	1.02
				C	-0.29	0.88	1.13
				D	-0.05	1.11	0.90
				E	-0.20	0.93	1.07
				F	0.17	0.92	1.08
II		0.10	4	A	0.16	1.00	1.00
				B	-0.06	1.02	0.98
				C	0.14	0.98	1.02
				D	-0.36	0.97	1.03
III		0.48	9	A	0.19	1.06	0.95
				B	-0.18	0.92	1.09
				C	-0.11	0.95	1.05
				D	-0.06	1.02	0.98
				E	0.20	1.06	0.94
				F	-0.02	1.05	0.96
				G	-0.18	0.92	1.09
				H	-0.03	0.98	1.02
				I	0.18	1.02	0.98
IV		0.74	6	A	0.15	1.00	1.00
				B	0.10	0.99	1.01
				C	-0.14	1.00	1.00
				D	0.18	1.01	0.99
				E	-0.02	0.99	1.00
				F	0.10	0.99	1.00
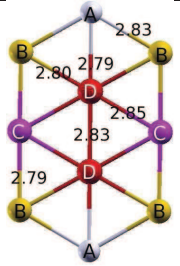
4.4.4 Au_9

The lowest two conformations of Au_9 are built upon the lowest energy conformations of Au_6 and Au_7 as shown in Table 4.4. Conformation (I) is made up of one additional atom to the first high energy isomer of Au_8, with six unique reactive sites. As in the earlier clusters, the central atoms are negatively charged.

First high energy isomer is also planar and looks like two Au_6-configurations fused at the bottom. The structure has C_{2v} symmetry and four unique reactive sites. The other two conformations given in the Table 4.4 are the lowest non-planar structures in the present study with a flat cage shape. It is noteworthy, that from Au_9 onwards we begin to see non-planar structures having a flat cage conformation. One of the non-planar conformations with C_1 symmetry has nine distinct reactive sites. As in earlier cases, atoms with the higher co-ordination are negatively charged and are bonded to each other with largest inter atomic bond distances in all of the above configurations.

The number and types of reactive sites in each of these three clusters are given in Table 4.4. All the atoms in the lowest energy structure except "B" and "D" sites are viable for an electrophilic attack. The other planar conformation (conformation (II) in contrast has the central atom clearly preferable for electrophilic attack with rest of atoms being amphiphilic in nature. Conformation (IV), which is more symmetric of the two non-planar has all the atoms with amphiphilic behavior. On the other hand, another conformation III has 6 chemically distinct reactive sites of which the four corner atoms "A", "E", "F" and "I" are favorable for a nucleophilic attack. Thus, conformation (III), which is a high energy isomer, offers more sites susceptible to nucleophilic attack as compared to the ground state conformation.

TABLE 4.5: Structural, Electronic and Reactivity Parameters of Au$_{10}$ Conformations. The values in red, blue and black are electrophilic, nucleophilic and amphiphilic attack sites respectively. The values given next to the conformations in Column II of the Table correspond to the inter-atomic distances (in Å) between various unique sites.
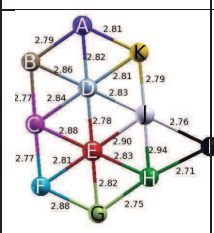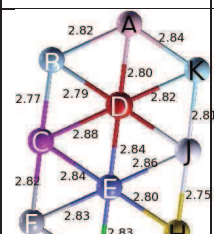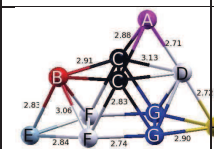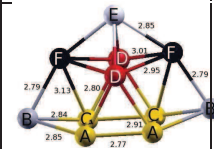
	Structure	$\triangle$ E (eV)	No. of Unique sites	Site	Charge	f_{el}	f_{nu}
I		0.00	4	A	0.06	0.75	1.33
				B	0.09	1.04	0.96
				C	0.02	1.47	0.68
				D	-0.25	0.86	1.17
II		0.31	5	A	0.16	0.52	1.91
				B	-0.07	0.26	3.80
				C	-0.08	0.84	1.19
				D	0.23	2.02	0.50
				F	-0.17	1.67	0.60
III		0.67	6	A	0.12	1.32	0.76
				B	-0.07	1.10	0.91
				C	-0.16	1.19	1.19
				D	-0.06	0.91	0.91
				E	0.18	1.35	1.35
				F	0.12	1.32	0.76

4.4.5 Au_{10}

Table 4.5 gives the structural details and reactivity parameters for Au_{10} cluster. The lowest energy conformation is built upon Au_9 conformation (I). The geometry does not change significantly from that of Au_9 in spite of one additional atom. However, it increases the symmetry of the structure to C_{2v} there by reducing the atoms with distinct chemical environment to four. As in case of earlier clusters, the central atoms are negatively charged. The two non-planar structures are reasonably symmetric and lie about 0.3 eV and 0.7 eV higher than the planar ground state configuration.

In conformation (I), the outer edge atoms "B-C-B" are most vulnerable for an nucleophilic attack, while the atoms forming an inner edge "A-D-D-A" are better for an electrophilic attack. The lowest non-linear conformation (II) is a very interesting geometry where its entire upper part (A-B-B-C) is highly favorable for an electrophilic attack leaving only three atoms at the bottom, D-E-D, for a nucleophilic attack. Another non-linear conformation (III), in contrast has only four atoms, two "C" sites and two "E" sites for an electrophilic attack. Thus, the non-planar cluster is a better alternative for adsorption of molecules seeking electrons, while the lower planar structure is better for adsorption of electron donating molecules such as CO.

TABLE 4.6: Structural, Electronic and Reactivity Parameters for Au_{11} Conformations. The values in red, blue and black are electrophilic, nucleophilic and amphiphilic attack sites respectively. The values given next to the conformations in Column II of the Table correspond to the inter-atomic distances (in $\mathring{A}$) between various unique sites.
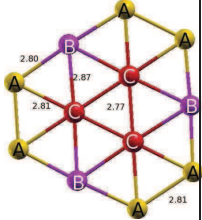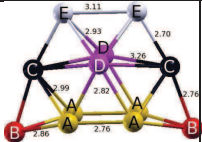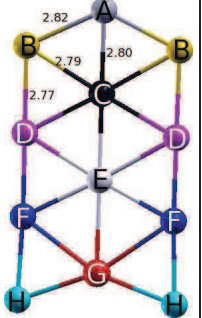
	Structure	$\triangle$ E (eV)	No. of Unique sites	Site	Charge	f_{el}	f_{nu}
I		0.00	11	A	0.06	1.00	0.99
				B	0.09	0.97	1.03
				C	0.00	0.91	1.10
				D	-0.21	1.09	0.92
				E	-0.24	1.15	0.87
				F	0.09	0.98	1.03
				G	0.11	0.99	1.01
				H	-0.05	0.99	1.01
				I	0.17	1.03	0.97
				J	-0.13	0.93	1.08
				K	0.11	1.01	0.98
II		0.06	11	A	0.06	1.00	1.00
				B	0.09	1.01	0.99
				C	0.02	1.02	0.99
				D	-0.26	0.97	1.03
				E	-0.23	1.03	0.97
				F	0.13	1.00	1.00
				G	-0.08	1.00	1.00
				H	-0.05	1.00	1.00
				I	0.15	0.99	1.01
				J	0.05	0.98	1.02
				K	0.10	1.01	0.98
III		0.53	8	A	0.23	1.08	0.93
				B	-0.02	0.92	1.09
				C	-0.14	0.89	1.12
				D	-0.13	1.08	0.92
				E	0.18	1.01	0.99
				F	-0.05	1.02	0.98
				G	-0.05	1.02	0.98
				H	0.21	1.07	0.94
IV		0.64	5	A	0.01	1.02	0.98
				B	0.17	1.03	0.97
				C	-0.08	1.00	1.00
				D	-0.05	0.97	1.03
				E	-0.19	0.98	1.01
				F	0.17	1.01	0.99
				G	-0.07	0.94	1.06

4.4.6 Au_{11}

Table 4.6 gives the details of Au_{11} conformations. Conformations (I) and (II) are lowest energy configurations with C_1 point group and are built upon Au_{10} conformation. Both of them have 11 unique reactive sites. The two central atoms and the atoms bonded to the new additional atom (I) in both cases are negatively charged. The two lowest non-planar configurations shown are very similar except for the position of the top cap atom which makes configuration (IV) more symmetric as compared to the configuration (III).

Analysis of the relative reactivity descriptors shows that in conformation (I), the two central atoms "D", "E" and the projecting atom "I" are most viable atoms for an nucleophilic attack, while, the atoms forming the left edge "B", "C", "F", and "G" are favorable for an electrophilic attack. In contrast, conformation (II) has only one site for a nucleophilic attack which is the central atom "E". Thus, difference in position of a single atom modifies the number and type of reactive sites in a cluster. Going to a non planar conformation III results in a geometry with several sites (six unique sites) favorable for a nucleophilic attack (eight atoms). Rest of the three atoms "B" and "C" are favorable sites for an electrophilic attack. However, the more symmetric non-planar structure has only two central atoms favorable for an electrophilic attack viz., "D". The two edge atoms on both sides, "B", and "F" are favorable for an nucleophilic attack.

TABLE 4.7: Structural, Electronic and Reactivity Parameters of Au_{12} Conformations. The values in red, blue and black are electrophilic, nucleophilic and amphiphilic attack loving sites respectively. The values given next to the conformations in Column II of the Table correspond to the inter-atomic distances (in Å) between various unique sites.
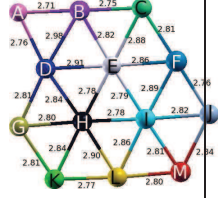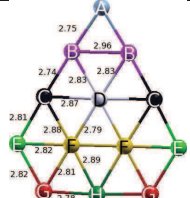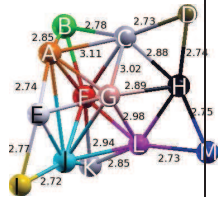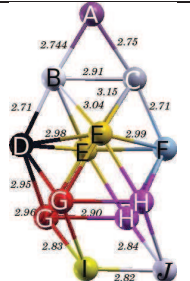
Structure	$\triangle$ E (eV)	No. of Unique sites	Site	Charge	f_{el}	f_{nu}
I	0.00	3	A	0.10	1.05	0.95
			B	-0.01	0.60	1.66
			C	-0.19	1.83	0.55
II	0.52	5	A	-0.05	0.82	1.21
			B	0.21	1.23	0.81
			C	-0.08	1.26	0.79
			D	-0.20	0.84	1.19
			E	-0.16	1.03	0.97
III	0.73	8	A	0.06	1.24	0.81
			B	0.11	1.03	0.98
			C	-0.28	0.93	1.08
			D	0.03	0.74	1.35
			E	-0.19	1.26	0.79
			F	-0.01	1.22	0.82
			G	-0.21	0.73	1.37
			H	0.17	1.06	0.95
IV	0.91	9	A	0.06	0.69	1.46
			B	0.10	0.63	1.60
			C	0.04	1.04	0.96
			D	-0.02	1.14	0.88
			E	0.20	1.13	0.88
			F	-0.21	1.54	0.65
			G	-0.04	1.22	0.82
			H	-0.38	0.71	1.41
			I	0.09	0.99	1.01

4.4.7 Au_{12}

Table 4.7 describes the lowest energy geometry and a few higher energy conformers of Au_{12}. Conformation (I) is planar and is the lowest energy structure with a symmetry of D_{3h}. The high symmetry of the structure reduces the number of chemically distinct sites to three. Other planar structure of Au_{12} which is also built upon the structure of Au_{11} is less symmetric than Conformation (I) with 8 distinct reactive sites and C_{2v} symmetry. Conformation (III) is the lowest energy of all non-planar ones and corresponds to the flat cage. This structure is also built upon the lowest energy non-planar structure of Au_{11} and has 5 distinct reactive sites. Conformation (IV) is the higher energy non-planar structure of Au_{12} with a point group of C_s. It has one mirror plane passing through the atoms A, B, C, H and I thereby dividing the cluster into two halves due to which distinct reactive sites reduces to 9.

The lowest energy conformation of Au_{12}, which is a Au_6 cluster with 2 atoms capping each edge has one reactive site "B", which is favorable for an electrophilic attack. The three central atoms, "C", are the only atoms favorable for a nucleophilic attack. The next low lying planar configuration, conformation (II), results in one less site for an nucleophilic attack with the central atom, "C", atoms "D", and "E" site preferring an electron loving guest. In the non-planar conformation, conformation (III), all the atoms with maximum coordination, viz., "D" and "A", prefer an electrophilic attack, with rest of the atoms favoring and nucleophilic attack. The other non-planar structure shows an interesting feature where the entire lower part of the structure is a electron loving region, thereby preferring to react with electron donating molecules, leaving the upper three atoms "A", "B", and "H" for a electrophilic attack. Thus, interestingly, most of the Au_{12} clusters are favorable for an nucleophilic attack.

TABLE 4.8: Structural, Electronic and Reactivity Parameters of Au$_{13}$ Conformations. The values in red, blue and black are electrophilic, nucleophilic and amphiphilic attack loving sites respectively. The values given next to the conformations in Column II of the Table correspond to the inter-atomic distances (in Å) between various unique sites.

	Structure	$\triangle$ E (eV)	No. of Unique	Site	Charge	f_{el}	f_{nu}
I		0.00	13	A	0.19	0.98	1.02
				B	-0.05	1.00	0.99
				C	0.15	1.01	0.99
				D	-0.14	1.03	0.97
				E	-0.18	0.99	1.01
				F	-0.01	1.02	0.98
				G	0.10	0.99	1.00
				H	-0.15	0.99	1.00
				I	-0.19	1.00	1.00
				J	0.10	1.00	1.00
				K	0.10	0.99	1.00
				L	-0.01	1.03	0.98
				M	0.01	0.97	1.03
II		0.04	8	A	0.15	0.99	1.01
				B	-0.04	1.05	0.96
				C	0.03	0.94	1.07
				D	-0.16	1.02	0.98
				E	0.11	1.03	0.98
				F	-0.19	0.93	1.07
				G	0.99	1.04	0.96
				H	0.00	1.00	1.01
III		0.47	13	A	0.01	1.00	1.00
				B	0.22	1.00	1.00
				C	-0.18	0.97	1.03
				D	0.21	1.05	0.95
				E	0.01	0.92	1.08
				F	-0.28	0.96	1.05
				G	-0.16	1.02	0.98
				H	-0.12	0.95	1.06
				I	0.11	1.03	0.97
				J	-0.18	1.05	0.95
				K	0.24	1.00	1.00
				L	-0.17	0.95	1.06
				M	0.20	1.06	0.94
IV		0.99	9	A	0.16	1.01	1.00
				B	-0.03	1.01	0.99
				C	-0.01	0.99	1.01
				D	0.09	0.95	1.05
				E	-0.16	1.03	0.97
				F	0.07	1.01	0.99
				G	0.02	0.98	1.02
				H	-0.10	1.02	0.98
				I	0.02	1.01	0.99

4.4.8 Au_{13}

Table 4.8 gives the lowest energy structure and a few characteristic high energy conformations of Au_{13}. It is clearly seen that there are two lowest nearly degenerate planar conformations which are both built upon planar conformation of Au_{12}. Conformation III, is the lowest energy structure among the all non-planar conformations and is built upon the lowest non-planar conformation of Au_{12}. There are no major changes in the inter atomic bond distances due to the additional atom. Structure IV is a higher energy conformer which is non planar with no clear symmetry (C_1) and thus has 13 distinct sites.

Analysis of the reactivity parameters indicates that most of the sites in the lowest energy planar configuration and two non-planar configurations are amphiphilic in nature. The planar configuration nearly degenerate to the ground state conformation has alternating electrophilic and nucleophilic loving sites. This arrangement of amphiphilic sites or alternating electrophilic and nucleophilic sites makes then ideal catalysts for CO reduction as discussed before.

TABLE 4.9: HOMO and LUMO energies, the corresponding energy gaps and hardness in Au clusters

System	$-E_H(eV)$	$-E_L(eV)$	$E_{gap}(eV)$	Hardness, $\eta(eV)$
$Au_6 - I$	6.041	3.837	2.204	1.102
$Au_6 - II$	5.795	4.029	1.767	0.883
$Au_6 - III$	5.514	5.117	0.397	0.199
$Au_6 - IV$	5.270	4.496	0.774	0.387
$Au_7 - I$	5.139	3.950	1.188	0.594
$Au_7 - II$	4.632	4.550	0.081	0.041
$Au_7 - III$	4.664	3.879	0.785	0.392
$Au_7 - IV$	4.981	3.833	1.148	0.574
$Au_7 - V$	4.866	3.943	0.924	0.462
$Au_8 - I$	6.045	4.340	1.706	0.853
$Au_8 - II$	5.461	4.623	0.837	0.419
$Au_8 - III$	5.816	3.987	1.829	0.914
$Au_8 - IV$	5.666	4.623	1.043	0.521
$Au_8 - V$	5.823	3.903	1.921	0.960
$Au_9 - I$	5.135	4.356	0.778	0.389
$Au_9 - II$	4.706	4.530	0.176	0.088
$Au_9 - III$	4.803	4.050	0.753	0.377
$Au_9 - IV$	4.581	3.912	0.669	0.335
$Au_{10} - I$	5.735	4.439	1.297	0.648
$Au_{10} - II$	5.527	4.132	1.395	0.698
$Au_{10} - III$	5.396	4.178	1.218	0.609
$Au_{11} - I$	5.239	4.247	0.992	0.496
$Au_{11} - II$	4.468	4.468	0.541	0.271
$Au_{11} - III$	4.927	4.036	0.891	0.446
$Au_{11} - IV$	4.801	4.189	0.612	0.306
$Au_{12} - I$	5.642	4.707	0.935	0.467
$Au_{12} - II$	5.514	4.408	1.106	0.553
$Au_{12} - III$	5.599	4.556	1.044	0.522
$Au_{12} - IV$	5.219	4.380	0.839	0.420
$Au_{13} - I$	5.219	4.525	0.695	0.347
$Au_{13} - II$	4.991	4.780	0.210	0.105
$Au_{13} - III$	4.801	4.062	0.740	0.370
$Au_{13} - IV$	4.854	4.393	0.461	0.230
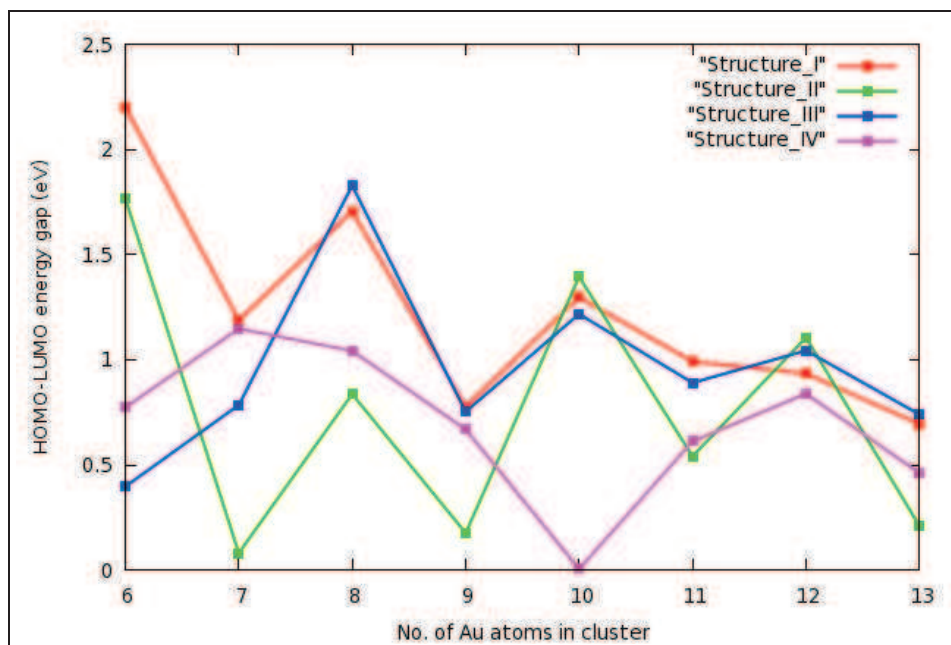
FIGURE 4.2:   Size dependence of HOMO-LUMO energy gaps for the low-lying energy structures of Au cluster

4.4.9   HOMO-LUMO Energy Gap

The HOMO-LUMO energy gap reflects the possibility of electrons to jump from the occupied orbitals to unoccupied orbitals and is a fair indicator of the electronic stability of the cluster. It partially indicates the electronic perturbation required to loose the assembly of molecule undergoing a chemical reaction or a thermal isomerisation. Table 4.9 gives the HOMO-LUMO energy gaps for various conformations of Au clusters. From the values of HOMO-LUMO energy gap as obtained, the planar Au_6 has a very noticeable value for E_{gap} which is in well agreement with the literature [69] and calculations performed by Wang et al. [70] The experimental [71] value of HOMO-LUMO transition energy has been reported to be 2.5 eV which is in reasonable accordance with our calculated value of 2.2 eV.

Thus, the HOMO-LUMO energy gap of Au_6 ground state conformation is found to be higher than that of two most stable Au clusters reported to date, viz., Au_{20} (with a reported energy gap of 1.77 eV experimentally [72] and 1.85 eV theoretically [73]) and Au_2 (1.97 eV from our calculations against 1.96 eV in literature. [69]) The Au_6 ground state conformation also has a much higher energy gap value as compared to the corresponding values of Au_7-Au_{13} ground state conformations. The order of electronic stability of the ground state conformation as understood from the HOMO-LUMO energy gap is $Au_6 > Au_2 > Au_{20} > Au_8 > Au_7 > Au_{10} > Au_{11} > Au_{12} > Au_{13}$, with also Au_6 as the most stable cluster among Au_n (n=1-20) clusters. The higher energy conformations of Au_6 have much lower E_{gap} values, indicating that Au_6 ground state conformation is also exceptionally stable compared to its higher energy conformations.

In the context of higher energy clusters of Au_7, conformation (I) shows the highest stability followed by nonplanar conformation (IV) and (V). The nonplanar conformation (V) of Au_8 is the most stable one, having stability higher than the lowest energy conformation of Au_7 and is followed by conformations (III) and (I).

Conformation (I) of Au_9 is the most stable one followed by the conformations (III) and (IV). This also indicates that the most stable conformation of Au_9 is a planar one in contrary to the results of nonrelativistic CCSD (T). [22] Au_{10} has the lowest energy conformation which is planar and first three conformations show similar stability. Continuing to the higher numbered cluster Au_{11}, the relativistic DFT calculation shows that the lowest energy conformation is electronically more stable with HOMO-LUMO energy difference as 0.99 eV. The next higher energy conformation is (III) which is close to structure (I) in terms of stability. Furthermore, for Au_{12} cluster, all the clusters show similar stability in terms of HOMO-LUMO energy gap and hardness which is further calculated from the energy gap. For Au_{13} cluster, conformation (III) shows the maximum hardness followed by conformations (I), (IV) and (II).

It is thus observed that even-numbered gold clusters are more stable electronically as compared to the odd numbered ones. Moreover the stability reduces as the number of atoms in the cluster increases and so is the odd-even oscillation which has been displayed in Figure 4.4.8. This may suggest that the even numbered clusters upto ten atoms are relatively more stable as compared to their neighboring odd numbered ones.

4.5   Discussion on the Shape Sensitivity of Reactivity in Au$_n$ (n=6-13) Clusters

From the above results, it is seen that the lowest energy conformation is a planar one within the studied cluster range. All of these planar configurations have an alternating arrangement of nucleophilic and electrophilic attack loving sites (a central nucleophilic site surrounded by electrophilic sites or vice-verse). Interestingly in odd-atom clusters, the electrophilic attack loving sites form the tips or easily accessible edges of the clusters. This feature, in conjunction with the odd

unpaired electron within them makes them more favorable for reactions such as O_2 reduction. The presence of nearby nucleophilic sites facilitates the adsorption of CO molecules and its subsequent oxidation following the for O_2 reduction. These could be key factors to why the odd-planar Au gas phase clusters in this size range as favorable catalysts for CO oxidation among many experimentalists. The even-atom clusters are seen to have most of the electrophilic sites located in the interior/inner locations of the cluster. One exception to this case is Au_6 whose edges are electrophilic sites. Interestingly, Au_2 and Au_6 are the two even-atom clusters, which show high binding energies with O_2 molecule.[74–76]

However, it may be recalled that Au clusters adsorbed on oxide surfaces are more efficient catalysts for O_2 reduction.[77] This has been attributed to the additional electrons which the cluster absorbs from the oxide support making it more feasible for conversion of O_2 molecule to super-oxide (O_2^-). This type of adsorption involves most nucleophilic loving Au site orienting towards the oxide surface. Thus, it can be envisaged from the reactivity descriptors that the planar configurations consisting of both electrophilic and nucleophilic reactive sites are not the best candidates for this case. Instead, a structure, consisting of a nucleophilic attack loving base and few electrophilic and nucleophilic attack loving sites as shown in Figure 4.3(a) or a 3D cluster with amphiphilic attack loving sites at the base such as shown in Figure 4.3(b) are better suited for adsorption and subsequent catalytic reactions. Some of the earlier reports [49, 50]document the fact that mostly the 3D conformations are adsorbed on the surface.

4.6   Summary and Conclusions

Our calculations show that the lowest energy structure is a planar one up to Au_{13}. The lowest energy conformations in Au clusters grow in a directional fashion by adding one atom to the ground state of the cluster of previous size from Au_6 to
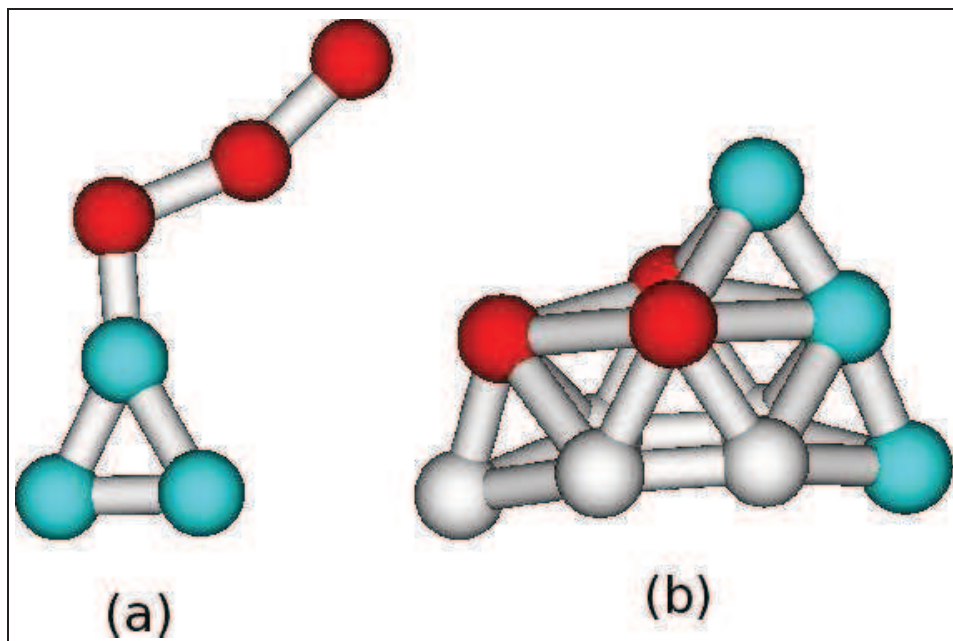
FIGURE 4.3: Some of the possible favorable Au cluster conformations for adsorption on oxide supports. Atoms in red, blue and black correspond to sites favorable for an electrophilic, nucleophilic and amphiphilic attack respectively.

Au_{13}. However, analysis of IR spectra of various isomers of Au_7 and their comparison with the experimental Au_7 IR spectrum indicate that many conformations are likely to co-exist in this cluster range. Interestingly, all the Au cluster conformations (planar as well as non-planar) in Au_n (n=6-13) have a central negatively charged core surrounded by positively charged atoms. These negatively charged centers are bonded through the largest inter-atomic bond distances. Finally, the reactivity of a cluster depends on the position and number of electrophilic and nucleophilic sites in a cluster. The reactivity descriptors indicate that while planar conformations are best suited gas phase catalysts for concomitant oxidation and reduction reactions, 3D conformations are better suited for adsorption on a surface and subsequent oxidation and reduction reactions.

Bibliography

[1] Haruta, M.; Yamada, N.; Kobayashi, T.; Iijima, S. *J. Catal.* **1989**, *115*, 301.

[2] Hutchings, G. J. *J. Catal.* **1985**, *96*, 292.

[3] Teles, J. H.; Brode, S.; Chabanas, M. *Angew. Chem.* **1998**, *99*, 2589.

[4] Hashmi, A. S. K. *Gold Bull.* **2003**, *3*, 36.

[5] Landman, U.; Luedtke, W. D.; Burnham, N.A.; Colton, R. J. *Science* **1990**, *248*, 454.

[6] Yang, Y.; Chen, S. *Nano. Lett.* **2003**, *3*, 75.

[7] Pyykko, P. *Inorg. Chim. Acta.* **2005**, *358*, 4113.

[8] Krishnamurty, S.; Shafai, G. S.; Kanhere, D. G.; Soule de Bas, B.; Ford, M.J. *J. Phys. Chem. A.* **2007**, *111*, 10769.

[9] Dyson, P. J.; Mingos, D. M. P. *Gold: Progress in Chemistry, Biochemistry and Technology*, edited by H. Schmidbaur, Wiley, New York, 511 (1999).

[10] Shaw III, C. F. *Chem. Rev.* (Washington D.C.) **1999**, *99*, 2589.

[11] Haruta, M. *Catal Today* **1997**, *36*, 153.

[12] Valden, M.; Lai, X.; Goodmanm, D. W. *Science* **1998**, *281*, 1647.

[13] Yoon, B.; Hakkinen, H.; Landman, U.; Worz, A. S.; Antonietti, J. M.; Abbet, S.; Judai, K.; Heiz, U. *Science* **2005**, *307*, 403.

[14] Haruta, M.; Takase, T.; Kobayashi, T. in *Catalytic Science and Technology*, Eds.: S. Yoshida, N. Takezawa, T. Ono, Kodansha, Tokyo **1991**, *1*, 331.

[15] Hashmi, A. S. K.; Hutchings, G. J. *Angew. Chem. Int. Ed.* **2006**, *45*, 7896.

[16] Coquet, R.; Howard, K. L.; Willock, D. J. *Chem. Rev.* **2008**, *37*, 2046.

[17] Hakkinen, H.; Landman, U. *Phys. Rev. B* **2000**, *62*, 2287.

[18] Wang, J.; Wang, G.; Zhao, J. *Phys. Rev. B* **2002**, *66*, 035418.

[19] Furche, F.; Ahlrichs, R.; Wies, P.; Jacob, C.; Gilb, S.; Bierweiler, T.; Kappes, M. M. *J. Chem. Phys.* **2002**, 117, 6982.

[20] Zhao, J.; Yang, J.; Hou, J. G. *Phys. Rev. B.* **2003**, 67, 085404.

[21] Hakkinen, H.; Yoon, B.; Landman, U.; Li, X.; Zhai, H.J.; Wang, L. S. *J. Phys. Chem. A.* **2003**, *107*, 6168.

[22] Hakkinen, H.; Moseler, M.; Kostko, O.; Morgner, N.; Hoffmann, M. A.; Bon Issendorff, B. *Phys. Rev. Lett.* **2004**, *93*, 093401.

[23] Olson, R. M.; Vargonov, S.; Gordon, M. S.; Metiu, H.; Chretien, S.; Piecuch, P.; Kowalski, K.; Kucharski, S. A.; Musial, M. *J. Am. Chem. Soc.* **2005**, *127*, 1049.

[24] Walker, A. V. *J. Chem. Phys.* **2005**, 122, 94310.

[25] Remacle, F.; Kryachko, E. S. *J, Chem. Phys.* **2005**, *122*, 44304.

[26] Gronnbeck, H.; Broqvist, P. *Phys. Rev. B* **2005**, *71*, 073408.

[27] Yuan, D. W.; Wang, Y.; Zeng, Z. *J. Chem. Phys.* **2005**, *122*, 114310.

[28] Li, X-B.; Wang, H-Y.; Yang, X-D; Zhu, Z-H.; Tang, Y-J. *J. Chem. Phys.* **2007**, *126*, 084505.

[29] Xiao, L.; Tollberg, B.; Hu, X.; Wang, L. *J. Chem. Phys.* **2006**, *124*, 114309.

[30] Li, J.; Li, X.; Zhai, H-J; Wang, L-S. *Science* **2003**, *299*, 864.

[31] Gao, Y.; Zeng, X. C. *J. Am. Chem. Soc.* **2005**, *127*, 3698.

[32] Gruene, P.; Rayner, D. M.; Redlich, B.; Van der Meer, A. F. G.; Lyon, J. T.; Meijer, G.; Fielicke, A. *Science* **2008**, *321*, 674.

[33] Bulusu, S.; Li, X.; Wang, L-S.; Zeng, X. C. *Proc. Natl. Acad. Sci.* **2006**, *103*, 8326.

[34] Hakkinen, H.; Moseler, M.; Landman, U. *Phys. Rev. Lett.* **2002**, *89*, 033401.

[35] Wang, L.; Ge, Q. *Chem. Phys. Lett.* **2002**, *366*, 368.

[36] Pawluk, T.; Hirata, Y.; Wang, L. C. *J. Phys. Chem. B.* **2005**, *109*, 20817.

[37] Wilson, N. T.; Johnston, R. L. *Eur. Phys. J.* **2000**, *12*, 161.

[38] Zhang, Z.; Berg, A.; Levanon, H.; Fessenden, R.; Meisel, W. D. *J. Am. Chem. Soc.* **2003**, *125*, 7959.

[39] Hakkinen, H. *Chem. Rev.* **2008**, *37*, 1847.

[40] Pyykko, P. *Angew. Chem. Int. Ed.* **2004**, *43*, 4412.

[41] Pyykko, P. *Inorg. Chim. Acta* **2005**, *358*, 4113.

[42] Pyykko, P. *Chem. Rev* **2008**, *37*, 1967.

[43] Wallace, W. T.; Wyrwas, R. B.; Wheten, R. L.; Mitric, R.; Bonacic-Koutecky, V. *J. Am. Chem. Soc.* **2003**, *125*, 8408.

[44] von Issendorff, B.; Hakkinen, H.; Moseler, M.; Landman, U. *Chem. Phys. Chem.* **2007**, 8, 157.

[45] Luo, C.; Fa, W.; Dong, J. *J. Chem. Phys.* **2006**, 125, 84707.

[46] Barton, D. G.; Podkolzin, S. *J. Phys. Chem. B.* **2005**, *109*, 2262.

[47] Barrio, L.; Lui, P.; Rodriguez, J.; Campos-Martin, J. M.; Fierro, J. L. G. *J. Phys. Chem. C.* **2007**, *111*, 19001.

[48] Wallace, W. T.; Wheten, R. L. *J. Am. Chem. Soc.* **2002**, *124*, 7499.

[49] Okumura, M.; Haruta, M.; Kitagawa, Y.; Yamaguchi, K. *Gold. Bull.* **2007**, *40*, 40.

[50] Chretien, S.; Metiu, H. *J. Chem. Phys.* **2007**, *126*, 104701.

[51] Shafai, G.; Hong, S.; Bertino, M.; Rahman, T. S. *J. Phys. Chem. C.* **2009**, *113*, 12072.

[52] Hohenberg, P.; Kohn, W. *Phys. Rev. B* **1964**, *136*, 864.

[53] Pearson, R. G. *J. Am. Chem. Soc.*, **1963**, *85*, 3533.

[54] Parr, R. G.; Yang, W. Density Functional Theory of Atoms and Molecules; Oxford University Press: New York, 1989.

[55] Parr, R. G.; Yang, W. *J. Am. Chem. Soc.*, **1984**, *106*, 4049.

[56] (a) Perdew, J. P.; Parr, R. G.; Levy, M.; Balduz, J. L., Jr. *Phys. Rev. Lett.*, **1982**, *49*, 1691. (b) Zhang, Y.; Yang, W. *Theor. Chem. Acc.*, **2000**, *103*, 346. (c) De Proft, F.; Amira, S.; Choho, K.; Geerlings, P. *J. Phys. Chem.*, **1994**, *98*, 5227.

[57] Yang, W.; Mortier, W. *J. Am. Chem. Soc.* **1986**, *108*, 5708.

[58] Roy, R. K.; Krishnamurti, S.; Geerlings, P.; Pal S. *J. Phys. Chem. A*, **1998**, *102*, 3746.

[59] Roy, R. K.; Proft, F. de and Geerlings, P. *J. Phys. Chem. A*, **1998**, *102*, 7035.

[60] deMon2k, Koster, A. M.; Calaminici, P.; Casida, M. E.; F-Moreno, R.; Geudtner, G.; Goursot, A.; Heine, T.; Ipatov, A.; Janetzko, F.; del Campo, J. M.; Patchkovskii, S.; Reveles, J. U.; Vela, A.; Salahub, D. R. deMon Developers (2006).

[61] Becke, A. D. *Phys. Rev. A* **1988**, *38*, 3098; Lee, C.; Yang, W.; Parr, R. G. *Phys. Rev. B* **1988**, *37*, 785.

[62] (a) Schwerdtfeger, P.; Dolg, M.; Schwarz, W.H.E.; Bowmaker, G.A.; Boyd, P.D.W. *J. Chem. Phys.*, **1989**, 91, 1762. (b) Dolg, M. Effective Core Potentials. In Modern Methods and Algorithms of Quantum Chemistry; John von Neumann Institute for Computing: Julich, 2000; Vol. 1, p 479.

[63] Godbout, N.; Salahub, D. R.; Wimmer, J. A. E. *Can. J. Phys.*, **1992**, *70*, 560.

[64] Schwerdtfeger, P.; Dolg, M.; Schwarz, W. H. E.; Bowmaker, G. A.; Boyd, P. D. W. *J. Chem. Phys.* **1989**, *91*, 1762.

[65] De, H. S.; Krishnamurty, S.; Pal, S. *J. Phys. Chem. C.* **2009**, *113*, 7101.

[66] Lowdin, P. -O., *J. Chem. Phys.*, **1950**, *18*, 365.

[67] Wells, D. H., Jr.; Delgass, W. N.; Thomson, K. T. *J. Chem. Phys.*, **2002**, *117*, 10597.

[68] James, A. M.; Kowalczyk, P.; Simard, B.; Pinegar, J. C.; Morse, M. D. *J. Mol. Spectrosc.* **1994**, 168, 248.

[69] Hakkinen, H; Landman, U. *Phys. Rev. B*, **2000**, *62*, R2287.

[70] Wang, J.; Wang, G.; Zhao, J. *Phys. Rev. B*, **2002**, *66*, 354181.

[71] Taylor, K.J.; Jin, C.; Conceicao, J.; Wang, L.-S.; Cheshnovsky, O.; Johnson, B.R. *J. Chem. Phys.*, **1990**, *93*, 7515.

[72] Li, J.; Li, X.; Zhai, H. J.; Wang, L.-S. *Science*, **2003**, *299*, 864.

[73] Gao, Y; Bulusu, S; Zeng, X. C. *J. Am. Chem. Soc.*, **2005**, *127*, 15680.

[74] Mitric, R.; Burgel, C.; Koutecky, V. B. *Proc. Acad. Natl. Sci.* **2007**, *104*, 10315.

[75] Candan, T. D.; Aksoylu, A. E.; Yildrim, R. *J. Mol. Cat. A: Chemical* **2009**, *306*, 118.

[76] Yoon, B.; Hakkinen, H.; Landman, U. *J. Phys. Chem.* **2003**, *107*, 4066.

[77] Joshi, A. M.; Delgass, W. N.; Thomson, K. T. *J. Phys. Chem. B.* **2006**, *110*, 16439.

Chapter 5

Sensitivity of Exchange correlation Functionals on Structure and Properties of Au Clusters

Abstract

We analyze the Relativistic Density Functional Theory based calculation for gold clusters with six to thirteen atoms on the ground of various exchange-correlation functionals. The work discusses that the electronic structures, energetics and vibrational spectra are sensitive towards the exchange correlation functionals used in density functional (DF) calculations whereas the density of states and Fukui functions are more or less independent of functionals. The 2D-3D transition in this cluster size is also quite dependent on the functional. This makes the choice of the appropriate functionals to speculate the correct lowest or low lying isomers and their properties highly complicated within DF based methods.

139

5.1 Introduction

Gold is preferentially used to construct nanoclusters for its surprising chemical reactivity as compared to the bulk gold which is well known for its chemical inertness. Small gold clusters, however, show distinctively different chemical properties compared to the bulk. Gold clusters of a few nanometers in diameters is reported to possess high catalytic activity [1–4], high relativistic effects [5–9] and correlation of a large number of electrons in the clusters [10] and so on. Apart from these, there are properties like electronic transport [11, 12], magnetic [13, 14] and optical [15, 16] properties which makes gold a potential material for for application in the field of molecular electronic devices, catalysis and as probes for biological diagnostics and so on [17].

Besides chemical applications of bare gold clusters, the properties vary distinctively depending upon the nature of support, geometry and shape of the Au cluster. Various theoretical [18–31] and experimental studies in concordance with theoretical calculations exist in literature to understand the electronic and structural properties as a function of shape and size. The importance of Au clusters in chemistry presents an additional motivation to study its energetics, vibrational spectrum, reactivity, density of states and potential energy curves (PECs) [32].

Density Functional Theory [33] combined with approximate exchange correlation (XC) functionals [34] has become a popular method to calculate various properties of molecules. An advantage of DFT is the relatively less computational time and less memory space without compromising the much of accuracy as compared to wave-function based theory[35]. With increase in size of the system, wave-function based method becomes unfeasible because of the high computational cost and the only first principle method available is DFT. This motivated immense efforts in development and testing of various XC functionals within the framework of DFT. Without the advent of various functionals DFT it would have remained mere a semiemperical theory. Despite these limitations, various XC functionals

are widely used for modeling of various systems. Formerly XC functionals relied upon the homogeneous electron density, and were solely based upon Local Density Approximation (LDA). Later on XC functionals included energy dependence on the gradient of density, Generalized Gradient Approximations, GGA. Further developments on kinetic energy density dependent functionals, which are known as meta-Generalized Gradient Approximations, meta-GGA.

In the present study we have used both GGA and meta-GGA and LDA XC functionals and compared the results obtained by them. As a consequence of the above discussion we explore the sensitivity of these functionals on neutral gas phase Au clusters in the region of 6-13 atoms, examine the lowest energy state in their lowest spin multiplicity and analyze variations in energetics, vibrational spectra, DOS, reactivity and PECs.

5.2 Computational Details

DFT calculations were performed as implemented in the deMon2K code (ver.2.2.6) [43]. Pseudopotentials modified with relativistic corrections were used to describe the nineteen valence electrons for all atoms and rest electrons are treated as core [42]. Six different exchange-correlation functionals, the Becke exchange (1988) plus Lee-Yang-Parr correlation [44] (B88-LYP), Perdew-Burke-Ernzerhof correlation (PBE) [45], Perdew-Wang (PW91) [46], Vosko-Wilk-Nusair (VWN) [47], *meta*-GGA functionals of Tao, Perdew, Staroverov, and Scuseria (TPSS) [48, 49] and Perdew, Kurth, Zupan, and Blaha (PKZB) [50] were considered for comparision. Geometry optimizations were performed without any symmetry constraint with Broyden-Fletcher-Goldfarb-Shanno algorithm (BFGS) [51–53]. The convergence and of the geometries were based on gradient and displacement criteria with a threshold value of 10^{-5} au and the criteria for convergence of SCF cycles was set to 10^{-9}. Only one spin multiplicity was has been investigated depending upon

the cluster-size. Only lowest spin-state has been considered for all the Au clusters. The spin multiplicities for even electron (even number of Au atoms) clusters were singlets and doublets for odd electron (odd number of Au atoms) clusters.

5.3   Results and Discussions

5.3.1   Energetics

The relative energies of various conformations for Au_n(n=6-13) are given in Tables 5.1-5.8. The relative trends are quite similar for all functionals for the case of Au_6 with a planar conformation as the lowest energy conformation. However, the trends begin to differ from Au_7 onwards. The LDA functional predicts a non-planar conformation as the lowest energy conformation. With the exception of B88LYP, rest of the GGA functionals predict a non-planar conformation as the lowest energy conformation. With the further increase in the cluster size, the trends begin to vary more widely. Intrestingly, however, all of the GGA functionals except the B88LYP show a 2D-3D transition at Au_{13}. However, the prediction of ground state geometry is different for different functionals. PKBZ and TPSS (the meta-GGA functionals) predict one non-planar conformation, while PBE and PW91 show that the planar and non-planar conformations are nearly degenerate. The structures obtained are in agreement with the earlier theoretical reports.[56, 57] Relativistic calculations for Au_n involving meta-GGA XC-functionals are not available in literature. In the past, smaller Au_n clusters, viz., Au_2 to Au_5 have been reported for the comparision of various basis sets and functionals.[58] Thus the prediction of the ground state geometry is quite functional dependent. A debate on the 2D-3D transition has been earlier well documented.

5.3.2 Properties

We have tabulated the harmonic frequencies for the Au_7 cluster for the complete set of XC functionals in figure 5.1. The structures with imaginary frequencies were avoided to ensure the minima on the PES. The vibrational frequencies were computed for all sets of XC-functionals. Experimental results for harmonic frequencies of Au_7 cluster is reported to be 220 cm^{-1}, [55] having a full width at half maximum of less than 4 cm^{-1}. The trend of the frequencies obtained from six sets of XC functional has appreciable differences in terms of the frequencies. The modelled frequency, PBE XC functionals when compared against the experimental results of Au_7 by Gruene et al.,[55] which confirms the computed frequencies to be agreement with the experimental frequencies. Moreover the minimum energy structure obtained of neutral gas phase Au_7 has been previously reported to be global minimum [59], for the meta-GGA XC functionals, the frequency shows a red shift by 40 cm^{-1} although the intensity pattern remains the same. LSD-VWN XC functional shows peaks at 203, 228 and 250 cm^{-1} respectively which is vastly different from the experimental spectrum. The reason that can be attributed for such deviation of spectra from the experimental results is the absence of HF exchange in meta-GGA functionals,[48] unlike PBE GGA which shows proper agreement with the experimental spectrum. Thus the harmonic frequencies are also functional dependent like the case of the potential energies. In contrast the Density of States (see Figure 5.2) and Fukui functions (see Table 5.9) quite functional independent. The trends are uniform across all the functionals. Interstingly, these both properties are are differential in nature. Thus, it can be concluded that the functional choice is not so critical in case of calculation of differential properties.

TABLE 5.1:   Relative energies computed for various Au$_6$ conformations using various exchange-correlation potentials are listed. The comparision of energy is done with respect to lowest total energy of cluster for a given functional.
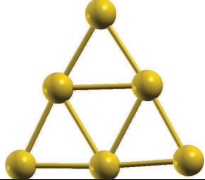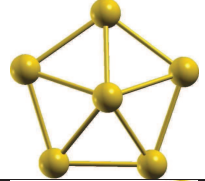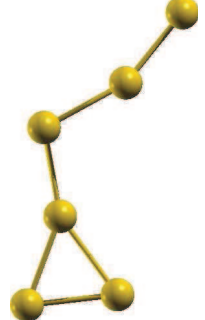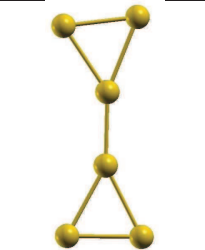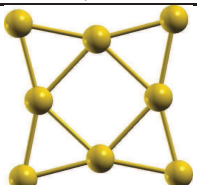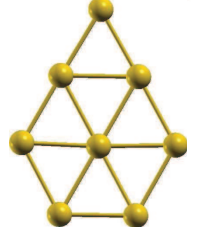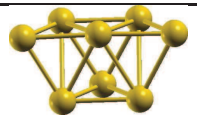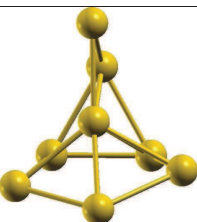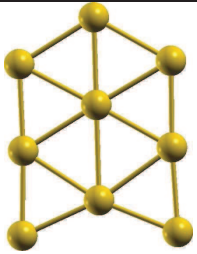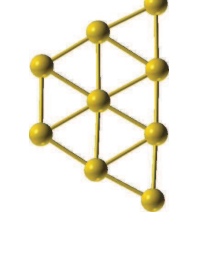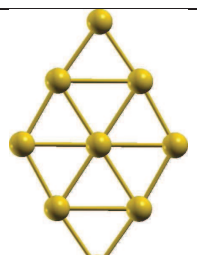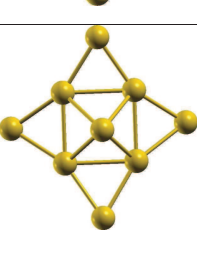
Conf./Funct.		$E_{(B88LYP)}$	$E_{(PBE)}$	$E_{(PKZB)}$	$E_{(PW91)}$	$E_{(TPSS)}$	$E_{(VWN)}$
I		0.00	0.00	0.00	0.00	0.00	0.00
II		0.90	0.87	0.92	0.87	0.89	0.86
III		0.00(I)	0.00(I)	0.00(I)	0.00(I)	0.00(I)	0.00(I)
IV		1.61	1.87	1.89	1.89	1.97	2.36

TABLE 5.2: Relative energies computed for various Au_7 conformations using various exchange-correlation potentials are listed. The comparison of energy is done with respect to lowest total energy of cluster for a given functional
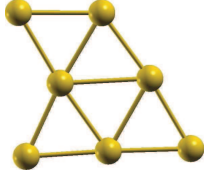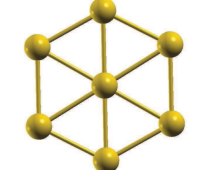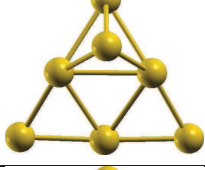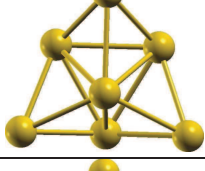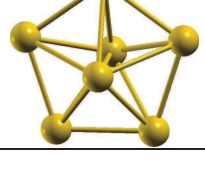
Conf./Funct.		$E_{(B88LYP)}$	$E_{(PBE)}$	$E_{(PKZB)}$	$E_{(PW91)}$	$E_{(TPSS)}$	$E_{(VWN)}$
I		0.00	0.00	0.00	0.00	0.00	0.01
II		0.37	0.29	0.31	0.29	0.28	0.21
III		0.45	0.22	0.19	0.21	0.19	0.16
IV		0.68	0.42	0.36	0.41	0.30	0.08
V		0.74	0.42	0.33	0.40	0.26	0.00

TABLE 5.3: Relative energies computed for various Au_8 conformations using various exchange-correlation potentials are listed. The comparison of energy is done with respect to lowest total energy of cluster for a given functional
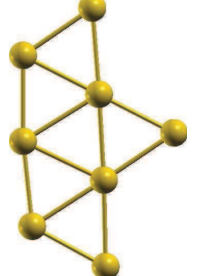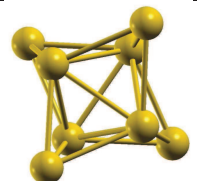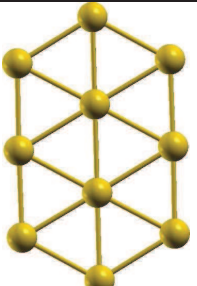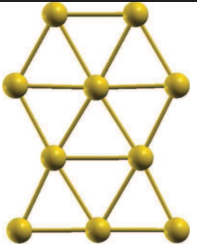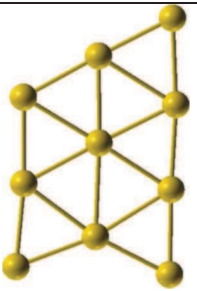
	Conf./Funct.	$E_{(B88LYP)}$	$E_{(PBE)}$	$E_{(PKZB)}$	$E_{(PW91)}$	$E_{(TPSS)}$	$E_{(VWN)}$
I		0.00	0.00	0.00	0.00	0.00	0.28
II		0.44	0.32	0.33	0.31	0.27	0.43
III		0.71	0.37	0.29	0.35	0.20	0.00
IV		0.54	0.46	0.49	0.44	0.34	0.37
V		0.56	0.53	0.52	0.53	0.51	0.77
VI		0.78	0.41	0.31	0.39	0.22	0.17

TABLE 5.4: Relative energies computed for various Au_9 conformations using various exchange-correlation potentials are listed. The comparison of energy is done with respect to lowest total energy of cluster for a given functional
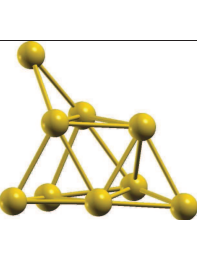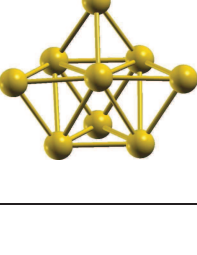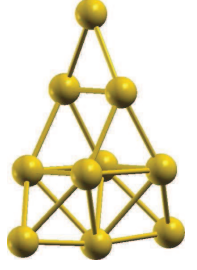
Conf./Funct.		$E_{(B88LYP)}$	$E_{(PBE)}$	$E_{(PKZB)}$	$E_{(PW91)}$	$E_{(TPSS)}$	$E_{(VWN)}$
I		0.00	0.00	0.00	0.00	0.00	0.17
II		0.08	0.10	0.09	0.96	1.00	0.28
III		0.10	0.14	0.14	0.13	0.15	0.30
IV		0.20	0.20	0.15	0.20	0.19	0.29
V		0.58	0.36	0.25	0.35	0.23	0.00
VI		0.75	0.43	0.30	0.41	0.26	0.14

TABLE 5.5: Relative energies computed for various Au_{10} conformations using various exchange-correlation potentials are listed. The comparison of energy is done with respect to lowest total energy of cluster for a given functional
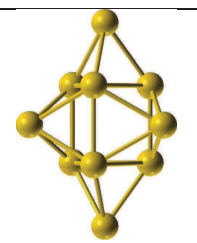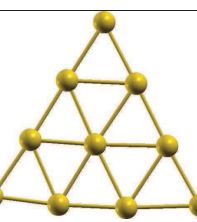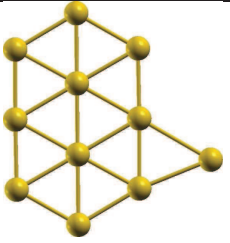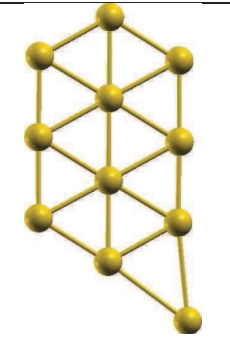
	Conf./Funct.	$E_{(B88LYP)}$	$E_{(PBE)}$	$E_{(PKZB)}$	$E_{(PW91)}$	$E_{(TPSS)}$	$E_{(VWN)}$
I		0.00	0.00	0.00	0.00	0.00	0.08
II		0.02	0.12	0.11	0.13	0.16	0.34
III		0.08	0.21	0.20	0.21	0.25	0.42
IV		0.33	0.19	0.14	0.19	0.14	0.00
V		0.65	0.41	0.30	0.41	0.27	0.03
VI		0.82	0.95	0.95	0.95	1.01	1.14

TABLE 5.6: Relative energies computed for various Au_{11} conformations using various exchange-correlation potentials are listed. The comparison of energy is done with respect to lowest total energy of cluster for a given functional
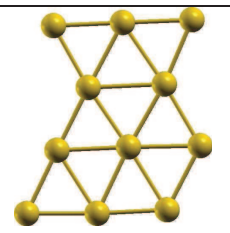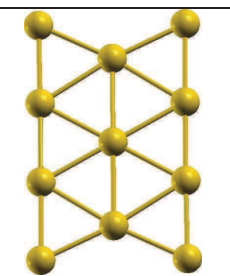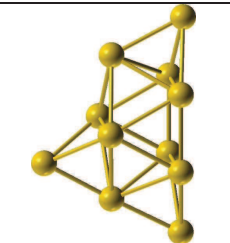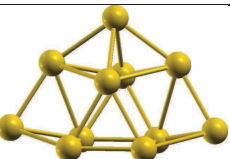
	Conf./Funct.	$E_{(B88LYP)}$	$E_{(PBE)}$	$E_{(PKZB)}$	$E_{(PW91)}$	$E_{(TPSS)}$	$E_{(VWN)}$
I		0.00	0.00	0.00	0.00	0.00	0.34
II		0.06	0.09	0.07	0.08	0.08	0.42
III		0.06	0.17	0.16	0.18	0.20	0.66
IV		0.06	0.18	0.17	0.18	0.21	0.34
V		0.53	0.22	0.06	0.18	0.03	0.00
VI		0.64	0.32	0.14	0.29	0.08	0.02

TABLE 5.7: Relative energies computed for various Au_{12} conformations using various exchange-correlation potentials are listed. The comparison of energy is done with respect to lowest total energy of cluster for a given functional
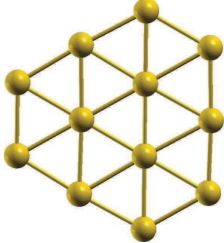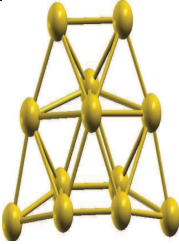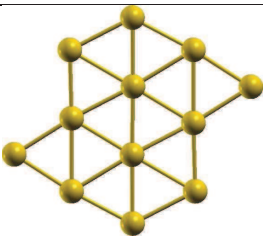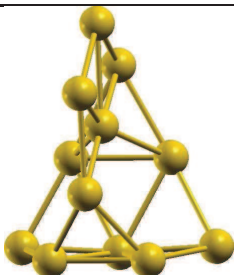
	Conf./Funct.	$E_{(B88LYP)}$	$E_{(PBE)}$	$E_{(PKZB)}$	$E_{(PW91)}$	$E_{(TPSS)}$	$E_{(VWN)}$
I		0.00	0.00	0.00	0.00	0.00	0.34
II		0.52	0.21	0.02	0.18	0.01	0.00
III		0.47	0.49	0.48	0.49	0.49	0.81
IV		0.53	0.67	0.67	0.68	0.72	1.20
V		0.71	0.85	0.87	0.86	0.92	1.38
VI		0.91	0.76	0.62	0.75	0.61	0.76

TABLE 5.8: Relative energies computed for various Au_{13} conformations using various exchange-correlation potentials are listed. The comparison of energy is done with respect to lowest total energy of cluster for a given functional
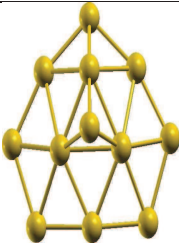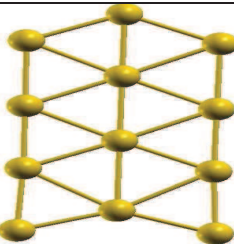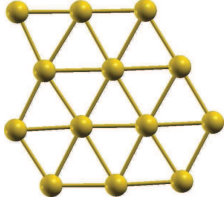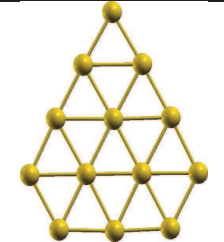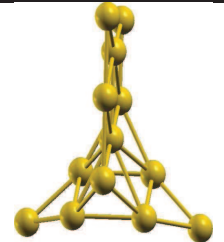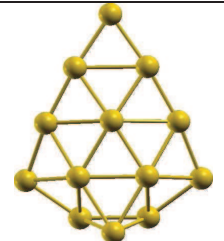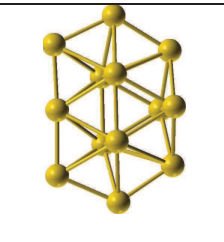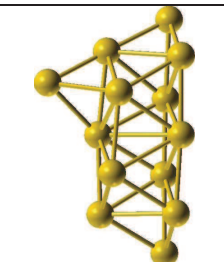
	Conf./Funct.	$E_{(B88LYP)}$	$E_{(PBE)}$	$E_{(PKZB)}$	$E_{(PW91)}$	$E_{(TPSS)}$	$E_{(VWN)}$
I		0.00	0.00	0.08	0.00	0.16	0.72
II		0.04	0.03	0.11	0.03	0.18	0.73
III		0.43	0.43	0.44	0.43	0.55	1.17
IV		0.61	0.58	0.67	0.57	0.73	1.21
V		0.69	0.14	0.00	0.11	0.00	0.00
VI		0.85	0.40	0.25	0.37	0.28	0.44

FIGURE 5.1: Vibrational Spectra for Various Functionals of Au$_7$ Lowest Energy Conformations.
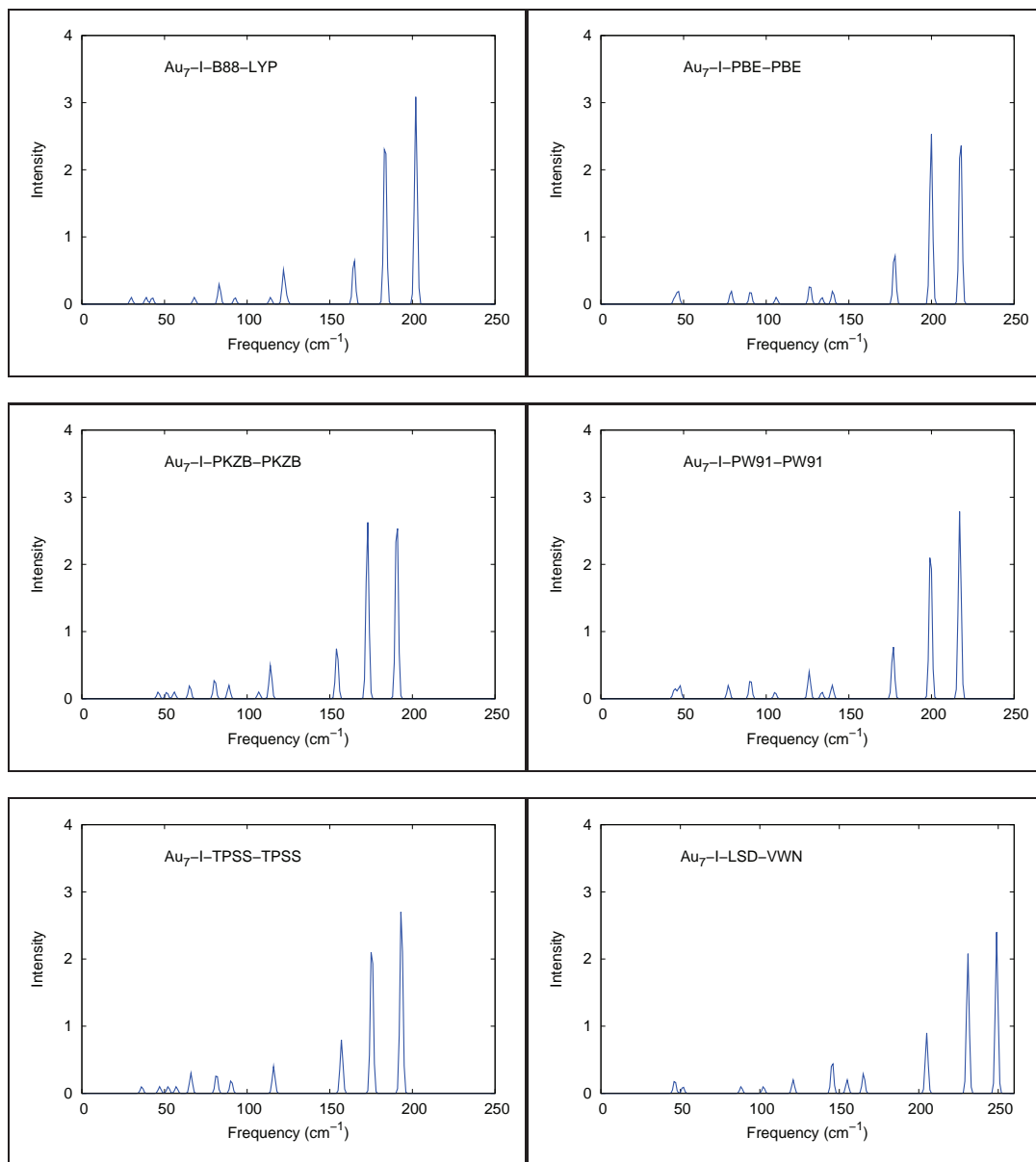
FIGURE 5.2: Relativistic Density of States (DOS) for Various Functionals of Au$_7$ Lowest Energy Conformation.
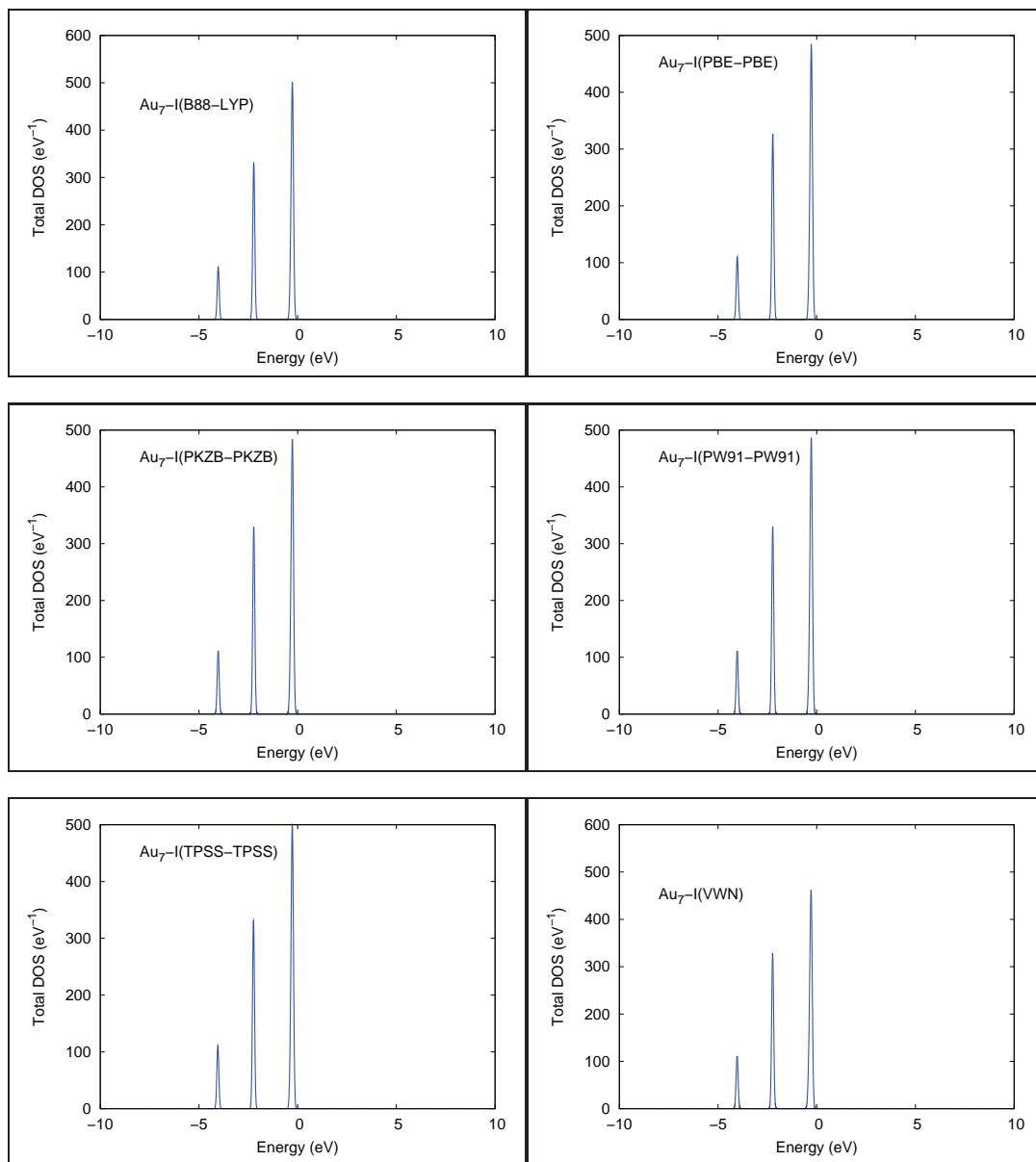
5.3.3 Conclusions

Based on relativistic density functional theory, we report that GGA XC functional PBE96-PBE is best for determining structures and vibrational spectroscopic properties those are in agreement with the experiment than those obtained for meta-GGA or LDA based XC functionals. A higher contribution of HF exchange in GGA XC functionals are capable of predicting the IR frequencies more accurately as compared to neglecting HF exchange in meta-GGA XC functionals or consideration of homogeneous electron gas in LDA functionals. We find no difference in results of density of states, relative nucleophilicity and relative electrophilicity of atoms by condensed FF method due to the alteration in XC functionals.

TABLE 5.9: Fukui Functions computed for the ground state geometry of Au_7 with various functionals

System	XC Functional	Unique sites	Site	Charge	f_{nu}	f_{el}
$Au_7 - I$	B88-LYP	7	A	0.038	0.931	1.073
			B	-0.102	0.975	1.025
			C	0.154	0.940	1.063
			D	-0.138	1.024	0.976
			E	0.176	0.993	1.007
			F	-0.248	1.108	0.902
			G	0.122	1.031	0.970
	PBE96-PBE	7	A	0.046	0.934	1.071
			B	-0.115	0.964	1.038
			C	0.166	0.931	1.074
			D	-0.143	1.018	0.982
			E	0.186	0.983	1.017
			F	-0.267	1.122	0.892
			G	0.127	1.043	0.959
	PKZB-PKZB	7	A	0.039	0.935	1.070
			B	-0.105	0.977	1.023
			C	0.156	0.318	-0.017
			D	-0.140	1.021	0.979
			E	0.178	0.990	1.010
			F	-0.251	-0.091	-0.393
			G	0.122	1.032	0.969
	TPSS-TPSS	7	A	0.039	0.935	1.069
			B	-0.107	0.982	1.018
			C	0.159	0.933	1.071
			D	-0.142	1.016	0.984
			E	0.180	0.985	1.015
			F	-0.254	1.114	0.898
			G	0.125	1.037	0.964
	LSD-VWN	7	A	0.050	0.938	1.065
			B	-0.129	0.948	1.055
			C	0.178	0.935	1.069
			D	-0.147	1.013	0.987
			E	0.198	0.978	1.022
			F	-0.285	1.118	0.894
			G	0.135	1.050	0.952

Bibliography

[1] Haruta, M.; Yamada, N.; Kobayashi, T.; Iijima, S. *J. Catal.*, **1989**, *115*, 301.

[2] Hutchings, G. J. *J. Catal.*, **1985**, *96*, 292.

[3] Teles, J. H.; Brode, S.; Chabanas, M. *Angew. Chem.*, **1998**, *99*, 2589.

[4] Hashmi, A. S. K. *Gold Bull.*, **2003**, *3*, 36.

[5] Pyykko, P. *Chem. Rev.*, **1988**, *88*, 563.

[6] Hakkinen, H.; Moseler, M.; Landman, U. *Phys. Rev.Lett.* **2002**, *89*, 033401.

[7] Pyykko, P. *Angew. Chem.*, **2002**, *114*, 3723.

[8] Pyykko, P. *Angew. Chem. Int. Ed.*, **2002**, *41*, 3573.

[9] Pyykko, P. *Angew. Chem. Int. Ed.*, **2004**, *43*, 4412.

[10] Estiu, G. L.; Zerner, M. C. *J. Phys. Chem.*, **1996**, *100*, 16874.

[11] Yu, J-X.; Chen, X-R.; Sanvito, S. *Phys. Rev. B.*, **2010**, *82*, 085415.

[12] (a) Torma, V.; Vidoni, O.; Simon, U.; Schmid, G. *Eur. J. Inorg. Chem.*, **2003**, 1121. (b) Clarke, L.; Wybourne, M. N.; Yan, M.; Cai, S. X.; Keana, J. F. W. *Appl. Phys. Lett.*, **1997**, *71*, 617.

[13] (a) Li, X.; Kiran, B.; Cui, Li-Feng.; Wang, L-S. *Phys. Rev. Lett.*, **2005**, *95*, 253401. (b) Pundlik, S. S.; Kalyanaraman, K.; Waghmare, U. V. *J. Phys. Chem. C*, **2011**, *115*, 3809.

[14] Sessoli, R.; Gatteschi, D.; Caneschi, A.; Novak, M. A. *Nature*, **1993**, *365*, 141.

[15] Pyykko, P. *Inorg. Chim. Acta.*, **2005**, *358*, 4113.

[16] Li, Q.; Wu, K.; Wei, Y.; Sa, R.; Cui, Y.; Lu, C.; Zhu, J.; He, J.; *Phys. Chem. Chem. Phys.*, **2009**, *11*, 4490.

[17] *Gold. Progress in Chemistry, Biochemistry and Technology*; Schmidbaur, H., ed.; Wiley: Chichester, 1999; p 894.

[18] Xie, Y. P.; Gong, X. G. *J. Chem. Phys.*, **2010**, *132*, 244302.

[19] Suzuki, Y.; Yamashita, K. *Chem. Phys. Lett.*, **2010**, *486*, 48.

[20] Chandrachud, P.; Joshi, K.; Krishnamurty, S.; Kanhere, D. G. *Pramana*, **2009**, *72*, 845.

[21] Bonacic-Koutecky, V.; Mitric, R. ;Buergel, C.; Nossler, M. *Chem. Phys.*, **2008**, *350*, 111.

[22] Krishnamurty, S.; Shafai, G. S.; Kanhere, D. G.;de Bas, B. S.; Ford, M. J. *J. Phys. Chem. A*, **2007**, *111*, 10769.

[23] Stanzel, J.; Burmeister, F.; Neeb, M.; Eberhardt, W.; Mitric, R.; Burgel, C.; Bonacic-Koutecky, V. *J. Chem. Phys.*, **2007**, *127*, 164312.

[24] Mitric, R.; Werner, U.; Burgel, C,; Bonacic-Koutecky, V. *Eur. Phys. J. D*, **2007**, *43*, 201.

[25] Koskinen, P.; Hakkinen, H.; Huber, B.; von Issendorff, B.; Moseler, M. *Phys. Rev. Lett.*, **2007**, *98*, 015701.

[26] Kimble, M. L.; Moore, N. A.; Johnson, G. E.; Castleman A. W.; Burgel, C.; Mitric, R.; Bonacic-Koutecky, V. *J. Chem. Phys.*, **2006**, *125*, 204311.

[27] Yildirim, E. K.; Guvenc, Z. B. *Modeling Simul. Mater. Sci. Eng.*, **2006**, *14*, 947.

[28] Fernandez, E. M.; Soler, J. M.; Balbas L. C. *Phys. Rev. B*, **2006**, *23*, 235433.

[29] Zhao, X.; Wang, S. Q.; Zhang, C. B. *J. Mater. Sci. Technol.*, **2006**, *22*, 123.

[30] Pyykko, P. *Inorg. Chim. Acta*, **2005**, *358*, 4113.

[31] Yildirim, E. K.; Atis, M.; Guvenc, Z. B. *Int. J. Mod. Phys.* **2005**, *16*, 99.

[32] Sohnel, T.; Brown, R.; Kloo, L.; Schwerdtfeger, P. *Chem.-Eur. J.* **2001**, *7*, 3167.

[33] Parr, R. G.; Yang, W. *Density Functional Theory of Atoms and Molecules*; Oxford University Press: New York, 1989.

[34] Geerlings, P.; De Proft, F.; Langenaeker, W. *Chem. Rev. (Washington, D.C.)* **2003**, *103*, 1793.

[35] Pettersson, L. G. M.; Bauschlicher, C. W.; Langhoff, S. R.; Partridge, H. *J. Chem. Phys.*, **1987**, *87*, 481.

[36] Parr, R. G.; Yang, W. *J. Am. Chem. Soc.*, **1984**, *106*, 4049.

[37] (a) Perdew, J. P.; Parr, R. G.; Levy, M.; Balduz, J. L., Jr. *Phys. Rev. Lett.*, **1982**, *49*, 1691. (b) Zhang, Y.; Yang, W. *Theor. Chem. Acc.*, **2000**, *103*, 346. (c) De Proft, F.; Amira, S.; Choho, K.; Geerlings, P. *J. Phys. Chem.*, **1994**, *98*, 5227.

[38] Yang, W.; Mortier, W. *J. Am. Chem. Soc.* **1986**, *108*, 5708.

[39] Roy, R. K.; Krishnamurti, S.; Geerlings, P.; Pal S. *J. Phys. Chem. A*, **1998**, *102*, 3746.

[40] Roy, R. K.; Proft, F. de and Geerlings, P. *J. Phys. Chem. A*, **1998**, *102*, 7035.

[41] Pearson, R. G. *J. Am. Chem. Soc.* **1963**, *85*, 3533.

[42] deMon2K, Koster, A. M.; Calaminici, P; Casida, M. E.; F-Moreno, R; Geudtner, G.; Goursot, A.; Heine, T.; Ipatov, A; Janetzko, F.; del Campo, J. M.; Patchkovskii, S.; Reveles, J. U.; Vela,A.; Salahub, D. R.; deMon Developers, 2006.

[43] Schwerdtfeger, P.; Dolg, M.; Schwarz, W. H. E.; Bowmaker, G. A.; Boyd, P. D. W. *J. Chem. Phys.* **1989**, *91*, 1762. (b) Dolg, M. *Effective Core Potentials. In Modern Methods and Algorithms of Quantum Chemistry*; John von Neumann Institute for Computing: Julich, 2000; Vol. 1, p 479.

[44] Lee, C.; Yang, W.; Parr, R. *Phys. Rev. B* **1988**, *37*, 785.

[45] Perdew, J. P.; Burke, K.; Ernzerhof, M. *Phys. Rev. Lett.* **1996**, *77*, 3865.

[46] Perdew, J. P.; Wang, Y. *Phys. Rev. B* **1992**, *45*, 13244.

[47] Vosko, S. H.; Wilk, L.; Nusair, M. *Can. J. Phys.* **1980**, *58*, 1200.

[48] Tao, J.; Perdew, J. P.; Staroverov, V. N.; Scuseria, G. E. *Phys. Rev.Lett.* **2003**, *91*, 146401.

[49] Perdew, J. P.; Tao, J.; Staroverov, V. N.; Scuseria, G. E. *J. Chem. Phys.*, **2004**, *120*, 6898.

[50] Perdew, J. P.; Kurth, S.; Zupan, A.; Blaha, P. *Phys. Rev. Lett.* **1999**, *82*, 2544.

[51] Broyden, C. G. *J. Inst. Math. Its Appl.* **1970**, *6*, 76.

[52] Fletcher, R. *Comput. J.* **1970**, *13*, 317.

[53] Goldfarb, D. *Math. Comput.* **1970**, *24*, 23.

[54] Becke, A. D. *Phys. Rev. A* **1988** *38*, 3098.

[55] Gruene, P., Rayner, D. M., Redlich, B. ; Van der Meer, A. F. G.; Lyon, J. T.; Meijer, G.; Fielicke, A. *Science*, **2008**, *321*, 674.

[56] Hakkinen, H.; Yoon, B.; Landman, U.; Li, X.; Zhai, H.-J.; Wang, LDeviations in Energy from *ab initio* data for neutral Au_6 cluster with various XC functionals..-S. *J. Phys. Chem. A*, **2003**, *107*, 6168.

[57] Li, X.-B.; Wang, H.-Y.; Yang, X.-D.; Zhu, Z.-H.; Tang, Y.-J. *J. Chem. Phys.*, **2007**, *126*, 084505.

[58] Shi, Y. -K.; Li, Z. H.; Fan, K. -N. *J. Phys. Chem. A*, **2010**, *114*, 10297.

[59] Bonacic-Koutecky, V.; Burda, J.;Roland, M., and Maofa, G.; Zampella, G.; Fantucci, P. *J. Chem. Phys.*, **2002**, *117*, 3120.

[60] (a) De, H. S.; Krishnamurty, S.; Pal, S. *J. Phys. Chem. C.*, **2009**, *113*, 7101. (b) De, H. S.; Krishnamurty, S.; Pal, S. *J. Phys. Chem. C.*, **2010**, *114*, 6690.

Chapter 6

Finite Temperature Behavior Of Small Au Clusters

Abstract

Relativistic Density Functional Theory (DFT) based molecular dynamical simulations are performed on gold clusters with three to ten atoms (Au_n; n=3-10) with an aim of understanding their finite temperature behavior in this chapter. Conformations of a cluster coexisting at different temperatures are analyzed. The simulations reveal that the finite temperature behavior of Au clusters can be classified into three regions viz., a 'solid-like' region, a 'structural fluctionality' region, and a 'liquid-like' state. The 'structural fluctionality' region is when the cluster dynamically inter converts between two conformations through a metastable intermediate. For Au_n; n$\leq$ 7, where the atoms reorient continuously such that two planar conformations co-exist. On the other hand, for Au_n; n$\geq$ 8, the cluster behaves as a quasi-planar liquid where the outer edge atoms of the cluster bend and relax alternatively around a central planar region. In 'liquid-like' state the cluster is predominantly in a 3D conformation and transits through various conformations. The onset and duration of each of the above three regions is seen to

be size dependent. Au_6 is the most stable cluster and remains in its ground state conformation (or 'solid-like' region) up to nearly 1100 K. Au_9 is the least stable among the studied clusters with a 'liquid-like' state around room temperature itself. All the clusters with the exception of Au_6 enter the 'liquid-like' state at much lower temperatures as compared to that of bulk gold.

6.1   Introduction

With respect to the bulk and atomic scale chemistry, the gas phase chemistry of metal clusters is surprisingly different. One of the most important features is their higher catalytic activity as compared to that of bulk.[1, 2] This along with the other notable features such as electronic transport,[3, 4] magnetic,[5, 6] and optical properties[7, 8] have led to a surge in the research activity on them. This is especially the case for clusters comprising 2-50 atoms (also referred to as zero dimensional quantum dots) where the quantum confinement of electrons results in size specific physical and chemical properties.

These research works have established that clusters at finite temperatures undergo a physical transformation (phase transformation) from a 'solid-like' state to a 'liquid-like' state. At low temperatures, the atoms in a cluster vibrate around their equilibrium positions similar to the case of a bulk solid and hence the name 'solid-like' state. As the temperature increases, atoms in the clusters diffusively reorient their equilibrium positions and transform into other minimum energy conformations. At much higher temperatures, these transitions are observed to happen at higher frequencies (i.e., transits through several conformations in a few femto seconds). These conformational reorientations/isomerization increases dramatically beyond a temperature specific to each cluster after which the cluster begins to resemble a liquid droplet and hence the name 'liquid-like' state. This phenomenon has been widely explored in several clusters such as silicon,[9] gallium,[10] aluminum,[11] tin,[12] sodium,[13] and gold[14] using either experimental and/or theoretical methods.

From the chemical point of view, small clusters have highly active coordination sites for catalytic activity unlike periodic surfaces, which makes them more important, apart from the above discussed physical features. These sites and their activities vary with size and shape of the cluster. The catalytic reactions on these sites occur at various finite temperatures.[15] Due to isomerization discussed

above, there is an observable correlation between the shape of the cluster and its temperature. Following this, the type and the number of surface reactive sites available for a reacting molecule, (in other words, the cluster's functional catalytic activity) is modified. Hence, stability of a given geometry or an understanding of different isomers co-existing for a cluster at its working temperature is significant. This information is lacking in the literature and hence a limitation in its practical applications.

In this context, the catalytic properties of Au clusters have been the most prominent. Hence, the potential energy surface of Au_n ($4 \leq n \leq 15$) has been the most studied topic using theoretical,[16] experimental,[17] and a combination of both these methods.[18] One of the reports using Photo Electron Spectroscopy (PES) demonstrates the possibility of 'liquid-like' states co-existing for Au_7 when generated at 100 K.[19] Along the same lines, Wang and co-workers using PES and Density Functional Theory (DFT) have demonstrated the co-existence of several planar isomers in Au_{10}^- and Au_{12}^-.[20] Studies using ion mobility spectrometry and trapped electron diffraction propose that there is a co-existence of several isomers at room temperature[21] in cationic and anionic Au_n ($n \leq 9$) clusters. The existence of this 'liquid-like' state is also validated by a debate on 2D-3D (2 dimensional-3 dimensional) transition within the Au clusters.[22] Apart from the above mentioned few works, stability and various isomers present at a given working temperature of Au clusters is not well explored experimentally.

Theoretically, the finite temperature property/behavior of intermediate sized gold clusters has been investigated by few groups using classical MD simulations.[23] One such report[24] mentions that Au clusters with 13-2869 atoms undergo a phase transition between 600-750 K. In an other work, Cleveland et *al.* using an embedded atom potential show that the Au_n ($n < 250$) clusters undergo a solid (from a low temperature structure) to solid transformations (an icosahedral, I_h structure) before a 'solid-like' to 'liquid-like' transformation around 760 K.[25] One of the interesting conclusions on the Au cluster dynamics using classical mechanics

based methods is that surface mobility of atoms within the Au clusters enhances their catalytic activity from 300 K onwards. BOMD was also applied to a limited extent to study the finite temperature behavior of Au clusters.[14, 26, 27]

However, the most interesting point raised so far is by Moseler and co-workers, who have reported a co-existence of two hetero-dimensional phases (a free planar Au liquid phase which co-exists with the usual three dimensional liquid) in anionic Au_n (11≤ n ≤ 14) clusters from tight binding DFT simulations.[27] Their work has further emphasized on the complications in validating the theoretically proposed ground state geometries. Thus, there seems to exist a more complex potential energy surface within Au clusters, with several conformations co-existing (the co-existence is likely to be more pronounced with increasing cluster size) at various working temperatures.

In light of the above discussion, in the present chapter, we explore the finite temperature behavior/ thermodynamic stability of neutral gas phase Au clusters with three to ten atoms (Au_n, n=3-10). In this range, due to their planarity, the Au clusters are proposed to be highly reactive.[28] Further, all the atoms in this size range are surface atoms. For this purpose, we have carried out *ab initio* molecular dynamical simulations on Au_n, n=3-10, clusters at various temperatures. From the simulations, we discuss the geometrical rearrangements of atoms within different sized and shaped clusters.

The chapter is organized as follows. In Section 6.2, we discuss the computational methodology and clusters for which the simulations are carried out. In Section 6.3, we note the results from the simulation studies. Section 6.4 discusses the implication of various molecular dynamical results reported in Section 6.3. We conclude the chapter in brief in Section V.

6.2   Computational Details

All calculations are performed in the framework of Density Functional Theory (DFT), using a linear combination of Gaussian orbitals as implemented in *de-Mon2k* code.[29] Several conformations are generated for each cluster size. All such generated conformations are optimized using the Perdew-Burke-Ernzerhof (PBE) exchange and correlation functional[30] with 1997 Stuttgart-Dresden Relativistic Effective Core Potential's (RECP)'s[31] as the basis set for the valence electrons. 5s, 5p, 5d and 6s electrons are considered to constitute the valence electrons. We note that these ECP's are now documented for the accurate prediction of structure as well as spectroscopic properties of Au clusters.[32, 33] No additional polarization functions are added. The A2 auxiliary functions are used to fit the charge density.[34] The convergence of the geometries is based on gradient and displacement criteria with a threshold value of 10^{-5} a.u. and the criteria for convergence of an SCF cycle was set to 10^{-9}. Only the lowest spin state is considered for all the Au clusters. Thus, the spin multiplicity for even electron (even number of Au atoms) cluster is singlet and doublet for odd electron (odd number of Au atoms) clusters. It has also been reported in an earlier literature that Au clusters prefer to be in their lowest spin state.[35] Following the geometry optimization, harmonic vibrational frequencies are computed for various conformations of Au_n ($3 \leq n \leq 10$). All of the frequencies are found to be positive, thereby, indicating the conformations to be a local minima.

The lowest energy conformation is chosen as the starting conformation for all of the Molecular Dynamical (MD) simulations. The finite temperature simulation for each cluster is carried out implementing Born-Oppenheimer Molecular Dynamics (BOMD) using the same exchange-correlation functionals and RECPs as described above. The simulations are carried out between 200 K to 2000 K. At each temperature, the cluster is equilibrated for a time period of 10 ps followed

by a simulation time of 30 ps. The temperature of the cluster is maintained using the Berendsen's thermostat ($\tau = 0.5$ps). The nuclear positions are updated using velocity Verlet algorithm with a time step of 1 fs. The atomic positions and bond length fluctuations of atoms are analyzed using traditional parameters such as Root Mean Square bond length fluctuations (δ_{rms}) and the Mean Square ionic Displacements (MSD)'s. The δ_{rms} is defined as

$$\delta_{rms} = \frac{2}{N(N-1)} \sum_{i<j} \frac{\sqrt{\langle R_{ij}^2 \rangle_t - \langle R_{ij} \rangle_t^2}}{\langle R_{ij} \rangle_t} \tag{6.1}$$

where, N is the number of particles in the system, r_{ij} is the distance between the ith and j^{th} particle in the system and $<...>_t$ denotes a time average over the entire trajectory. The MSD of an individual atom is defined as,

$$\langle R_i^2 \rangle = \frac{1}{M} \sum_{m=1}^{M} [R_i(t_{0m} + t) - R_i(t_{0m})]^2 \tag{6.2}$$

where, $R_i(t_{0m})$ is the instantaneous position of atom i at t_0 and $R_i(t_{0m} + t)$ is the corresponding position of atom i after a time interval t.
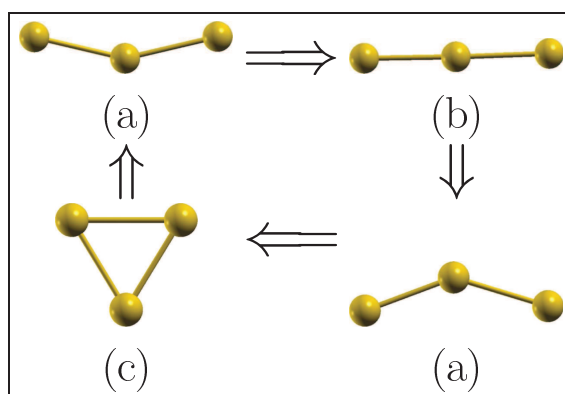
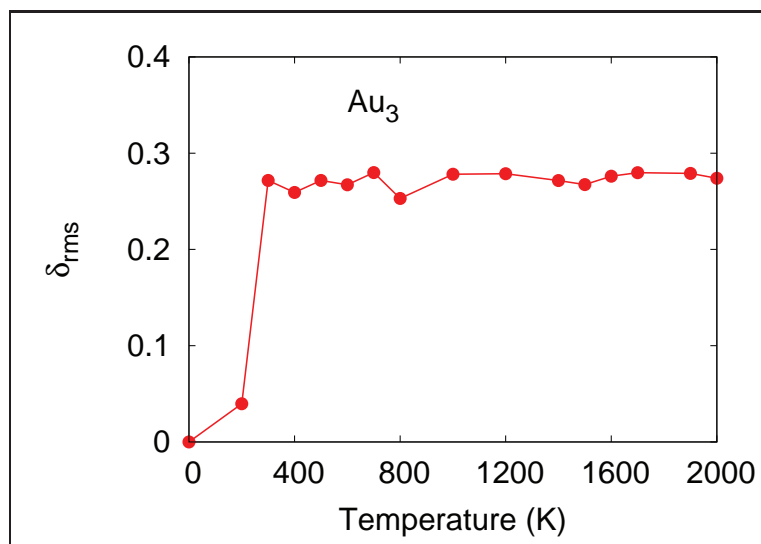FIGURE 6.1:   Cycle of conformational reorientation observed in Au$_3$ cluster between 200 K to 2000 K.

FIGURE 6.2: δ_{rms} of Au$_3$ as a function of temperature.

6.3   Results

6.3.1   Au$_3$

The cluster with three atoms is quite small with limited conformational reorientation available within. The ground state conformation of Au$_3$ is a bent structure with an Au-Au-Au angle of 162° (conformation shown as (a) in Figure 6.2). This conformation is nearly degenerate (the energy difference between both the conformations is just 0.3 kcal/mol) with that of a linear conformation shown as (b) in Figure 6.2. The simulations are carried out with bent structure as the starting conformation. An analysis of ionic motion around 200 K shows that the cluster evolves smoothly from the bent structure to the linear one and further to a triangular conformation (see Figure 6.2 (c)). Incidentally, this triangular conformation is just 5 kcal/mol higher in energy with respect to the ground state conformation. Thus, even at a low temperature of 200 K, there is an evolution between all possible conformations within a three atom cluster. Around 200 K, the triangular conformation is an obtuse angle triangle with an Au-Au-Au angle reaching a minimum of 100° with respect to the linear conformation. 300 K and above, the triangular conformation is equilateral with all the bond angles around 60°. This is reflected clearly in the δ_{rms} plot shown in Figure 6.2. The value is lower for 200 K where the two end atoms of bent conformation come close enough to only form an obtuse angle triangle. Interestingly, the cluster does not dissociate even up to 2000 K and the cluster undergoes a cyclic path of conformational reorientation between 200 K to 2000 K as shown in Figure 6.2.
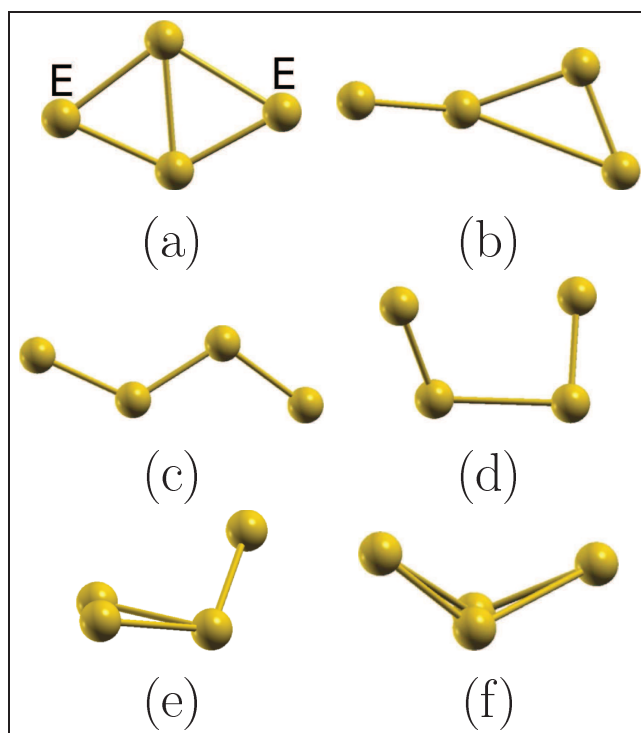
FIGURE 6.3:   Various conformations of Au$_4$ observed during an MD simulation. (a) corresponds to the ground state conformation.
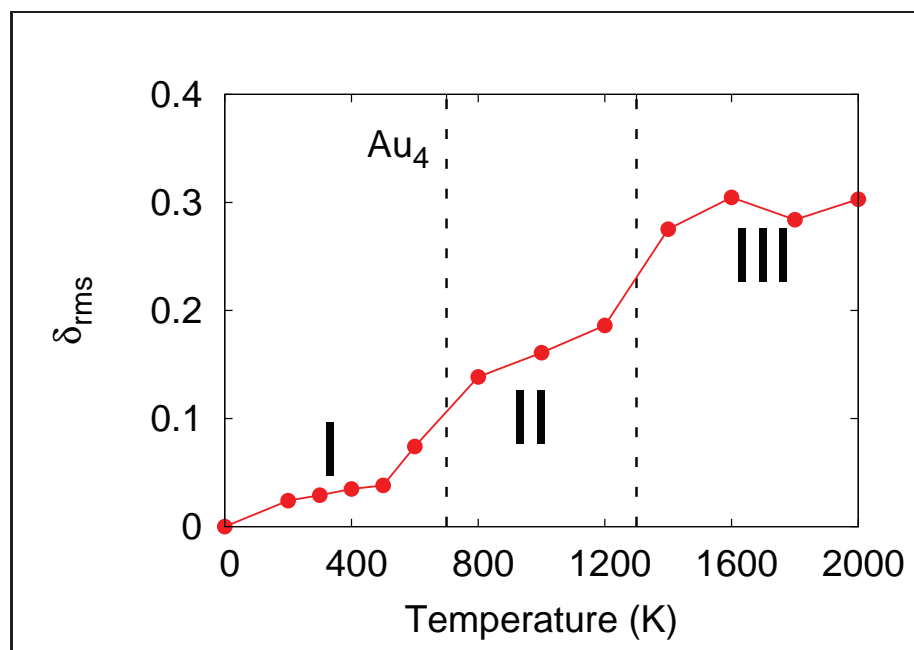
FIGURE 6.4: δ_{rms} of Au_4. I, II, III correspond to different states of a cluster as a function of temperature.

6.3.2 Au_4

The ground state geometry of Au_4 is a cyclic rhombus conformation shown in Figure 6.3.1(a). MD simulations with this conformation as the starting geometry are carried out between 200 K - 2000 K. Based on the conformational reorientation seen in Au_4, the behavior of the cluster can be classified into three regions/states. Region I is between 200 K-600 K, where atoms vibrate around their equilibrium position of the ground state conformation. Significantly, the two edge atoms (atoms indicated by E in Figure 6.3.1(a)) show higher displacements as compared to the central atoms of the ground state conformation. Region II is between 800-1200 K, where the cluster transits between ground state and next excited state conformation (see Figure 6.3.1(b)). During this transition, the dangling atom in Figure 6.3.1(b) bonds and dissociates in a cyclic fashion with alternating edges of the triangle. Such a transition from one conformation to another is more commonly referred to as 'structural fluctionality'.[36] This can be also envisaged as a region of 'planar fluidity' where, the cluster essentially retains its 2D orientation, while, the dynamic movements of few significant atoms reorient the cluster into two or three different planar configurations. Region III is 1400 K and above, where the cluster frequents some high energy planar conformations and 3D conformations in addition to the two conformations noted in the region II (see Figure 6.3.1(c)-(f)). This state is a thus a 'liquid-like' state. The above mentioned ionic movements reflect in Figure 6.3.1. The δ_{rms} hovers around 0.3 between 200 K-600 K. It shows a linear increase between 600 K- 1200 K where the cluster oscillates between the ground state and an excited state which is 0.32 kcal/mol above the ground state conformation. Other planar conformations which lie around 6-10 kcal/mol above the starting conformation are observed around 1400 K. Also it is only around this temperature that the atoms in the cluster diffuse enough to orient into 3D conformations. These conformations lie about 20 kcal/mol above the ground state conformation. One of the conformations shown in Figure 6.3.1(f) is a distorted T_d conformation. Thus, the Au_4 ground state conformation is seen to be stable up to

at least 600 K. Interestingly, Na_4 also exhibits similar finite temperature behavior as Au_4.[37]
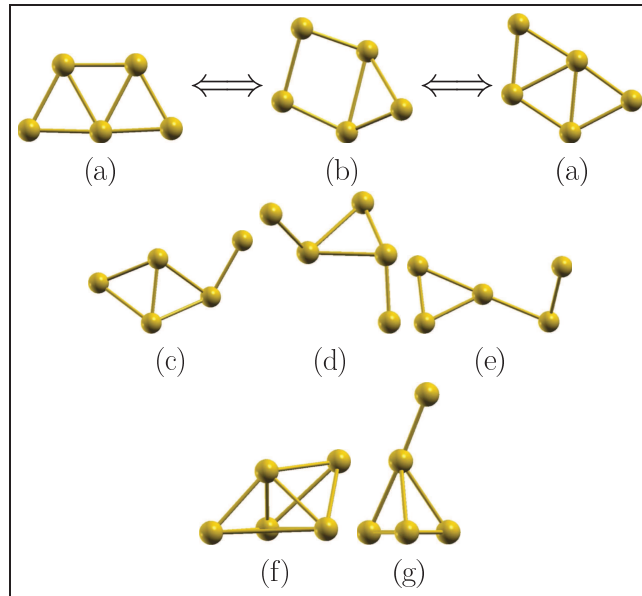
FIGURE 6.5: Various conformations seen during the MD simulation of Au_5. (a) corresponds to the ground state conformation.
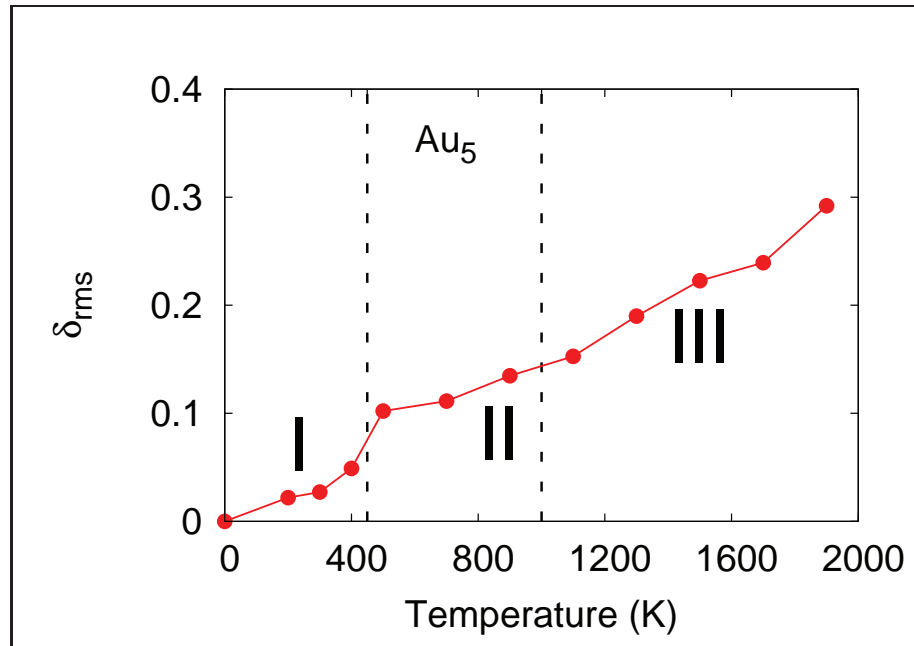

FIGURE 6.6: δ_{rms} of Au_5 with various regions highlighted.

6.3.3 Au_5

The ground state geometry of Au_5 is an extension of Au$_4$, with an additional edge of a triangle being capped (see Figure 6.3.2(a)). As in case of Au$_4$, the finite temperature behavior of the cluster can be classified into three regions, viz.,: (a) A 'solid-like' region where the atoms vibrate around their ground state region (from 200-400 K), called region I. (b) a planar 'liquid-like' region, where the the ground state transits through a metastable state (see Figure 6.3.2(b)) before returning back to its original configuration. This involves a rearrangement of the two cap atoms of the triangle between 500 K to 1000 K. Thus, Au_5, like in case of Au_4 also exhibits 'structural fluctionality'. (c) Around 1100 K, few high planar high energy conformations such as Figure 6.3.2(c), Figure 6.3.2(d) are seen. Above 1500 K, the 3D conformations are also seen. These conformations lie typically about 15-20 kcal/mol above the ground state conformation. These atomic movements reflect in the root mean square displacement values plotted in Figure 6.3.2.
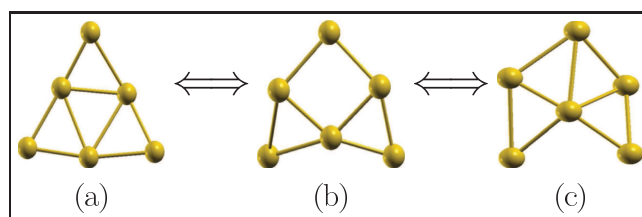
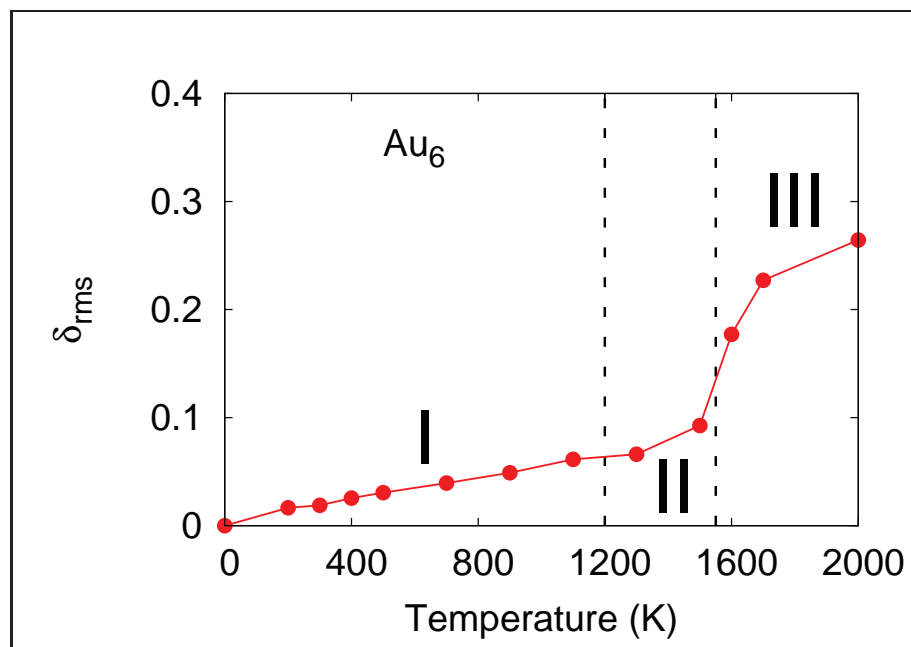FIGURE 6.7: "Structural fluctionality" observed in Au_6 between 1300 K to 1500 K.

FIGURE 6.8: δ_{rms} for Au_6. The cluster retains its ground state conformation upto 1100 K.

6.3.4 Au_6

The ground state geometry of Au_6 which corresponds to three capped edges of
a triangle (see Figure 6.3.3(a)), is the most stable conformation among all the
clusters studied with the cluster remaining in its ground state conformation up to
considerably high temperatures. Figure 6.3.3 gives the δ_{rms} for Au_6 cluster. An
analysis of ionic motion shows that the atoms vibrate around their equilibrium
positions in the ground state geometry up to a temperature of 1100 K. Above
this temperature, the cluster undergoes a transition between the ground state
planar structure and a next high energy planar conformation which is 7 kcal/mol
higher in energy via a metastable conformation (shown as (b) in Figure 6.3.3).
Interestingly, the same 'structural fluctionality' seen above has been reported in
one of the earlier works on $Au_6{}^-$ cluster The report indicates this transition to
have an energy barrier of nearly 9 kcal/mol.[15][a] which is seen to be reduced
by the chemical adsorption of various ligands. It is only around 1600 K that the
cluster transforms into a 'liquid-like' state where it transits through a several high
energy planar and 3D conformations. This temperature of 1700 K is remarkably
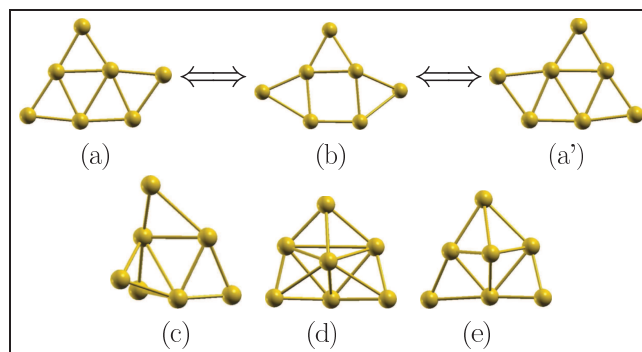high as compared to the melting temperature of bulk gold which is around 1337
K.

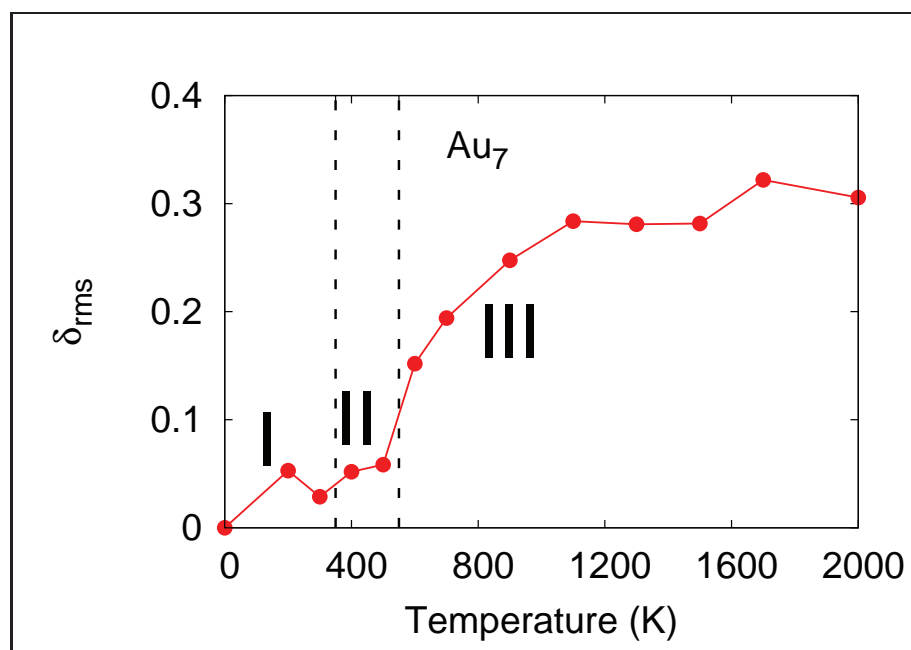FIGURE 6.9:   Various conformations seen during the MD simulation of Au$_7$.

FIGURE 6.10:   Root Mean Square (RMS) displacement in Au$_7$.

6.3.5 Au_7

The ground state geometry of Au_7 is a capped Au_6 conformation (see Figure 6.3.4(a)). The atoms in the cluster vibrate about their equilibrium positions in ground state conformation around 200 and 300 K. Around 400 and 500 K, the cluster shows a structural rearrangement from ground state geometry to a metastable conformation (see Figure 6.3.4(b)) before collapsing back into its mirror image (see Figure 6.3.4(a')). At 600 K and above, the system enters a a 'liquid-like' state with the cluster visiting several 3D conformations shown in Figure 6.3.4(c)-(e). Thus, the planar-liquid like region is quite small and and limited to 400-500 K in Au_7. The various regions of cluster behavior are clearly demarcated in figure 6.3.4.
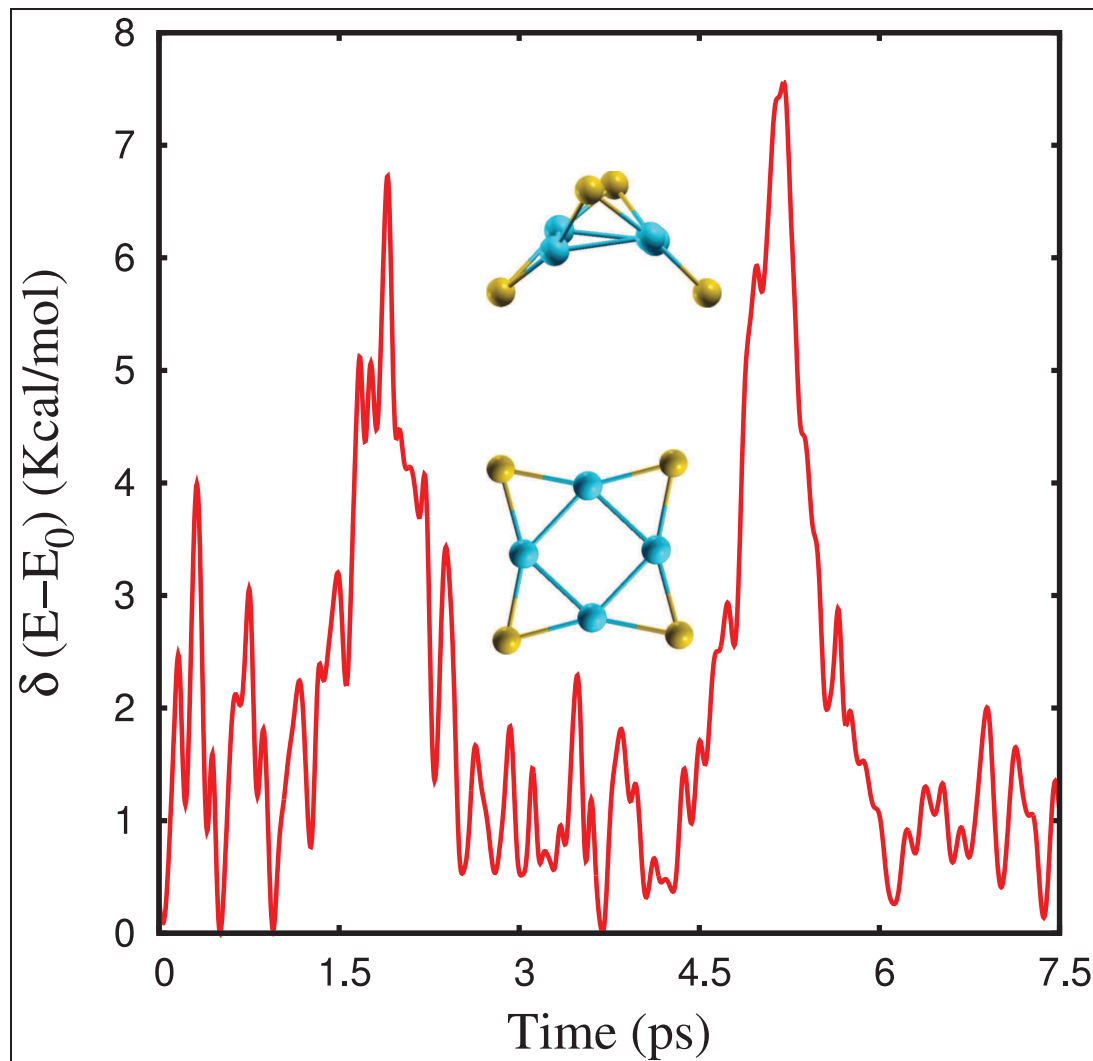
FIGURE 6.11: Oscillations in the potential energy (PE) given in kcal/mol for Au$_8$ at 200 K. Also shown are the two conformers corresponding to extrema in the PE. The four blue atoms correspond to the central plane. Rest of the atoms bend around this plane in a symmetric fashion.
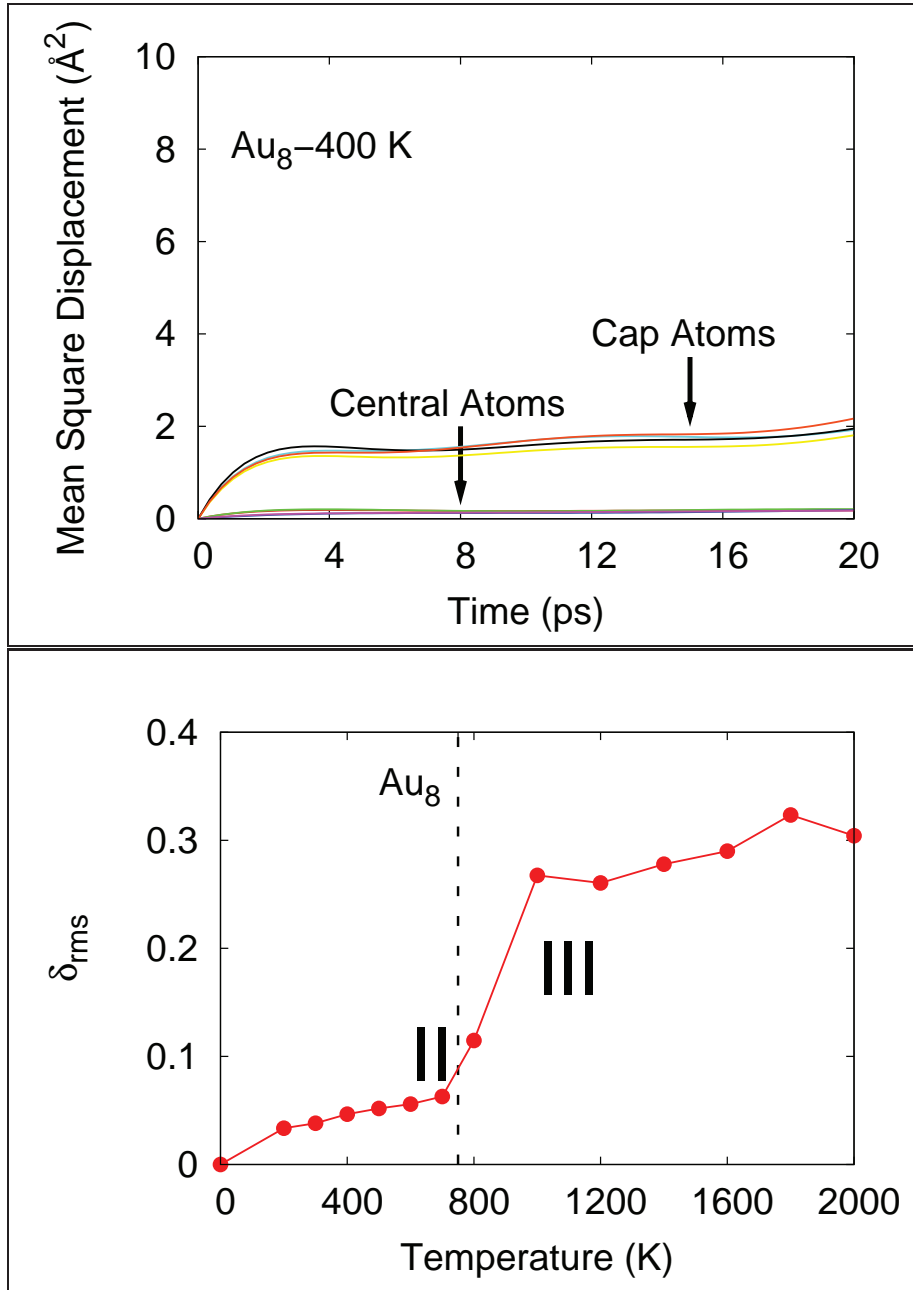
FIGURE 6.12:   MSD and δ_{rms} for Au8 of individual atoms in Au8 as seen at 400 K.

6.3.6 Au_8

The ground state geometry of Au_8 consists of a square with each of its edges capped by an Au atom.[33] An analysis of the ionic motion around 200 K reveals a slightly different behavior as compared to clusters discussed so far. The four cap atoms bend around the central square in a symmetric fashion. This is more clearly understood from Figure 6.3.5. The Figure demonstrates the fluctuations within potential energy with the ground state conformation referenced as zero. During the course of simulation the potential energy increases in spikes of ∼6-7 kcal/mol. During these increments, the cluster gets enough kinetic energy and the cap atoms bend around the plane of the central atoms. These distortions are very symmetric with the two diagonally placed caps bending downwards and the other two bending upwards. Figure 6.3.5 gives the individual mean square displacements of atoms from their equilibrium positions and this clearly shows that while the central four atoms are more rigid and remain very close to their equilibrium positions, the cap atoms undergo larger displacements. This behavior extends up to 700 K with the cap atoms undergoing the displacement with increasing frequency and amplitude as a function of temperature. Around 800, the additional 3D conformations are seen. 900 K and above, the cluster begins to resemble a liquid droplet transiting through several 3D conformations in addition to the ground state conformation and other planar conformations. This transition is clearly seen from δ_{rms} in Figure 6.3.5.
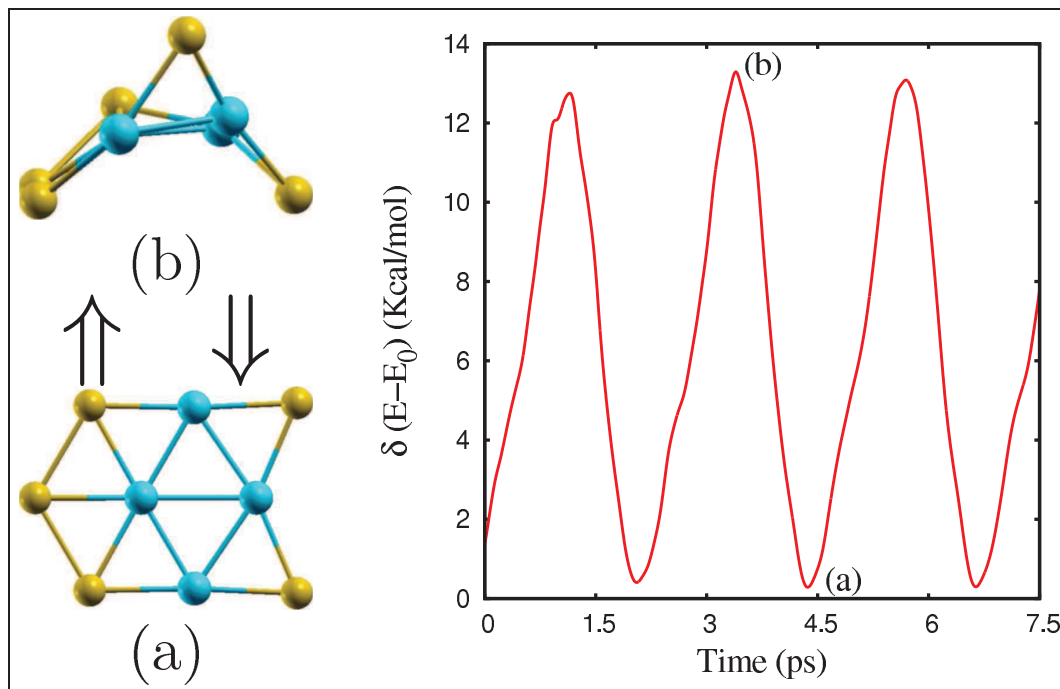
FIGURE 6.13: The two conformational orientations seen for Au_9 at 200 K. The atoms highlighted in blue correspond to the plane of atoms which vibrate around their equilibrium positions. Rest of the atoms undergo symmetric displacements about the plane. Also shown in the Figure is the corresponding oscillation in the potential energy for (a) and (b) conformations.
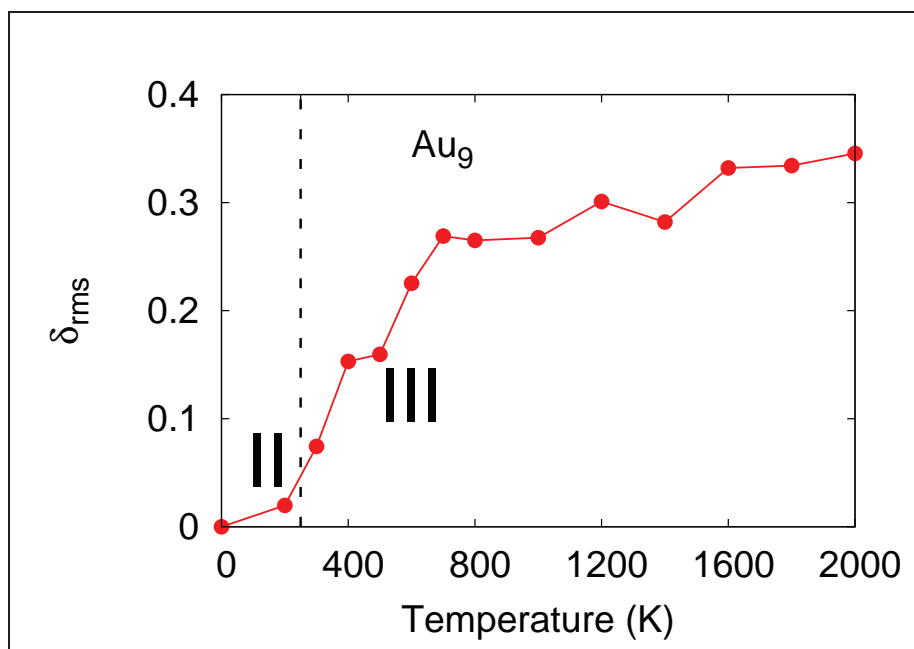
FIGURE 6.14: δ_{rms} for Au_9 of individual atoms in Au_9 as seen at 400 K.

6.3.7 Au_9

Au_9 ground state geometry being a growth over Au_8, is seen to be quite unstable. Around 200 K, the ground state geometry undergoes a 'structural fluctionality' as in case of Au_8 as shown in Figure 6.3.6. However, above 300 K, the cluster is seen to transit through various high energy planar and other non-planar conformations. Thus, the cluster already begins to resemble a liquid droplet. The cluster is in a complete 'liquid-like' state by 600 K as is clearly seen from the δ_{rms} plot in the Figure 6.3.6.
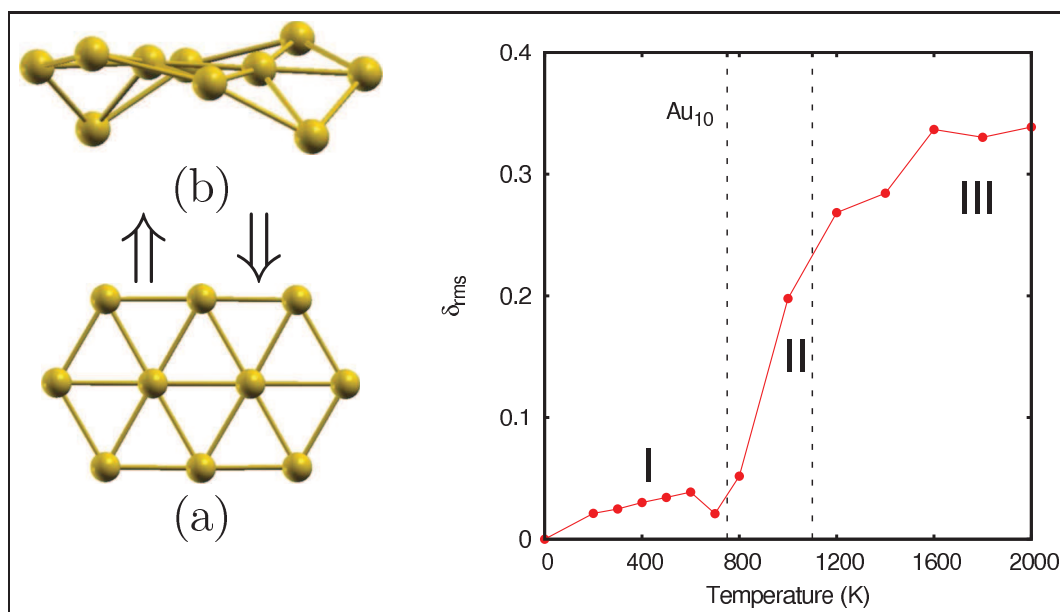
FIGURE 6.15: The conformational orientation seen in Au_{10} between 800 K - 1000 K (region II). Also shown in the Figure is the δ_{rms} for Au_{10}.

6.3.8 Au_{10}

Au_{10} ground state geometry is stable up to 700 K with the atoms vibrating about their equilibrium positions. Around 800 K, the cluster undergoes constrained deformation about the plane of the cluster as shown in the Figure 6.15. Above 1000 K, the cluster transits through several 3D conformations in addition to several excited state planar conformations thereby resembling a liquid state system.

6.4   Discussion on the finite temperature behavior of Au$_n$ (n=3-10) Clusters

Traditionally, clusters are known to transit from a 'solid-like' state and a 'liquid-like' state as a function of temperature. Each of these states have their own significance. The 'solid-like' region/state is significant due to the structural stability and an assurance of a constant electronic and geometric configuration. This state is important for applications where the clusters are applied for their response properties, which are size and shape sensitive. The 'liquid-like' state is a more dynamic state, which is significant during the synthesis of bigger nanoparticles where a soft electronic and geometric structure is needed. Interestingly, all the gold clusters studied in the present chapter exhibit a 'structural rearrangement' state (where they transit through two or three isomers) before they enter into a 'liquid-like' state.

TABLE 6.1:   Charge on individual atoms based on Lowdin population analysis for various conformations observed in Au$_6$ between 1100 and 1600 K and in Au$_8$ between 200 and 800 K.
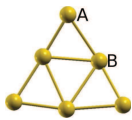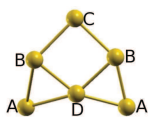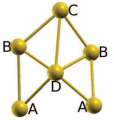
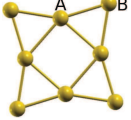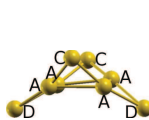| Cluster					
Reactivity Site	Au$_6$(a)	Au$_6$(b)	Au$_6$(c)	Au$_8$(a)	Au$_8$(b)
A	-0.164	-0.120	-0.070	-0.173	-0.185
B	0.165	0.151	0.144	0.173	–
C	–	-0.150	-0.259	–	0.183
D	–	0.133	0.103	–	0.186

Table 6.1 shows the conformations in Au_6 and Au_8 clusters respectively and the Lowdin charge distribution on them as they undergo the above 'structural rearrangement'. It is clearly evident from the values in the Table that a structural rearrangement is accompanied by a moderate to considerable charge redistribution. For example, site 'A' in Au_6 undergoes a significant charge depletion, while the site 'C' (which is site 'A' before the structural change) gains some charge. When a ligand molecule such as CO is adsorbed on site 'B' through carbon atom, presence of a more negatively charged 'C' site adjacent to it will help in an easier reduction process of it. Similar analysis can be drawn for other ligand molecules such as O_2, CH_3OH etc. In case of Au_8 also there is some charge redistribution leading to more negatively and positively charged atoms. Thus, the cluster is more polarized during the process. Hence, presence such a structural rearrangement appears to be important for many catalytic reactions where the atoms need to reorient with a modified charge distribution on adsorption of ligands. This facilitates the oxidation and reduction reaction mechanisms to have a lower barrier. Similar significance of this 'structural rearrangement' is also proposed by other experimental and theoretical studies.[36, 38]
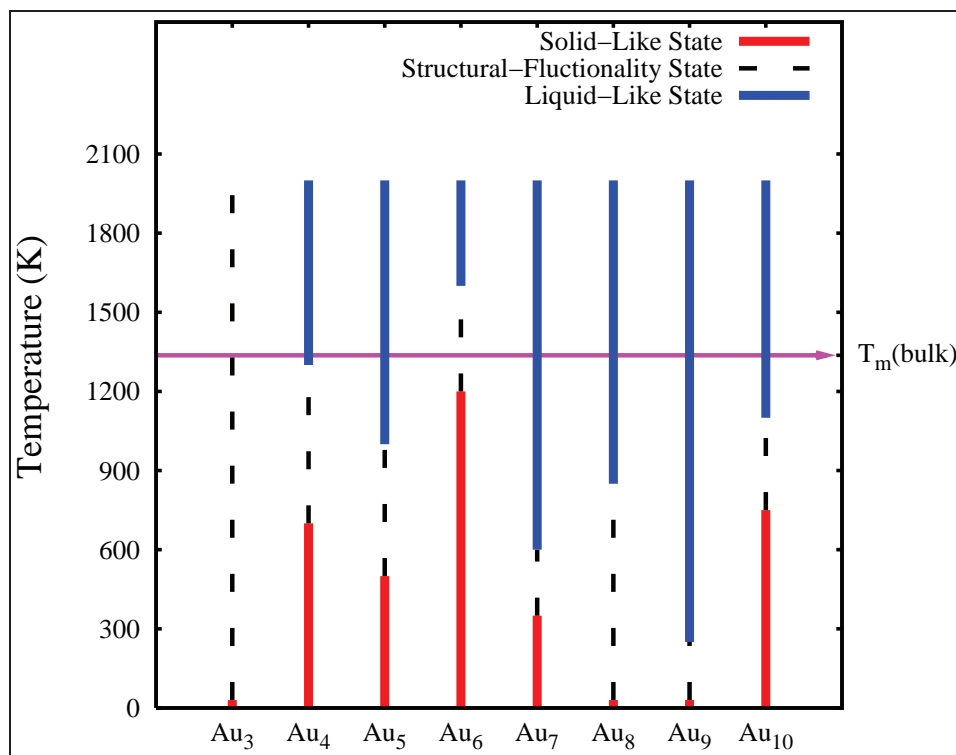
FIGURE 6.16: Summary of various thermodynamic states within Au_n clusters. The arrow indicates the melting temperature of bulk gold (T_m (bulk)).

In Figure 6.16, we summarize the observed finite temperature behavior of Au_n (n=3-10) clusters. The Figure clearly shows that Au_3, Au_8 and Au_9 clusters do not exhibit a 'solid-state' like behavior even at low temperatures. On the other hand, Au_6 is stable up to nearly 1100 K, highest among all the clusters studied. In general, it can be commented that that 'solid-like' region is comparatively larger for clusters with even atoms. The 'structural fluctionality' region is comparatively large for Au_8 and Au_3.

FIGURE 6.17: δ_{rms} of Au$_7$ with non-planar conformation as starting geometry.

In order to understand the significance of this 'structural rearrangement' in case of different starting conformations, we have carried out a BOMD simulation with a non-planar isomer of Au_7 as the starting conformation. This isomer is reported to co-exist along with the planar conformations in the recent experimental and theoretical reports.[19, 33]. An analysis of the ionic motion as a function of temperature in this simulation clearly shows that the finite temperature behavior of this conformation can be divided clearly 'solid-like' and 'liquid-like' states. The regions are demarcated and shown in Figure 6.4. The atoms in the cluster vibrate around their equilibrium positions up to 300 K. 400 K and above the cluster visits several other high energy 3D conformations along with few planar conformations. This was found to be consistently true in case of BOMD simulations with a no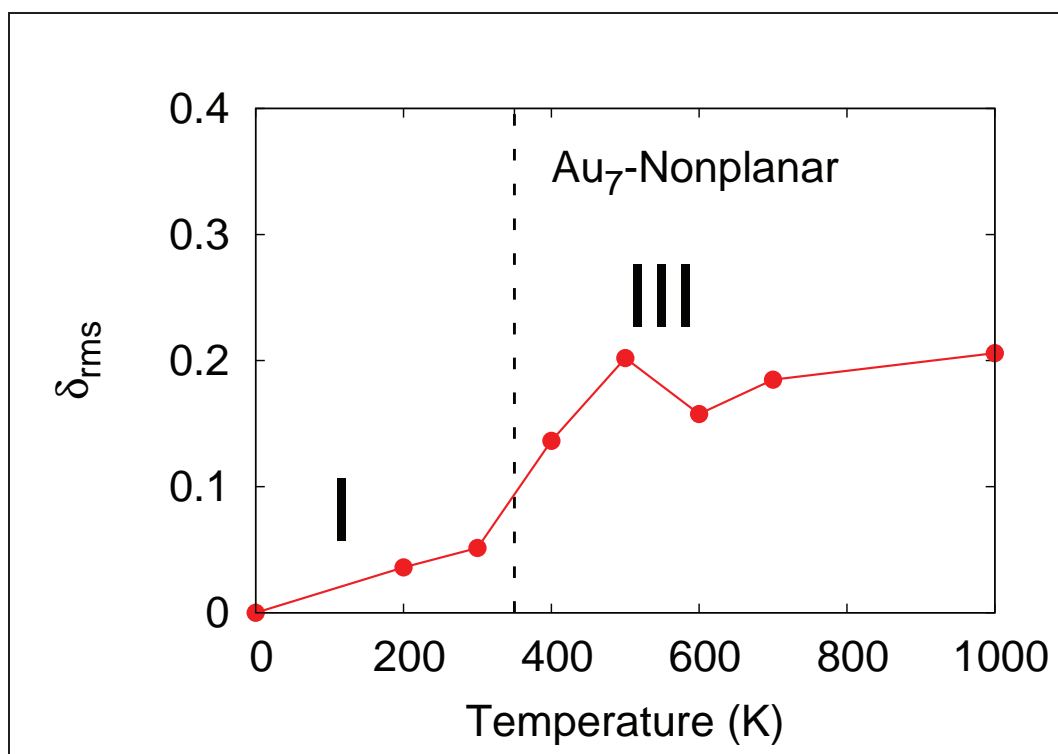n planar conformation as the starting geometry in Au_8 as well as Au_9. Thus, the 'structural fluctionality/rearrangement' appears to be characteristic of planar Au conformations. This behavior is probably an explanation to the higher catalytic activity of the small planar Au clusters[39] in comparison to their non-planar conformations.

6.5   Conclusions

Born Oppenheimer molecular dynamical simulations on Au_n (n=3-10) reveal a size dependent finite temperature behavior of clusters. The study shows that in clusters such as Au_3, Au_8 and Au_9 more than one isomer may co-exist at 300 K. Au_6 is the most stable conformation with only the ground state conformation dominating up to nearly 1100 K. A dynamic transition between two isomers or two conformations is observed in all the clusters between the 'solid-like' state and 'liquid-like' state. Such a fluctionality is seen to be size-specific and characteristic of planar conformations in this study. This transition called 'thermally driven structural fluctionality' may be quite significant and contribute positively to catalytic property of the planar gold clusters.

Bibliography

[1] (a) Haruta, M.; Yamada, N.; Kobayashi, T.; Iijima, S. *J. Catal.* **1989**, *115*, 301. (b) Hashmi, A. S. K. *Gold Bull.* **2003**, *36*, 3.

[2] (a) Hutchings, G. J. *J. Catal.* **1985**, *96*, 292. (b) Teles, J. H.; Brode, S.; Chabanas, M. *Angew. Chem.* **1998**, *110*, 1475.

[3] Yu, J-X.; Chen, X-R.; Sanvito, S. *Phys. Rev. B.* **2010**, *82*, 085415.

[4] (a) Torma, V.; Vidoni, O.; Simon, U.; Schmid, G. *Eur. J. Inorg. Chem.* **2003**, 1121. (b) Clarke, L.; Wybourne, M. N.; Yan, M.; Cai, S. X.; Keana, J. F. W. *Appl. Phys. Lett.* **1997**, *71*, 617.

[5] (a) Li, X.; Kiran, B.; Cui, Li-Feng.; Wang, L-S. *Phys. Rev. Lett.* **2005**, *95*, 253401. (b) Pundlik, S. S.; Kalyanaraman, K.; Waghmare, U. V. *J. Phys. Chem. C*, **2011**, *115*, 3809.

[6] Sessoli, R.; Gatteschi, D.; Caneschi, A.; Novak, M. A. *Nature* **1993**, *365*, 141.

[7] Pyykko, P. *Inorg. Chim. Acta.* **2005**, *358*, 4113.

[8] Li, Q.; Wu, K.; Wei, Y.; Sa, R.; Cui, Y.; Lu, C.; Zhu, J.; He, J.; *Phys. Chem. Chem. Phys.* **2009**, *11*, 4490.

[9] Krishnamurty, S.; Joshi, K.; Kanhere, D. G.; Blundell, S. A. *Phys. Rev. B.* **2006**, *73*, 045419.

[10] (a) Breaux, G. A.; Cao, B.; Jarrold, M. F. *J. Phys. Chem. B.* **2005**, *109*, 16575. (b) Breaux, G. A.; Hillman, D. A.; Neal, C. M.; Benirschke, R. C.; Jarrold, M. F. *J. Am. Chem. Soc.* **2004**, *126*, 8628.

[11] (a) Breaux, G. A.; Neal, C. M.; Cao, B.; Jarrold, M. F. *Phys. Rev. Lett.* **2005**, *94*, 173401. (b) Bagrets, A.; Werner, R.; Evers, F.; Schneider, G.; Schooss, D.; Wolfle, P. *Phys. Rev. B.* **2010**, *81*, 075435.

[12] Shvartsburg, A. A.; Jarrold, M. F. *Phys. Rev. Lett.* **2000**, *85*, 2530.

[13] Schmidt, M.; Kusche, R.; von Issendorff, B.; Haberland, H. *Nature* **1998**, *393*, 238.

[14] Krishnamurty, S.; Shafai, G. S.; Kanhere, D. G.; Soule de Bas, B.; Ford, M.J. *J. Phys. Chem. A.* **2007**, *111*, 10769.

[15] (a) Lang, S. M.; Bernhardt, T. M.; Barnett, R. N.; Yoon, B.; Landman U. *J. Am. Chem. Soc.* **2009**, 131, 8939. (b) Cox, D. M.; Brickman, R. O; Creegan, K.; Kaldor, A. *Mater. Res. Soc. Symp. Proc.* **1991** 206, 43. (c) Sun, Q.; Jena, P.; Kim Y. D.; Fischer, M.; Gantefor, G.; *J. Chem. Phys.* **2004**, 120, 6510.

[16] (a) Xiao, L.; Tollberg, B.; Xiankui, B.; Wang, L. *J. Chem. Phys.* **2006** 124, 114309. (b) Chen, G.; Wang, Q.; Sun, Q.; Kawazoe, Y.; Jena, P. *J. Chem. Phys.* **2010**, 132, 194306. (c) Shi, Y-K.; Li, Z-H.; Fan, K-N.; *J. Phys. Chem. A.* **2010**, 114, 10297.

[17] Hakkinen, H.; Landman, U. *Phys. Rev. B* **2000**, *62*, R2287.

[18] (a) Lechtken, A.; Schooss, D.; Stairs, J. R.; Blom, M. N.; Furche, F.; Morgner, N.; Kostko, O.; von Issendroff, B.; Kappes, M. M. *Angew. Chem. Int. Ed.* **2007**, *46*, 2944. (b) Walter, M.; Frondelius, P.; Honkala, K.; Hakkinen, H.; *Phys. Rev. Lett.* **2007**, *99*, 096102. (c) Hockendorf, R.F.; Cao, Y.; Bayer, M. K. *Organometallics* **2010**, *29*, 3001. (d) Iwasa, T.; Nobusada, K. *J. Phys. Chem. C.* **2007**, *111*, 45. (e) Shao, N.; Huang, W.; Gao, Y.; Wang, L-M.; Lim, X.;

Wang, L-S; Zeng, X. C. *J. Am. Chem. Soc.* **2010**, *132*, 6596. (f) Glib, S.; Weis, P.; Furche, F.; Ahlrichs, R.; Kappes, M. M.; *J. Chem. Phys.* **2002**, *116*, 4094.

[19] Gruene, P.; Rayner, D. M.; Redlich, B.; Van der Meer, A. F. G.; Lyon, J. T.; Meijer, G.; Fielicke, A. *Science* **2008**, *321*, 674.

[20] (a) Wang, L-M.; Pal, R.; Huang, W.; Zeng, X. C.; Wang, L-S. *J. Chem. Phys.* **2010**, *132*, 114306. (b) Huang, W.; Wang, L-S. *Phys. Rev. Lett.* **2009**, *102*, 153401.

[21] Schooss, D.; Weis, P.; Hampe, O.; Kappes, M. M.; *Phil. Trans. R. Soc. A.* **2010**, *368*, 1211.

[22] (a) Olson, R. M.; Vargonov, S.; Gordon, M. S.; Metiu, H.; Chretien, S.; Piecuch, P.; Kowalski, K.; Kucharski, S. A.; Musial, M. *J. Am. Chem. Soc.* **2005**, *127*, 1049. (b) Walker, A. V. *J. Chem. Phys.* **2005**, 122, 94310. (c) Remacle, F.; Kryachko, E. S. *J. Chem. Phys.* **2005**, *122*, 44304. (d) Gronbeck, H.; Broqvist, P. *Phys. Rev. B* **2005**, *71*, 073408. (e) Yuan, D. W.; Wang, Y.; Zeng, Z. *J. Chem. Phys.* **2005**, *122*, 114310.

[23] (a) Chushak, Y.; Bartell, L. S.; *Eur. Phys. J. D.* **2001**, *16*, 43. (b) Wang, Y.; Rashkeev, S. N.; *J. Phys. Chem. C.* **2009**, *113*, 10517. (c) Wang, Y.; Teitel, S.; Dellago, C.; *J. Chem. Phys.* **2005**, *122*, 214722. (d) Cleveland, C. L.; Luedtke, W. D.; Landman, U.; *Phys. Rev. B.* **1999**, *60* 5065.

[24] Gomez, J. C. R.; Rincon, L. *Revista Mexicana de Fisica* **2007**, *53*, 208.

[25] Cleveland, C. L.; Luedtke, W. D.; Landman, U.; *Phys. Rev. Lett.* **1998**, *81*, 2036.

[26] (a) Soule de Bas, B.; Ford, M.J.; Cortie, M. B.; *J. Phys: Condensed Matter* **2006**, *18*, 55. (b) Chandrachud, P.; Joshi, K.; Krishnamurty, S.; Kanhere, D. G. *Pramana* **2009**, *72*, 845.

[27] Koskinen, P.; Hakkinen, H.; Huber, B.; von Issendorff, B.; Moseler, M. *Phys. Rev. Lett.* **2007**, *98*, 015701.

[28] Herzing, A. A.; Kiely, C. J.; Carley, A. F.; Landon, P.; Hutchings, G. J. *Science* **2008**, *321*, 1331.

[29] deMon2k, Koster, A. M.; Calaminici, P.; Casida, M. E.; F-Moreno, R.; Geudt- ner, G.; Goursot, A.; Heine, T.; Ipatov, A.; Janetzko, F.; del Campo, J. M.; Patchkovskii, S.; Reveles, J. U.; Vela, A.; Salahub, D. R. deMon Developers (2006).

[30] Perdew, J. P.; Burke, K.; Ernzerhof, M. *Phys. Rev. Lett.* **1996**, *77*, 3865.

[31] (a) Schwerdtfeger, P.; Dolg, M.; Schwarz, W.H.E.; Bowmaker, G.A.; Boyd, P.D.W. *J. Chem. Phys.* **1989**, *91*, 1762. (b) Dolg, M. Effective Core Potentials. In Modern Methods and Algorithms of Quantum Chemistry; John von Neumann Institute for Computing: Jülich, 2000; Vol. 1, p 479.

[32] De, H. S.; Krishnamurty, S.; Pal, S. *J. Phys. Chem. C.* **2009**, *113*, 7101.

[33] De, H. S.; Krishnamurty, S.; Pal, S. *J. Phys. Chem. C.* **2010**, *114*, 6690.

[34] (a) Godbout, N.; Salahub, D. R.; Wimmer, J. A. E. *Can. J. Phys.* **1992**, *70*, 560. (b) Köster, A. M.; Flores-Moreno, R.; Reveles, J. U. *J. Chem. Phys.* **2004**, *121*, 681.

[35] Wells, D. H., Jr.; Delgass, W. N.; Thomson, K. T. *J. Chem. Phys.* **2002**, *117*, 10597

[36] Hakkinen, H.; Abbet, S.; Sanchez, A.; Heiz, U.; Landman, U. *Angew. Chem. Int. Ed.* **2003**, *42*, 1297.

[37] Gamboa, G. U.; Calaminici, P.; Geudtner, G. G.; Köster, A. M. *J. Phys. Chem. A* **2008**, *112*, 11969.

[38] Giorgio, S.; Cabie, M.; Henry, C. R. *Gold Bull.* **2008**, *41*, 167.

[39] (a) Jeyabharathi, C.; Senthil Kumar, S.; Kiruthika, G. V. M.; Phani, K. L. N. *Angew. Chem. Int. Ed.* **2010**, *49*, 2925. (b) Zanchet, A.; D-Urra, A.; Aguado, A.; Roncero, O. *J. Phys. Chem. C* **2011**, *115*, 47.

Chapter 7

Molecular Dynamics Study Of Icosahedral Au_{32} Cluster

Abstract

Relativistic Density Functional Theory (DFT) based molecular dynamical simulations are performed on Au_{32} golden fullerene with an aim of understanding its thermal stability. Various conformations being populated at different temperatures of a cluster have been analyzed. The chapter shows that the icosahedral conformation is stable only up to 300 K and structure remains in a hollow conformation only up to 400 K. This clearly explains the reasons for failure by experimentalists in trapping the unique fullerene conformation in spite of the theoretical predictions of it being a very stable one.

7.1   Introduction

During the last decade new class of Au nano clusters have resulted in a substantial excitement in both experimental and theoretical chemists. Apart from the tetrahedral Au_{19} and Au_{20} clusters,[1] new class of golden cages[2] have been proposed using both experimental and theoretical methods. In addition several state of art theoretical studies have shown plausible existence of golden fullerenes.[3–7] Au_{32},[3, 4] Au_{50}[5, 6] and Au_{72}[7] are the sizes with fullerene structure as the ground state geometry at relativistic Density Functional Theory (DFT) methods. The fact metal clusters can have hollow fullerene structural orientations has led to a lot of excitement. Among the three sizes, Au_{32} has been most intriguing cluster. It started with a report by Johansson and co-workers[3] that ground state geometry of Au_{32} is a icosahedral golden fullerene. The report shows as to how the spherically hollow Au_{32} conformation with nearly 0.9 nm diameter is structurally similar to C_{60}. In addition to its shape uniqueness, the theoretical studies also revealed a record value of magnetic shielding at the center of the cage indicative of induced ring currents in the molecule. In other words, the ground state Au_{32} geometry has been proposed to be aromatic in nature.

The hollow nature combined with the ring currents in the center of Au_{32} can find use in distributing pharmaceuticals. However, the bottle neck in its practical application is the failure by the experimental methods to trap this conformation in spite of its high stability as predicted by theoretical methods. It has been proposed that maintaining the spherical aromaticity is critical in trapping the fullerene Au_{32} conformation experimentally.[8] Other reports propose that a C_1 is more stable conformation[4, 9]. Motivated by these findings, we in the present work report a finite temperature study in Au_{32} to evaluate its stability as a function of temperature.

The chapter is organized as follows. In Section 7.2, we discuss the computational methodology and clusters for which the simulations were carried out. In Section

7.3, we note the results and observations from the simulation studies. We conclude in brief the chapter in Section 7.4.

7.2 Computational Details

All calculations are performed in the framework of Density Functional Theory (DFT), using a linear combination of Gaussian orbitals as implemented in *de-Mon2k* code.[10] About 50 conformations are generated and optimized using the Perdew-Burke-Ernzerhof(PBE) exchange and correlation functional[11] with 1997 Stuttgart-Dresden Relativistic Effective Core Potential's (RECP)'s[12] as the basis set for the valence electrons. 5s, 5p, 5d and 6s electrons are considered to constitute the valence electrons. We note that these ECP's are now documented for accurate prediction of structure as well as spectroscopic properties of Au clusters.[13, 14] No additional polarization functions are added. The A2 auxiliary functions are set to fit the charge density. [15] The convergence of the geometries is based on gradient and displacement criteria with a threshold value of 10^{-5} au and the criteria for convergence of SCF cycles was set to 10^{-9}. Only the lowest spin state is considered for all the Au clusters. The spin multiplicities for even electron (even number of Au atoms) clusters are singlets and doublets for odd electron (odd number of Au atoms) clusters. It has also been reported in an earlier literature that Au clusters prefer to be in their lowest spin state.[16] Following the geometry optimization, harmonic vibrational frequencies are computed for various conformations. All of the frequencies are found to be positive, thereby, indicating the conformations to be a local minima.

The lowest energy conformation is found to be of icosahedral (I_h) symmetry. Finite temperature study was carried out on this cluster in order to evaluate its thermal stability. The finite temperature simulation is carried out using Born-Oppenheimer Molecular Dynamics (BOMD). The simulations are carried out between 200 K to

2000 K. For each temperature, the cluster is equlibrated for a time period of 10 ps followed by a simulation time of 30 ps. The temperature of the cluster is maintained using the Berendsen's thermostat ($\tau = 0.5$ps) in the NVT ensemble. The nuclear positions are updated with the velocity Verlet algorithm with a time step of 1 fs. The atomic positions and bond length punctuations of atoms are analyzed using traditional parameters such as root mean squared bond length fluctuations (δ_{rms}) and the Mean Squared ionic Displacements (MSD)'s[17, 18]. δ_{rms} is defined as

$$\delta_{rms} = \frac{2}{N(N-1)} \sum_{i<j} \frac{\sqrt{\langle R_{ij}^2 \rangle_t - \langle R_{ij} \rangle_t^2}}{\langle R_{ij} \rangle_t} \tag{7.1}$$

where, N is the number of particles in the system, r_{ij} is the distance between the ith and j^{th} particles in the system and $<...>_t$ denotes a time average over the entire trajectory. The MSD of an individual atom is defined as,

$$\langle R_i^2 \rangle = \frac{1}{M} \sum_{M-1}^{M} [R_i(t_{0m} + t) - R_i(t_{0m})]^2 \tag{7.2}$$

where, $R_i(t_{0m})$ is the instantaneous position of atom i at t_0 and $R_i(t_{0m} + t)$ is the corresponding position of atom i after a time interval t.

7.3   Results and Discussion

Figure 7.3 gives the root mean square displacement of Au_{32} as a function of various temperatures. It is clearly seen from the Figure that the structure undergoes systematic structural variations from 600 K onwards. The δ_{rms} around 300 and 400 K is minimal and is 0.03 and 0.04 respectively. However, around 600 K it jumps to a value 0.08 and around 700 K the value reaches to 0.1 indicate of significant displacements of atoms around 600 K onwards. Around 1200 K, the value reaches nearly 0.3. Several research works have by now established that

clusters at finite temperature undergo a transformation from solid-like state to a liquid-like state. At low temperatures, the atoms in a cluster vibrate around their equilibrium positions as in case of a bulk solid (and hence the name solid-like state). As the temperature increases, the atoms within the cluster reorient their positions. As they reorient, the cluster transits into other local minima through diffusive motion of atoms. Finally, at very high temperatures, clusters transit through several conformations within few femto seconds. These conformational reorientation's/isomerization increases dramatically beyond a temperature specific to each cluster and resembles a liquid droplet (and hence the name liquid-like state). This phenomenon has been very widely explored experimentally as well as theoretically in several clusters such as silicon,[19] gallium,[20] aluminum,[21] tin,[22] sodium,[23] and gold[24] experimentally and/or theoretically. A δ_{rms} value of 0.3 is indicative of a nearly liquid like state of the cluster.[24][a] In other words, Au_{32} is in a nearly liquid like state around 1200 K.
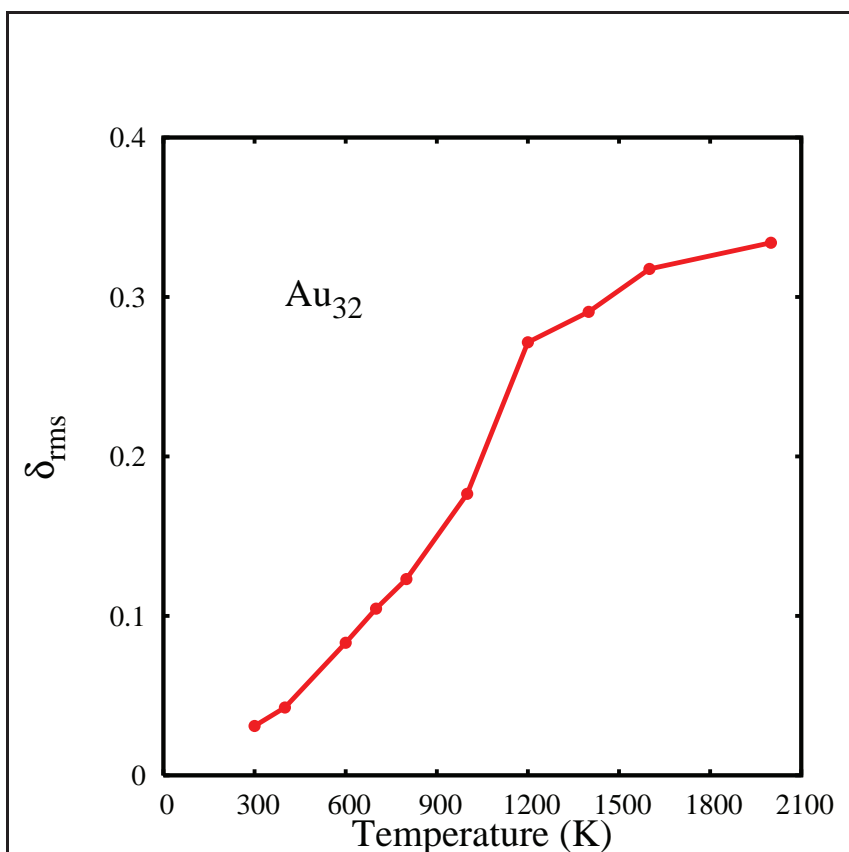
FIGURE 7.1: Root Mean Square displacement of Au_{32} as function of temperature.
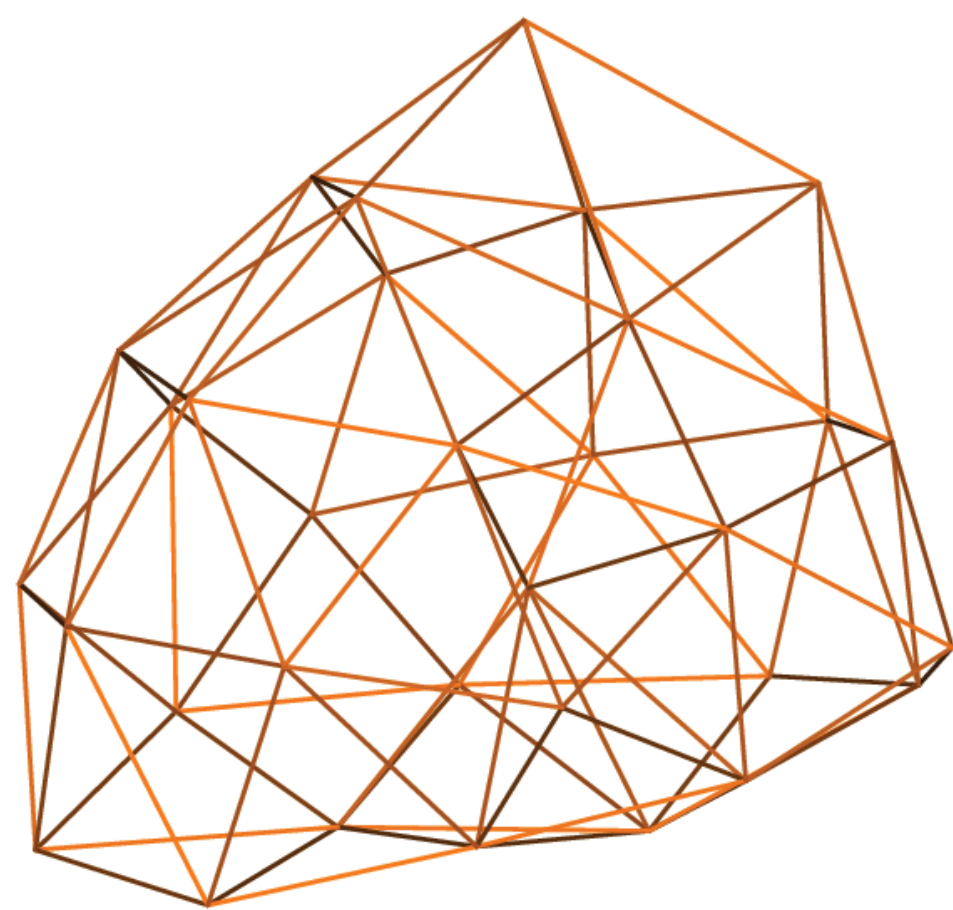
FIGURE 7.2: One of the space filling conformations seen at 500 K.

To get a more detailed insight, we have analyzed the ionic motions of the atoms. The analysis reveals that the cluster remains in the ground state icosahedral state up to 300 K. Around 400 K we note that the cluster oscillates between icosahedron and other hollow conformation which is of C_1 symmetry. Around 500 K, the cluster transits into other space filling conformations (see Figure 7.2. The atomic motions increase beyond 500 K and the cluster begins to resemble a liquid droplet by 1200 K.

7.4   Conclusions

Born Oppenheimer molecular dynamical simulations on Au_{32} reveal that the fullerene conformation is unstable beyond 300 K. This conformation gives way to other hollow conformations around 400 K. Space filling conformations dominate trajectories from 500 K. Clearly other factors such as capping agents are needed for stabilizing the much needed fullerene Au_{32} conformation.

7.5   Future Scope

In the future we plan to address the general stability of hollow cages, viz. Au_{18} at different temperatures with traditional molecular dynamics parameters. In addition to that, electron Localization Function (ELF) are to be calculated for Au_{32} clusters for various conformations in order to describe the nature of bonding within the Au clusters in critical manner.

Bibliography

[1] Gruene, P.; Rayner, D. M.; Redlich, B.; Van der Meer, A. F. G.; Lyon, J. T.; Meijer, G.; Fielicke, A. *Science*, **2008**, *321*, 674.

[2] Bulusu, S.; Li, X.; Wang, L-S.; Zeng, X.C. *Proc. Natl. Acad. Sci. U. S. A*, **2006**, *103*, 8326.

[3] Johansson, M. P.; Sundhlom, D.; Vaara, J. *Angew. Chem. Int. Ed.*, **2004**, *43*, 2678.

[4] Gu, X.; Ji, M.; Wei, S. H.; Gong, X. G. *Phys. Rev. B*, **2004**, *70*, 205401.

[5] Wang, J.; Jellinek.; Zhao, J.; Chen, Z.; King. R. B.; Schleyer, von R. P. *J. Phys. Chem. A.*, **2005**, *109*, 9265.

[6] Tian, D.; Zhao, J.; Wang, B.; King, R. B. *J. Phys. Chem. A.*, **2007**, *111*, 411.

[7] Karttunen, A. J.; Linnolahti, M.; Pakkanen, T. A.; Pyykko, P. *Chem. Commun.*, **2008**, 465.

[8] Johansson, M. P.; Vaara, J.; Sundholm, D. *J. Phys. Chem. C*, **2008**, *112*, 19311.

[9] Ji, M.; Gu, X.; Li, X. G.; Gong, G.; Li, J.; Wang, L-S. *Angew. Chem. Int. Ed.*, **2005**, *44*, 7119.

[10] deMon2k, Koster, A. M.; Calaminici, P.; Casida, M. E.; F-Moreno, R.; Geudtner, G.; Goursot, A.; Heine, T.; Ipatov, A.; Janetzko, F.; del Campo, J. M.;

Patchkovskii, S.; Reveles, J. U.; Vela, A.; Salahub, D. R. deMon Developers (2006).

[11] Perdew, J. P.; Burke, K.; Ernzerhof, M. *Phys. Rev. Lett.*, **1996**, *77*, 3865.

[12] (a) Schwerdtfeger, P.; Dolg, M.; Schwarz, W.H.E.; Bowmaker, G.A.; Boyd, P.D.W. *J. Chem. Phys.*, **1989**, 91, 1762. (b) Dolg, M. Effective Core Potentials. In Modern Methods and Algorithms of Quantum Chemistry; John von Neumann Institute for Computing: Jülich, 2000; Vol. 1, p 479.

[13] De, H. S.; Krishnamurty, S.; Pal, S. *J. Phys. Chem. C.*, **2009**, *113*, 7101.

[14] De, H. S.; Krishnamurty, S.; Pal, S. *J. Phys. Chem. C.*, **2010**, *114*, 6690.

[15] Godbout, N.; Salahub, D. R.; Wimmer, J. A. E. *Can. J. Phys.*, **1992**, *70*, 560.

[16] Wells, D. H., Jr.; Delgass, W. N.; Thomson, K. T. *J. Chem. Phys.*, **2002**, *117*, 10597

[17] Kanhere, D. G.; Vichare, A.; Blundell, S. A. *Reviews in Modern Quantum Chemistry*, edited by K. D. Sen, World Scientic, Singapore, 2001.

[18] Berry, R. S., Haberland, H. *Clusters of Atoms and Molecules I*, edited by H. Haberland Springer-Verlag, Berlin, 1994.

[19] Krishnamurty, S.; Joshi, K.; Kanhere, D. G.; Blundell, S. A. *Phys. Rev. B.*, **2006**, *73*, 045419.

[20] (a) Breaux, G. A.; Cao, B.; Jarrold, M. F. *J. Phys. Chem. B.*, **2005**, *109*, 16575. (b) Breaux, G. A.; Hillman, D. A.; Neal, C. M.; Benirschke, R. C.; Jarrold, M. F. *J. Am. Chem. Soc.*, **2004**, *126*, 8628.

[21] (a) Breaux, G. A.; Neal, C. M.; Cao, B.; Jarrold, M. F. *Phys. Rev. Lett.*, **2005**, *94*, 173401. (b) Bagrets, A.; Werner, R.; Evers, F.; Schneider, G.; Schooss, D.; Wolfle, P. *Phys. Rev. B.*, **2010**, *81*, 075435.

[22] Shvartsburg, A. A.; Jarrold, M. F. *Phys. Rev. Lett.*, **2000**, *85*, 2530.

[23] Schmidt, M.; Kusche, R.; von Issendorff, B.; Haberland, H.; *Nature*, **1998**, *393*, 238.

[24] (a) Krishnamurty, S.; Shafai, G. S.; Kanhere, D. G.; Soule de Bas, B.; Ford, M.J. *J. Phys. Chem. A.*, **2007**, *111*, 10769. (b) Cleveland, C. L.; Luedtke, W. D.; Landman, U. *Phys. Rev. B.* **1999**, *60* 5065. (c) De, H. S.; Krishnamurty, S.; Mishra, D.; Pal, S. *J. Phys. Chem. C*, **2011**, *115*, 17278.

Appendix A

List of Publications

- Himadri Sekhar De, Sailaja Krishnamurthy and Sourav Pal, **Density Functional Investigation of Relativistic Effects on the Structure and Reactivity of Tetrahedral Gold Clusters**, *J. Phys. Chem. C* **2009**, *113*, 7101.

- Himadri Sekhar De, Sailaja Krishnamurthy and Sourav Pal, **Understanding the reactivity Properties of Au_n ($6 \leq n \leq 13$) Clusters Using Density Functional Theory Based Reactivity Descriptors**, *J. Phys. Chem. C* **2010**, *114*, 6690.

- Himadri Sekhar De, Sailaja Krishnamurthy, Deepti Mishra and Sourav Pal, **Finite Temperature Behavior of Gas Phase Neutral Au$_n$ ($3 \leq n \leq 10$) Clusters: A First Principles Investigation**, *J. Phys. Chem. C* **2011**, *115*, 17278.

- Himadri Sekhar De, Sailaja Krishnamurthy and Sourav Pal, **Sensitivity of Exchange correlation Functionals on Structure and Properties of Au_n ($6 \leq n \leq 13$) Clusters**, *(In manuscript)*.

- Himadri Sekhar De, Sailaja Krishnamurthy and Sourav Pal, **Thermal stability of a golden fullerene: A First Principles Investigation.**, *(In manuscript).*

Appendix B

B.1 Computational Details

The software used was deMon2K which has been mentioned in brief in Chapter 2. For all the calculations in previous chapters deMon2k in the version 2.2.6 was used. For calculation of Mean-Squared Displacements (MSD), δ_{rms}-Bond Length Fluctuation (δ_{rms}-BLF) and potential energy surface spectra (PES), unix scripts and Fortran 90/95 codes were written.

B.2 Typical Computational Requirements

To present a brief idea on the computational resources used for the various simulations, the time needed to perform one wavefunction step is given in the table below:

TABLE B.1: Computational requirements of simulations in this thesis. In
the table the time needed for one wavefunction step is given in seconds.
It depends on the size of the studied system, the type of calculation and
the type of computer and the number of processors used.

System	Intel(R) Xeon(R) E7330@ 2.40 GHz		Intel(R) Xeon(R) 5160 @3.00 GHz	
	No. of processors	Time (s)	No. of processors	Time (s)
Au_{13}	1	755	16	6
Au_{12}	1	499	16	3

For one geometry step it takes about 7-30 iterations of the wavefunction. The number of geometry steps needed to find a minimum on the potential energy depends strongly on the initial configuration or guess, the degrees of freedom in the system and the convergence criterium used which have been discussed in detail under Chapter 2. In a typical optimization of Au_{12} it takes about 20-50 geometry steps, and sometimes more, with an initial configuration already optimized with a different XC-functionals, to arrive at a local minimum. For a typical vibrational spectrum calculation for an already optimized structure of Au_{12}, where computing the forces are more time consuming as compared to SCF, 12 processors typically takes 43606 seconds or 12 hours.

Molecular Dynamics studies are far more computationally expensive. A typical MD run with deMon.2.2.6 code for Au_{12}, takes around 23 seconds per step of unit femtosecond, where about 6-15 iterations are needed per time step.

B.2.1 Input File

B.2.1.1 Input File 1

TITLE: Au13 - gs-relativistic :PBE PBE

GEOMETRY CARTESIAN ANGSTROMS

AU 0.000000 0.000000 0.000000

AU 0.000000 0.000000 2.737941

AU 2.372637 0.000000 1.360859

AU -0.093301 0.000308 -2.754029

AU -2.446888 -0.000234 -1.316111

AU -2.464655 -0.000252 1.407726

AU -2.363373 -0.000190 4.162655

AU 2.357827 0.000367 -1.484028

AU 4.822296 0.000703 -2.627738

AU 4.802450 0.000217 0.043261

AU 4.820991 -0.000410 2.748570

AU 2.440336 -0.000050 4.154874

AU 0.080350 0.000019 5.502075

#

GUESS CORE

SCFTYPE ROKS MAX=600 TOL=1.0E-09

OPTIM MAX=400 TOL=1.0E-05

SHIFT -0.1

CHARGE 0.0

MULTIPLICITY 2

ERIS DIRECT

MIXING -0.3

DIIS ON

QUADRATURE GAUSS

GRID ADAPTIVE TOL=1.0E-6

VXCTYPE BASIS PBE PBE

PRINT XCE MOE

VISUALISATION FULL

BASIS (RECP19|SD)

ECPS (RECP19|SD)

AUXIS (GEN-A2)

END

B.2.1.2   Input File 2

TITLE $Au_7 T = 200K$

#

$CHARGE 0.0$

$DYNAMICS STEP = 1.0 MAX = 30000 INT = 5$

$BASIS$

$Au(RECP19|SD)$

ECPS (RECP19|SD)

Au (RECP19|SD)

AUXIS (GEN-A2)

MULTIPLICITY 2

SCFTYPE ROKS MAX=60 TOL=0.100E-04

VXCTYPE AUXIS PBE-PBE

TRAJECTORY

BATH BERENDSEN TAU=0.05 T=200

VELOCITIES RANDOM LP=0

LPCONSERVE TOL=1.E-08

ERIS DIRECT

GUESS CORE

DIIS ON

MIXING 0.1

GRID ADAPTIVE TOL=1.0E-06

VISUALISATION MOLDEN MD

QUADRATURE GAUSS

#

GEOMETRY CARTESIAN ANGSTROM

Au 1.755944 1.019298 -0.000524

Au 0.088055 3.081010 0.002022

Au 3.550309 -0.989056 -0.003492

Au -0.985158 0.622911 -0.001263

Au 0.928325 -1.675736 0.005280

Au -1.720038 -2.017094 -0.000203

Au -3.617436 -0.041333 -0.001820